UNIVERSIDADE FEDERAL DE PERNAMBUCO
CENTRO DE CIÊNCIAS EXATAS E DA NATUREZA
PROGRAMA DE PÓS-GRADUAÇÃO EM FÍSICA

MATEUS FRANCISCO BATISTA GRANHA

Scale-Free and Visibility Effects on Social and Economic Modeling

Recife

2025

MATEUS FRANCISCO BATISTA GRANHA

Scale-Free and Visibility Effects on Social and Economic Modeling

Dissertação apresentada ao Programa de Pós-Graduação em Física da Universidade Federal de Pernambuco, como requisito parcial para a obtenção do título de Mestre em Física.

Área de Concentração: Física Teórica e Computacional

Orientador (a): André Luis da Mota Vilela

Coorientador (a): Paulo Roberto de Araújo Campos

Recife

2025

.Catalogação de Publicação na Fonte. UFPE - Biblioteca Central

Granha, Mateus Francisco Batista.
Scale-Free and Visibility Effects on Social and Economic Modeling / Mateus Francisco Batista Granha. - Recife, 2025.
124f.: il.

Dissertação (Mestrado) - Universidade Federal de Pernambuco, Centro de Ciências Exatas e da Natureza, Programa de Pós-Graduação em Física, 2025.
Orientação: André Luis da Mota Vilela.
Coorientação: Paulo Roberto de Araújo Campos.
Inclui referências e apêndice.

1. Sociophysics; 2. Econophysics; 3. Monte Carlo simulation; 4. Phase transitions; 5. Complex networks. I. Vilela, André Luis da Mota. II. Campos, Paulo Roberto de Araújo. III. Título.

UFPE-Biblioteca Central

MATEUS FRANCISCO BATISTA GRANHA

SCALE-FREE AND VISIBILITY EFFECTS ON SOCIAL AND ECONOMIC MODELING

Dissertação apresentada ao Programa de Pós-Graduação em Física da Universidade Federal de Pernambuco como requisito parcial para a obtenção do título de Mestre em Física.

Área de Concentração: Física Teórica e Computacional

Aprovado em: 26/02/2025.

BANCA EXAMINADORA

_____

Prof. Dr. André Luis da Mota Vilela (Orientador)
Universidade de Pernambuco - UPE

_____

Prof. Dr. Luis Felipe Cavalcanti Pereira (Examinador Interno)
Universidade Federal de Pernambuco - UFPE

_____

Prof. Dr. José Fernando Fontanari (Examinador Externo)
Universidade de São Paulo - USP

To my family. For their unwavering support, encouragement, and belief in me. Your love and guidance have been my foundations throughout this journey.

ACKNOWLEDGEMENTS

I would like to express my deepest gratitude to those who have helped me build the academic and personal skills to become the scientist I am.

To my family, for their endless encouragement, love, and understanding. Your support has been the bedrock upon which I have built my professional growth. To my father, Marco, and mother, Andrea, for being my examples in life and for their long-lasting support in my academic path. To my sister, Mayara, for so many years of companionship. To my godmother, Valéria, and grandmother, Iraciny, for their attentive ears and necessary advice. I love you all dearly.

To my friends, thank you for standing by me during both the challenging and joyful moments. Your companionship has made this journey more meaningful. In particular, to my lab partners Giuliano Porciúncula and Igor Oliveira for the shared knowledge and laughs. This journey would not be possible without you.

To the faculty of the Materials Physics undergraduate program at Universidade de Pernambuco for shaping my academic and research skills. In particular, I thank Prof. André Vilela, Prof. Emerson Lima, Prof. Gilvânia Vilela, and Prof. Marcone Sena for the countless discussions and advice. You helped me understand the world through the lens of physics and the language of mathematics.

To the Department of Physics at Universidade Federal de Pernambuco for enabling me to enhance my academic skills. Through Prof. Ernesto Raposo, Prof. João Carlos and Prof. Paulo Campos, I extend my thanks to the entire faculty and staff for their commitment to advancing science in Brazil.

I owe special thanks to my advisors, Dr. André Luis da Mota Vilela and Dr. Paulo Roberto de Araújo Campos, for your mentorship, patience, and invaluable guidance. Your insights have inspired me to push the boundaries of my knowledge and capabilities.

To the *Conselho Nacional de Desenvolvimento Científico e Tecnológico* (CNPq) for the financial support.

Do not go gentle into that good night,
Old age should burn and rave at close of day;
Rage, rage against the dying of the light.

Though wise men at their end know dark is right,
Because their words had forked no lightning they
Do not go gentle into that good night.

Good men, the last wave by, crying how bright
Their frail deeds might have danced in a green bay,
Rage, rage against the dying of the light.

Wild men who caught and sang the sun in flight,
And learn, too late, they grieved it on its way,
Do not go gentle into that good night.

Grave men, near death, who see with blinding sight
Blind eyes could blaze like meteors and be gay,
Rage, rage against the dying of the light.

And you, my father, there on the sad height,
Curse, bless, me now with your fierce tears, I pray.
Do not go gentle into that good night.
Rage, rage against the dying of the light.

—Dylan Thomas, *Do Not Go Gentle into That Good Night*

RESUMO

Este estudo investiga a influência de redes livres de escala do tipo Barabási-Albert na dinâmica social, destacando seu papel na evolução do consenso e na formação de preços. Na primeira parte, estendemos o modelo de voto da maioria de dois estados ao incorporar um parâmetro de visibilidade V, que representa a probabilidade de um indivíduo considerar a opinião de um vizinho com uma posição divergente em um debate social. Essa modificação captura a influência assimétrica entre concordância e discordância, impulsionada por algoritmos na chamada *economia do clique*, na qual os usuários são expostos predominantemente a conteúdos alinhados às suas crenças pessoais. Simulações Monte Carlo revelam que o parâmetro crítico de ruído q_c aumenta com V, exibindo um exuberante diagrama de fases caracterizado por transições de fase de primeira e segunda ordem, dependendo do valor de V e do parâmetro de crescimento da rede z. Na segunda parte, analisamos um modelo de dinâmica de opinião de três estados para investigar a formação de preços em mercados financeiros. Nosso modelo inclui dois tipos de agentes financeiros em relação às suas estratégias de mercado: *investidores de ruído* e *fundamentalistas*, cujas opções financeiras evoluem sob influências locais ou globais, respectivamente. Simulações numéricas mostram que o modelo reproduz os principais fatos estilizados de mercados financeiros, como distribuições de retornos com caudas longas, volatilidade *clusterizada* e memória de longo prazo na volatilidade. O aumento na fração de agentes fundamentalistas reflete uma redução progressiva das caudas nas distribuições de retorno, à medida que transicionam de um regime leptocúrtico para um mesocúrtico. Nossos resultados destacam o impacto crucial das redes livres de escala em promover comportamentos emergentes em sistemas socioeconômicos, oferecendo uma estrutura abrangente para a investigação de sistemas complexos.

Palavras-chaves: Sociofísica. Econofísica. Simulações Monte Carlo. Transições de fase. Redes complexas.

ABSTRACT

This study investigates the influence of Barabási-Albert scale-free networks in shaping social dynamics, highlighting their role in driving two key phenomena: consensus evolution and price formation. In the first part, we extend the two-state majority-vote model by incorporating a visibility parameter V, which models a chance that an individual considers the opinion of a neighbor holding a differing stance in some social debate. This modification captures the asymmetric influence of agreement and dissent driven by algorithms in the so-called *click economy*, in which users are presented with content that agrees with their personal beliefs. Monte Carlo simulations reveal that the critical noise parameter q_c increases with V, exhibiting an exuberant phase diagram characterized by both first-order and second-order phase transitions depending on the value of V and the network growth parameter z. In the second part, we analyze a three-state opinion dynamics model to investigate price formation in financial markets. Our model comprises two types of financial agents regarding their market strategies: *noise traders* and *fundamentalists*, whose financial options evolve via local or global influences, respectively. Numerical simulations show that the model reproduces key stylized facts of financial markets, including heavy-tailed return distributions, volatility clustering, and long-term memory of the volatility. An increase in the fraction of fundamentalist agents reflects a progressive loss of tails in the return distributions as they transition from a leptokurtic to a mesokurtic regime. Our results underscore the crucial impact of scale-free networks in driving emergent behaviors in socioeconomic modeling, providing an extensive framework for complex systems investigation.

Keywords: Sociophysics. Econophysics. Monte Carlo simulation. Phase transitions. Complex networks.

LIST OF FIGURES

CONTENTS

1 INTRODUCTION TO COMPLEX SYSTEMS

"[...] complexity is not about what happens in laboratories. It is about what happens all around us. Our job as scientists is to illuminate for everyone the truths that we discover."

Giorgio Parisi

1.1 FUNDAMENTAL PROPERTIES OF COMPLEX SYSTEMS

How can one define *complexity*? Or, more specifically, what are the elements that compose a *complex system*? The most natural definition would be that such systems are simply challenging to define, model, and investigate. And by all means, this is not a false statement. Nevertheless, a slightly more formal description would state that complex systems comprise interdisciplinary areas of research in which their central topic of study is by definition entwined (MITCHELL, 2009). This intricacy is what drives such systems to be difficult to analyze and draw tangible conclusions from, hence the name.

Several features encompass the behavior of complex systems and thus may help us identify when we are dealing with one. Below, we identify some of these features:

- **Emergence**: interactions among individual components often lead to complex, large-scale behavior, which may not be directly predicted from the microscopic examination of individual parts. Essential observations of such property are found in opinion models, for example, where local connections between individuals are modeled to display rich social phenomena such as consensus formation, polarization and decision-making processes (SOOD; REDNER, 2005; DEFFUANT et al., 2000; SZNAJD-WERON; SZNAJD, 2000; STAUFFER; SOUSA; OLIVEIRA, 2000; OLIVEIRA, 1992).

- **Non-linearity**: the relationship between local interactions and the overall outcome in the system is not directly proportional. In this context, small changes in one part of the system may lead to largely unpredictable effects at the global level. In real-world scenarios, such as financial markets, for example, the strategy adopted by some agents to "follow the crowd," referred to as herding behavior, often leads to crucial consequences such as expectation bubbles formation and stock market crashes (LUX; MARCHESI, 1999; CONT; BOUCHAUD, 2000; BORNHOLDT, 2001)

- **Self-organization**: spontaneous emergence of structured patterns (order) arising from local interactions without the need for external driving forces. It is a central feature that may aid scientists in unveiling more resilient systems as they adapt and create order out of chaotic interactions. This feature has been largely investigated in biological physics models, highlighting its foundational role in shaping modern evolutionary theory (KAUFFMAN, 1993).

- **Feedback loops**: mechanism in which the outputs of a system directly influence its inputs, creating a cyclical feeding relationship. Such loops can either be positive, in which the observed behavior is strengthened or amplified, or negative, where fluctuations get stabilized. Positive feedback loops, for instance, are often related to self-organizing behaviors, where individual system components create localized feeding mechanisms that may rapidly grow into a collectively organized pattern. An interesting example of this feature is the artificial fabrication of local consensus bubbles, often observed in the algorithms of social networking platforms (VILELA et al., 2021).

Despite their inherent complexity, complex systems have been majorly investigated in recent years. It currently expands a wide range of research topics, from climate analysis (FELDHOFF et al., 2015) to applications in neuroscience and brain networks (REIJNEVELD et al., 2007). This recent effervescence in complex system analysis has fostered the development of independent research fields that substantiate the study of complex phenomena such as *network science*, largely investigated by Barabási (2016). In this context, the individual parts that compose a given system (individuals, websites, molecules, neurons, etc.) are represented as nodes, and their interactions (social relations, hyperlinks, biochemical bonds, synapsis, etc.) are described as links.

A curious finding within network science is the remarkable similarity in network properties and structures exhibited by real-world systems across diverse domains. For instance, studies of brain neural networks have identified two fundamental features that facilitate synaptic processes: the *small-world effect*, which ensures efficient communication across the network, and hubs, neurons with an exceptionally high number of connections that are fundamental in information integration and processing (BASSETT; BULLMORE, 2006; YAO et al., 2015). Interestingly, these features are also present in human social networks, metabolic networks, citation networks, and the World Wide Web, among others (BARABÁSI; ALBERT, 2002; ALBERT, 2005). The underlying idea is that, despite the differences in the nature of these systems, they often

share universal topological traits. This apparent universality highlights the impact of network structures on the macroscopic behavior of complex systems, in which network science stands out as a framework to explore their diverse manifestations.

1.2 SOCIOPHYSICS AND ECONOPHYSICS

Within complex systems, two phenomena are particularly relevant to this work: consensus formation in social debates and price formation in financial markets. In both cases, their dynamics are driven by thousands, if not millions, of individuals constantly interacting in order to decide which stance they should take in a political election or if they should buy or sell stocks of a given company. Furthermore, as previously mentioned, the topological structure of these socioeconomic connections between individuals, which may arise from personal or professional relationships, fundamentally impacts the behavior of macroscopic observables.

To properly address these phenomena, one must consider how to effectively model the underlying mechanisms that drive the collective behavior of millions of individuals. This brings us to an essential consideration: *what role do physics tools play in simulating socioeconomic-based problems?* The connection of these apparently unrelated fields is made via statistical mechanics, a branch of physics that investigates the dynamics of physical systems by analyzing the macroscopic behavior of their physical quantities rather than their individual components. This realization fostered the development of the interdisciplinary fields of sociophysics and econophysics, which use statistical mechanics, network science and nonlinear dynamics techniques to investigate collective human behavior and emergent phenomena in social and economic systems (GALAM, 2012; MANTEGNA; STANLEY, 2000).

The use of statistical tools to investigate social phenomena dates back to the late 18th century when the French astronomer Pierre-Simon Laplace studied the reasons that led to near-equal numbers of male and female births in Paris. He theorized that the birth process could be understood as a random process with equal probabilities rather than being shaped by divine intervention (BALL, 2002).

Later, in the early 19th century, the statistical view of human behavior began to take shape, particularly within the scientific community. During this period, the French philosopher Auguste Comte introduced the term "social physics," envisioning it as a field that could complement the scientific description of the world that classical mechanics could not capture. Building on this statement, the Belgian astronomer Adolphe Quetelet made pioneering contributions

that set the foundations for the quantitative study of social phenomena (BALL, 2002). His work focused on understanding statistical patterns in areas such as crime rates and mortality, introducing the concept of the "average man" (*l'homme moyen*) as a central figure in his analysis. In particular, in 1832, he wrote the following:

> It seems to me that whatever concerns the human species, considered *en masse*, belongs to the domain of physical facts; the greater the number of individuals, the more the individual will is submerged beneath the series of general facts which depend on the general causes according to which society exists and is conserved (QUETELET, 1832, p. 80).

The overarching idea of his statement is that there seems to be a *sociophysical* law that compels individuals to adopt reasonable collective behaviors, especially within large societies.

Ideas such as the ones proposed by Comte and Quetelet, along with the later development of computational tools, were responsible for the later effervescence of research within sociophysics. In particular, in 1982, Serge Galam, Yuval Gefen and Yonathan Shapir published for the first time a scientific work that linked strikes in industrial plants or factories with phase transitions in Ising-like systems (GALAM; GEFEN; SHAPIR, 1982). They investigated the stable state agents assumed, working or striking, by considering a competing effect between an external field, representing the individuals' effective salary, and nearest neighbor interactions. Furthermore, their work contained a call to the development of sociophysics, therefore being regarded as the founding paper of sociophysics, despite not being the first contribution in the field.

Since then, sociophysics has progressively become an essential field within statistical physics research, with several models being proposed to investigate social phenomena. For instance, Serge Galam introduced a variety of models to study problems such as minority opinion spreading in public debates (GALAM, 2002) and the effects of hierarchical voting in societies (GALAM, 1986; GALAM, 1990; GALAM, 1999; GALAM, 2000). Alternative approaches, such as the Sznajd model (SZNAJD-WERON; SZNAJD, 2000; STAUFFER; SOUSA; OLIVEIRA, 2000), attempt to model the effects of the outward flow of opinions in social discussions—an individual's opinion spreads out to their neighbors—in contrast to the voter model in which opinion flows inward (SOOD; REDNER, 2005; CASTELLANO; MUÑOZ; PASTOR-SATORRAS, 2009). Moreover, other implementations investigate how individuals with distinct opinions may interact in order to find common ground between their beliefs, a framework known as the Deffuant model (DEFFUANT et al., 2000).

Within the context of opinion dynamics, one model that is particularly relevant for the purpose of this work is the majority-vote model with noise proposed by Mário de Oliveira (OLIVEIRA, 1992). In his seminal work, he introduces a framework to explore the effects of social inertia—an intrinsic tendency of individuals to resist changing their beliefs. This resistance is quantified via a social anxiety parameter, which represents the probability that an individual acts in non-conformity with the majority opinion of their acquaintances. Using numerical simulations, Oliveira investigates how the average social order, or consensus, is influenced by this parameter, demonstrating that beyond some critical threshold, the system transitions into a polarized state. The majority-vote model has since become a cornerstone in the study of opinion dynamics and has been extensively explored in recent literature, where researchers have introduced modifications to the topological structure of the social connections (CAMPOS; OLIVEIRA; MOREIRA, 2003; PEREIRA; MOREIRA, 2005; LIMA, 2007; LIMA; SOUSA; SUMUOR, 2008) and to the dynamics of the model (VILELA; MOREIRA, 2009; VILELA; MOREIRA; SOUZA, 2012; VIEIRA; CROKIDAKIS, 2016; VILELA; STANLEY, 2018; VILELA et al., 2021; OLIVEIRA et al., 2024).

The growing interest in investigating complex social phenomena has not only advanced the field of sociophysics but has also catalyzed progress in related research areas. Among these, econophysics stands out as a particularly relevant application of insights from studies on human collective behavior, as financial markets are fundamentally composed of interacting individuals. Recent research in econophysics leverages statistical physics tools, mathematical modeling and computer simulations to reveal the fundamental mechanisms that shape price formation in modern financial markets. For the purpose of this work, we shall focus exclusively on agent-based modeling of economic systems for the impact of financial agents in shaping macroscopic market phenomena (CHAKRABORTI et al., 2011).

Some of the opinion models previously discussed were later extended to econophysics applications, investigating phenomena such as price evolution and the formation of market bubbles and crashes. In particular, Serge Galam adapted his local majority model to investigate the mechanisms behind market fluctuations, also exploring the effects of the presence of contrarians—agents who never adopt the local majority opinion (GALAM, 2013; GALAM, 2016). Similarly, the Sznajd model of outward opinion spreading was modified to analyze the process of price formation, offering a simple yet powerful framework for understanding how local interactions between financial agents shape global market trends (SZNAJD-WERON; WERON, 2002).

Yet, this work shall focus exclusively on the extension of the majority-vote model for

financial markets, which we shall refer to as the global-vote model, proposed by Vilela et al. (2019). In their work, the authors consider a heterogeneous composition of the market comprising two distinct market strategies: *noise traders* and *fundamentalists*. The former acts according to the regular majority-vote prescription, following the option of the majority of their friends, while the latter acts based on the market index. By relating changes in the average order parameter of the system with the returns of a financial asset, the authors are able to reproduce key stylized facts of financial markets, such as fat-tailed distribution of returns and volatility clustering. This framework has been investigated in its two-state (VILELA et al., 2019; GRANHA et al., 2022) and three-state (ZUBILLAGA et al., 2022b) configurations, differing by the number of financial options that the agents may adopt.

1.3 PROBLEM STATEMENT

Building on recent advances in sociophysics and econophysics, we propose an extension of the majority-vote framework to explore the effects of scale-free networks and biased visibility algorithms on social order and price formation. The body of this work is structured into two primary sections, each addressing distinct aspects of these phenomena.

In the first section, we define an opinion dynamics model that incorporates social network algorithms designed to reinforce converging opinions. Similar to the standard majority-vote model (OLIVEIRA, 1992; OLIVEIRA; MENDES; SANTOS, 1993), individuals assume one of two possible stances on some political issue, adopting the majority opinion of their acquaintances with a probability influenced by the social anxiety parameter q.

In this work, we shall extend this framework to explore the effects of biased visibility algorithms often present in modern social media platforms. In such a context, individuals tend to be disproportionately exposed to opinions that align with their current stance, while exposure to opposing views is limited. This approach simulates social media environments, where algorithms often amplify echo chambers and foster polarization. Our model implements a biased visibility parameter V, which measures the chance that an individual may access diverging opinions of his nearest acquaintances.

In the second section, we focus on expanding the three-state global-vote model for financial markets to encompass complex socioeconomic interaction network topologies. Our model comprises two types of economic strategies for their impact on price formation: *noise traders* and *fundamentalists*. We introduce a set of local update rules that drive noise traders' behavior

and global update rules that describe fundamentalist strategies based on the three-state Potts model (WU, 1982; BRUNSTEIN; TOMÉ, 1999; TOMÉ; PETRI, 2002).

This work builds upon recent investigations of the global-vote model framework by considering the effects of complex network topologies (GRANHA et al., 2022) on its three-state variant (ZUBILLAGA et al., 2022b). More specifically, we aim to shed light on the possible impacts of implementing complex networks with different average connectivities and how such topological structures influence the financial observables of our model. In this framework, we relate the time variations of the order parameter of the system with the logarithmic returns of real-world financial markets (BORNHOLDT, 2001; KAIZOJI; BORNHOLDT; FUJIWARA, 2002; TAKAISHI, 2005; CONT, 2007). As a result, we are able to explore crucial features of real-world financial time series via a fairly straightforward approach.

In both cases, individuals shall be represented as nodes in a Barabási-Albert network (BARABÁSI; ALBERT; JEONG, 2000), with links symbolizing socioeconomic interactions between them. The choice to use Barabási-Albert networks in our simulations stems from their ability to replicate key properties of real-world networks. These include the small-world effect, where distances between social media users are much smaller than their geographic separation, and the presence of hubs, which are highly influential individuals characterized by a disproportional number of connections.

1.4 ORGANIZATION OF THIS WORK

This work is organized as follows. Chapter 2 introduces the fundamental properties and basic vocabulary of network science. It shall present the concepts of graphs and complex network structures and their particular relevance to this work. Lastly, it introduces three critical models for the construction of distinct complex network topologies and their main properties.

Chapter 3 presents the theoretical background of stochastic processes and the Monte Carlo method. We shall discuss the mathematical description of Markovian processes, including the master equation. Finally, we discuss the theoretical basis of Monte Carlo sampling and its relation to time averages of thermodynamic quantities.

Chapter 4 presents and discusses the existing literature on opinion formation models for simulating social and economic systems. In particular, we define the majority-vote model, both in its two-state and three-state formulations, as well as the three-state global-vote model, an extension of the majority-vote framework for the investigation of price formation in stock

markets. Furthermore, we introduce a social opinion formation model that investigates filter bubble and echo chamber effects on consensus break. We shall also present a set of mathematical and statistical tools for analyzing critical systems, known as finite-size scaling, and obtain the unitary relation for critical exponents.

Chapter 5 and 6 present the numerical results of the Monte Carlo simulation of the models proposed in this work: a two-state majority-vote model that investigates the effects of artificial consensus bubbles on social order; and a three-state global-vote model for financial markets. In both cases, we consider the impacts of Barabási-Albert networks, a fundamental topology in investigating real-world complex systems.

In chapter 7, we present our concluding remarks, discussing the key conclusion of this work, as well as possible directions for future research on socioeconomic simulations.

2 NETWORK SCIENCE AND COMPLEX TOPOLOGIES

"The real world is controlled not by laws, but by networks."
Albert-László Barabási

2.1 A NETWORKED WORLD

As physicists, we are captivated by the possibility of solving what may at first glance seem unsolvable—of finding order in chaos and simplicity in complexity. This innate restlessness is what drove humankind, through the minds of brilliant scientists, to remarkable findings in diverse fields. Researchers often adopt a reductionist approach when dealing with such complex problems, breaking down the phenomena into simpler, treatable steps. Analyzing these manageable components enables them to gain insights into the mechanisms at play in the original problem, thus proving a valuable strategy for investigating complex phenomena.

Take, for instance, the study of the human brain. Billions of neurons form this highly complex structure, and their connections form what we understand as *cognition*. We expect that if an individual is affected by a neurological pathology, these connections should be altered somehow, negatively impacting their standard cognition. Thus, investigating and understanding the standard structure of the brain's neuronal connections could provide a non-invasive method to diagnose possible neurological conditions at an early stage. There are entire teams of neuroscientists devoted to defining this standard pattern of neuronal connections, a structure referred to as the *connectocome* (SPORNS; TONONI; KÖTTER, 2005).

Another interesting example lies in the study of the dynamic process involved in collective decision-making in political elections. Humans are complex beings that tend to interact with other individuals, family, friends, or even social influencers in order to form their opinions on a given social topic. Investigating how these influence webs are shaped can thus provide key insights into how opinions are formed and evolve. Ultimately, the study of opinion formation in modern societies can be a powerful tool in analyzing political election outcomes, providing a way to understand how consensus is reached or how polarization emerges in modern societies (WATTS; DODDS, 2007).

Finally, consider the behavior of financial assets in stock markets over time. We expect stock prices to fluctuate due to several factors, from individual strategies of investors to the arrival

of external news that impacts the market's public image. Predicting such fluctuations could provide one with the unique ability to navigate market price dynamics, hence the popularity of market prediction models (KIMOTO et al., 1990; GANDHMAL; KUMAR, 2019; JIANG, 2021). Yet, a simplified approach could suppose that the structure of socioeconomic interactions among market traders plays a fundamental role in shaping the global market behavior for the impact of collective buy-and-sell movements performed by financial agents.

The striking detail across these examples is observing the common thread they share, at least in a reductionist approach: the relationships among the components of these systems exert a deep influence on the outcomes observed. The substrate on which these dynamic processes unfold is known as a *network*, where the individual parts are denoted as *nodes* and their interactions as *links*. These are the basis of *network science*, an interdisciplinary field that investigates the mechanisms that shape the dynamics of complex systems via their underlying topological structure.

Network science, therefore, forms a crucial pillar of our work. In this chapter, we will explore the properties of networks that are relevant to our study, as well as discuss three essential models for the assembly of complex networks: Erdös-Rényi random graphs, Watts-Strogatz small-world networks, and Barabási-Albert scale-free networks.

2.2 BASIC DEFINITIONS AND KEY PROPERTIES

From a mathematical perspective, a network, or graph, comprises a set of elements called nodes (or vertices) and connections between them, known as links (or edges). These links represent various relationships, such as physical, social, political, or economic, between the network elements. Two connected nodes are usually referred to as *neighboring nodes*. Graphically, networks are typically depicted as dots representing the nodes and lines connecting them, symbolizing the links.

Let us now delve into a set of basic definitions that will compose the fundamental vocabulary for the study and comprehension of networks.

2.2.1 Connection Structure

Initially, networks can be divided into two groups regarding their links' structure: *directed* or *undirected*. A network is directed when there is an asymmetry in its connection structure,

i.e., a connection between node i and node j does not imply that there exists a connection between node j and node i. Such connections are usually graphically depicted as arrows and are referred to as *arcs*. On the other hand, a network is undirected if its connections do not obey a specific orientation. In this case, the network's connections are symmetric (if node i is connected to node j, node j is also connected to node i), and links are simply represented as lines connecting neighboring nodes.

Within the topic of the network's connections, another fundamental definition in network theory is that of *degree of connectivity* or, in simpler terms, *degree*. The degree k_i of node i measures the number of connections, or neighbors, it has. Note that we must extend this concept when regarding directed networks since, in this case, nodes have outward and inward connections. Hence, for directed networks, we introduce the idea of *in-degree* k^{in} (*out-degree* k^{out}), which relates to the number of connections of a given node that points towards (away from) it.

Still regarding the connectivity of the network, note that we may have two extreme cases:

1. *Disconnected regime*, in which there are no connections between any two nodes of the network. In this case, we say that each node of the network represents an independent *component* since there are no available paths from one element to another;

2. *Fully connected regime*, where each node i of the network is connected to all other nodes. In this way, every node in the network is accessible via any other node and the system is said to belong to a single component.

Typically, we find ourselves in some connectivity regime between these two extremes, in which there is a non-zero amount of links in the network and a comparatively small number of network components. Furthermore, note that once again, for directed networks, we must define an *in-component* (*out-component*) as the set of nodes that can reach (can be reached by) the node in question.

One particularly relevant way to mathematically store the topological features of networks is via the so-called *adjacency matrix*. For a network of size N, its adjacency matrix is defined as a $N \times N$ matrix in which its elements A_{ij} contain the information about the connection structure of the network: if there is a connection between nodes i and j, $A_{ij} = 1$, otherwise $A_{ij} = 0$. Furthermore, we remark that there is a unique correspondence between a network's

connection structure and its adjacency matrix, i.e., such a matrix can only represent one network.

Note that we may use the information contained in the adjacency matrix in order to identify the degree of the nodes in the network. For undirected networks, given its symmetry, the degree of a node i is identified as the sum of the elements in the row or column that contains it. Mathematically we have

$$k_i = \sum_{j=1}^{N} A_{ij} = \sum_{j=1}^{N} A_{ji}. \tag{2.1}$$

We can use this information to define the average connectivity of the network as

$$\langle k \rangle = \frac{1}{N} \sum_{i=1}^{N} k_i. \tag{2.2}$$

Conversely, as previously mentioned, we must differentiate the inward and outward connections for directed networks. Hence, for these networks, we have

$$k_i^{in} = \sum_{j=1}^{N} A_{ji}, \quad \text{and} \quad k_i^{out} = \sum_{j=1}^{N} A_{ij}, \tag{2.3}$$

where the total degree of connections is $k_i^{in} + k_i^{out} = k_i$. Additionally, their corresponding average degrees are expressed as

$$\langle k^{in} \rangle = \frac{1}{N} \sum_{i=1}^{N} k_i^{in}, \quad \text{and} \quad \langle k^{out} \rangle = \frac{1}{N} \sum_{i=1}^{N} k_i^{out}. \tag{2.4}$$

For the purpose of this work, we shall focus exclusively on undirected networks. In this case, the concept of inward and outward degrees becomes redundant, as all connections are symmetric. Consequently, each node i has a single degree k_i.

2.2.2 Degree Distributions

Naturally, we do not expect all nodes to have the same degrees in most real-world networks. In fact, in social networks, for example, we observe the presence of *hubs*—highly connected individuals—who tend to play a fundamental role in modern societal debates. In this way, we can define a *degree distribution* $P(k)$, which measures the dispersion of the degrees of the nodes within the network. As expected, since $P(k)$ represents a distribution of probabilities, it must obey the normalization condition

$$\sum_{k=0}^{\infty} P(k) = 1 = \sum_{k=k_{min}}^{k_{max}} P(k), \tag{2.5}$$

where k_{min} (k_{max}) represents the lowest (largest) number of connections of a node in the network. In other words, $P(k < k_{min}) = 0$ and $P(k > k_{max}) = 0$.

The degree distribution of a network plays a fundamental role in shaping many of its properties and associated phenomena. For instance, we may identify the network's average connectivity as

$$\langle k \rangle = \sum_{k=0}^{\infty} kP(k). \tag{2.6}$$

2.2.3 Average Path Length

Take a pair of nodes (i, j) in the network. The *path length* between the pair is defined as the number of edges required in the trajectory from node i to node j. In particular, we are often interested in the shortest path between each pair of nodes, a characteristic known as *geodesic distance* d_{ij}. Note that this definition does not require uniqueness (there may be more than one distinct geodesic path between a pair of nodes). Moreover, the length of the longest geodesic path in the network is referred to as the network's *diameter* d_{max}.

In particular, for undirected networks, we may define the average path length $\langle d \rangle$, which provides an overall measure of how effectively "small" the network is—a feature known as the *small-world effect*. Thus, the mean geodesic distance is defined as

$$\langle d \rangle = \frac{1}{N(N-1)} \sum_{i \neq j} d_{ij}. \tag{2.7}$$

Networks that exhibit the small-world property are characterized by relatively shorter average path lengths than their network size N. This phenomenon alludes to the renowned experiment conducted by the social psychologist Stanley Milgram, known as the six degrees of separation (MILGRAM, 1967). In this experiment, individual A was tasked with delivering a letter to individual B, and the delivery process could only be accomplished through manual transmission from person to person (TRAVERS; MILGRAM, 1977). Results showed that the average number of required individuals for the letter to reach its final recipient was close to six, which is small compared to the size of the population of the United States—where the experiment took place—hence the name of the effect.

2.2.4 Cliques and Clustering

Imagine we are investigating a network structure where each node represents a student in a given university, and links relate to their social relations. In real-world scenarios, individuals often have a high probability of interacting with the friends of their friends, forming social interaction triangles—a feature known as *cliques*. Formally, cliques are defined as a set of nodes in a network in which, for every pair in that set, there is a connection between them, such as a group of friends in which every individual interacts with the others.

As social beings, humans tend to organize themselves in groups, inducing the formation of cliques. This characteristic is commonly referred to as *clustering*, and we may quantify its impact via the *clustering coefficient* C (STROGATZ, 2001; NEWMAN, 2003; BARABÁSI, 2016). We define the local clustering coefficient of node i as follows:

$$C_i = \frac{2L_i}{k_i(k_i - 1)}, \tag{2.8}$$

where L_i represents the number of links between the k_i neighbors of site i. In practical terms, Eq. (2.8) equates the fraction of connections that actually exist between the neighbors of site i over the total number of possible links between those nodes $\frac{1}{2}k_i(k_i - 1)$. Furthermore, the network's clustering coefficient C is defined as the average of the local clustering coefficient C_i over all nodes, thus

$$C = \frac{1}{N}\sum_{i=1}^{N} C_i. \tag{2.9}$$

2.2.5 From Regular to Complex Networks

The properties discussed thus far form the fundamental theoretical apparatus for characterizing network structures. The investigation of real-world systems, such as the topology of the connections within the World Wide Web, the organization of power grid networks, or the structure of social relationships in social networking apps, have highlighted key features that regular networks failed to capture. This context spurred the development of complex networks, which aim to address some of the limitations displayed by regular structures.

In the following sections, we shall explore three of the most influential models for the assembly of complex networks: Erdös-Rényi random graphs, Watts-Strogatz small-world networks,

Figure 1 – Visual representation of three distinct complex network architectures with size $N = 16$, and average connectivity $\langle k \rangle = 4$. This visualization highlights key features of these topological structures: from the randomness of (a) random networks to the clusters and shortcuts of (b) small-world networks and hubs of (c) scale-free networks.

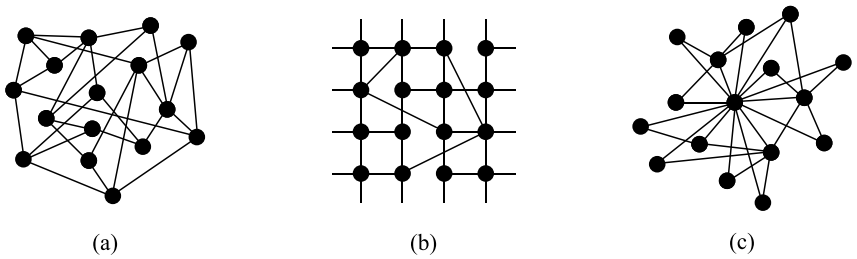

Source: The author (2025).

and Barabási-Albert scale-free networks. Each of these complex network models provides a specific set of features that attempt to reproduce the topological behavior of real-world complex systems. Random networks, for instance, provide a baseline for studying connectivity patterns through probabilistic link formation. In contrast, small-world networks simultaneously introduce a high clustering coefficient and short path lengths, a phenomenon widely observed in social and biological systems. Furthermore, scale-free networks include the presence of hubs, individuals with a higher number of connections, that tend to influence the dynamics of many natural and artificial systems.

Figure 1 provides a schematic visualization of the aforementioned properties of these three different complex networks. In the figure, we show (a) a random network, (b) a small-world network and (c) a scale-free network, each built with $N = 16$ nodes and average connectivity of $\langle k \rangle = 4$. The plot illustrates the disordered connectivity of random structures, the clusters and shortcuts that emerge in small-world networks and the hub-like structure of scale-free networks.

2.3 ERDÖS-RÉNYI RANDOM NETWORKS

Picture a scientific conference attended by N participants, none of whom know each other beforehand. After the formal sessions, the organizers host a cocktail party to encourage networking among attendees. As the evening progresses, conversations naturally begin to form, and by the end of the event, we expect that a network of connections will emerge, with nodes representing each participant and links representing social connections created at the gathering. If we lack detailed information about the exact formation of these connections,

a reasonable assumption is to consider that the connections were formed randomly between the participants. This framework is captured by the widely known *random networks* (ERDÖS; RÉNYI, 1959; ERDÖS; RÉNYI, 1960), representing an initial approach to the investigation of real-world complex systems.

In its original formulation, Paul Erdös and Alfréd Rényi define the construction of a random graph as taking a set of N isolated nodes and connecting every possible pair of nodes in the network $[N(N-1)/2]$ with chance $0 < w \leq 1$, while forbidding double connections (ERDÖS; RÉNYI, 1959). Note that in this formulation, the expected number of links present in the network depends on w and is given by

$$\langle L \rangle = \frac{wN(N-1)}{2}. \tag{2.10}$$

Furthermore, we remark that the average connectivity of the network is

$$\langle k \rangle = \frac{2\langle L \rangle}{N} = w(N-1), \tag{2.11}$$

where each link needs to be counted twice since we are dealing with undirected networks. Additionally, in the thermodynamic limit $(N \to \infty)$ we shall consider the approximation

$$\langle k \rangle = w(N-1) \approx wN. \tag{2.12}$$

In the construction process of random networks, each link has a probability w of being formed and a complementary chance $(1-w)$ of not being formed. Hence, random networks constructed via the Erdös-Rényi formulation clearly follow a binomial process, and their corresponding probability distribution are given by

$$P(k) = \binom{N-1}{k} w^k (1-w)^{N-1-k}. \tag{2.13}$$

Moreover, for large enough networks $(N >> k)$ and small values of the connection probability $(w << 1)$, while holding $wN \approx \langle k \rangle$, it can be shown that the binomial distribution tends to a Poisson distribution, given by

$$P(k) \approx e^{\langle k \rangle} \frac{\langle k \rangle^k}{k!}. \tag{2.14}$$

In Figure 2(a) to (d), we present an illustration of the connection process of random networks constructed using the Erdös-Rényi formulation with $N = 10$ and $L = 15$ links for an

Figure 2 – Representation of the Erdös-Rényi process for the assembly of random networks. From (a) to (d), consider a network with $N = 10$ initially isolated nodes which are connected by adding a total of $wN(N-1)/2 = 15$ random links between them. The final network has $\langle k \rangle = 3$. In (e), it is also shown the degree distribution $P(k)$ averaged over ten networks for $\langle k \rangle = 6, 8, 10$, and 20, each with $N = 2 \times 10^4$ nodes. The lines represent Poisson fits for the data.

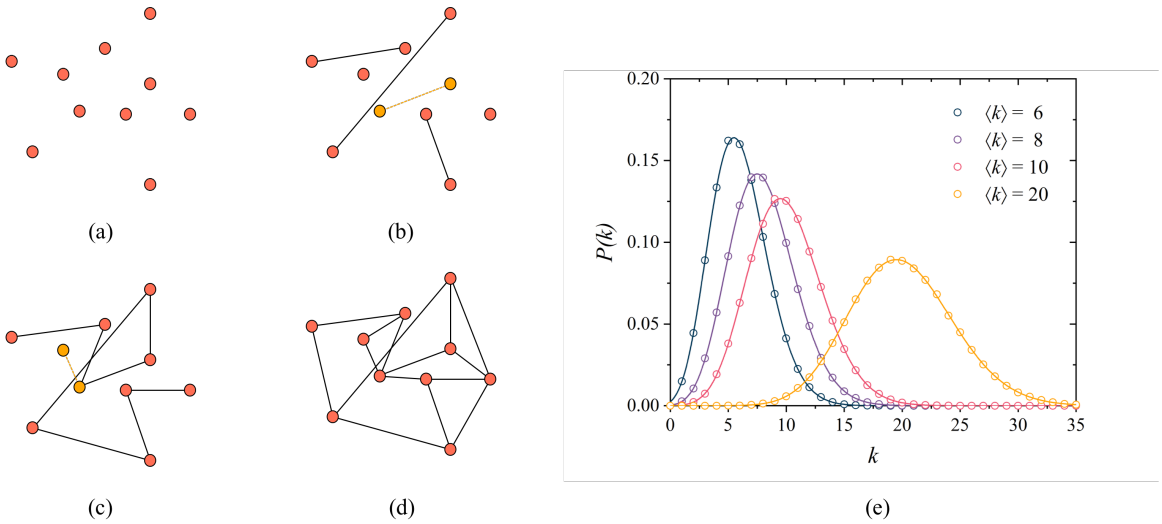

Source: Granha et al. (2022).

average connectivity $\langle k \rangle = 3$. Furthermore, Fig. 2(e) displays the degree distributions for networks built with $N = 2 \times 10^4$ nodes averaged over ten network realizations for several average connectivity values. Results show that the degree distributions closely follow the theoretical expected results for a Poisson distribution in such a limit.

As previously stated, random networks constitute an initial approach to studying complex systems, and as such, they lack certain structural properties that limit their capability to reproduce real-world network features. Since the chance of two randomly selected nodes being connected (w) is often held to small values, random graphs are characterized by a low clustering coefficient. This is a reflection of the absence of local links as a result of the random nature of the network's formation process. Still, random networks present a considerably small network diameter, indicating the presence of the small-world property. In general, while Erdös-Rényi random graphs display some aspects found in real-world networks, they fail to capture some subtleties of those systems, such as the presence of hubs or cliques.

2.4 WATTS-STROGATZ SMALL-WORLD NETWORKS

Prior to Watts and Strogatz's seminal paper (WATTS; STROGATZ, 1998), the theoretical study of complex systems involved the application of networks characterized by either com-

pletely regular or random topological structures. Yet, several real-world systems, from biological to social realms, are built on network structures that lie somewhere between these two limiting cases. Thus, the Watts-Strogatz network model proposes to interpolate between regularity and randomness by introducing a tunable parameter. Such structures are known as small-world networks, in allusion to the six degrees of separation experiment (MILGRAM, 1967).

In its original formulation, small-world networks are constructed according to the following prescription: start with a ring lattice of N nodes, where each is linked to its first K neighbors ($K/2$ neighbors on either side); each of the network's links will be rewired with probability p while forbidding that a link is rewired to the original node, self-connections and double connections (WATTS; STROGATZ, 1998). Note that when $p = 0$, we recover the standard regular lattice. Conversely, when $p = 1$, all links will be rewired, and we approach a random network regime. The probability p is often referred to as the rewiring parameter, and it tunes the degree of randomness present in the network.

The Watts and Strogatz model is remarkable for formulating networks encompassing small average path lengths $\langle d \rangle$ and high clustering coefficients C, a feature observed in many real-world networks. As they are built on a regular substrate, we still observe network cliques for intermediate values of p. Likewise, rewiring its regular links progressively introduces long-range interactions in the network, which reflect a decrease in the average path distances. Such effects are observed in Fig. 3, illustrating how small-world networks' average path length and clustering coefficient depend on the rewiring parameter. Indeed, we observe that for a particular range of values of p, Watts-Strogatz small-world networks can reproduce both features mentioned previously.

Before we rewire the network's links, the average connectivity of small-world networks is simply $\langle k \rangle = K$ (the number of links each node has in the original regular structure). Since no links are added to the network in the rewiring process, the average connectivity of the network shall be preserved, irrespective of the value of the rewiring parameter p.

Small-world networks represent a significant advancement in the investigation of real-world complex systems. They provide a clever bridge between the clustered structures of regular lattices and the small network diameter of random graphs. These features are often observed in systems such as social networking apps, where individuals tend to connect to those around them as well as people from other countries, eliminating the typical geographic constraints. Nevertheless, Watts-Strogatz small-world networks still fail to capture another crucial characteristic of social systems: the presence of highly connected and influential individuals. This is

a cornerstone of the Barabási-Albert model for the assembly of scale-free networks, presented in the following section.

Figure 3 – Plot of the average path length $L = \langle d \rangle$ and clustering coefficient C of Watts-Strogatz small-world networks as functions of the rewiring parameter p. Note that for a range of values of p, the resulting networks will present both the small-world effect and high clustering coefficients.

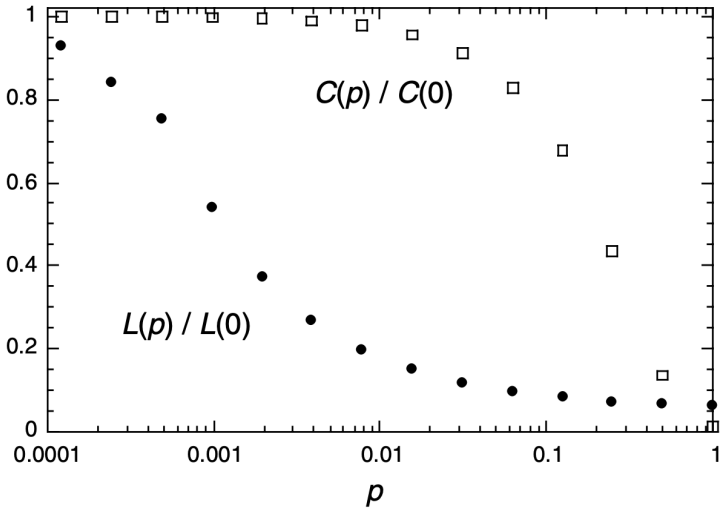

Source: Watts and Strogatz (1998).

2.5 BARABÁSI-ALBERT SCALE-FREE NETWORKS

In modern society, the presence of individuals known as *social influencers* has become increasingly prominent. Such social players tend to strongly influence trends across various fields, from lifestyle and fashion to politics and economics. A distinguishing characteristic of influencers is how they usually concentrate a large number of followers, often serving as opinion formers for their respective audiences. As previously discussed, this feature is not observed in random or small-world networks; it is actually a hallmark of a class of graphs known as scale-free networks. Mathematically, a scale-free network is a graph whose degree distribution follows a power law:

$$P(k) \sim k^{-\gamma}, \tag{2.15}$$

where γ is positive and real. Such networks are termed scale-free due to the lack of a characteristic scale in their degree distributions—the overall shape of the distributions is unchanged when altering the function's scale of observation.

A question that naturally arises at this point is: *is there a mechanism behind the emergence of the scale-free property?* And, if this is the case, *how can we define a network model so that it displays said property?* This was the central topic of the work by Barabási and Albert (2002), in which they discuss two fundamental characteristics observed in real-world networks regarding the emergence of the scale-free property:

1. **Growth**

   Most systems observed in the real world are not static—their number of nodes constantly evolves in time. The most distinguished example of this feature is the network of connections in the World Wide Web, where Web pages represent nodes and hyperlinks between pages represent edges. The World Wide Web represents the largest network ever built by humanity, and its size continues to grow daily (BARABÁSI, 2016). Random and small-world networks do not encompass this dynamic behavior observed in real-world complex networks.

2. **Preferential Attachment**

   Another curious behavior observed in systems such as social networking apps is individuals' innate tendency to connect themselves with influential players in the network. Thus, it is reasonable to assume that a mechanism is at play that reflects this "rich get richer" effect. This feature was formally termed *preferential attachment*, and it states that the probability that an existing node in the network receives new connections is proportional to its current degree (BARABÁSI; ALBERT, 2002).

Based on these two features, Barabási and Albert (2002) proposed the Barabási-Albert model for the construction of scale-free networks. The connection scheme considers an initial small set of nodes z_0 with n_0 links between them. Then, at each time step of the growth process, a new node with $z \leq z_0$ new links is added to the network, where double connections are forbidden. These connections are created via the aforementioned preferential attachment mechanism, in which the probability Π that a newly added node will link itself with node i depends linearly on the degree k_i of such node. Mathematically, we have

$$\Pi_i(k_i) = \frac{k_i}{\sum_j k_j}, \tag{2.16}$$

where the summation represents a normalization factor and runs over all nodes present in the network except the one currently being added. In this way, both the number of nodes

$N(t) = z_0 + t$ and the number of links $L(t) = n_0 + zt$ are functions of time.

For the purpose of this work, we shall consider Barabási-Albert networks constructed with a fully connected initial core of $z_0 = z + 1$ nodes. A new node with z links is added to the network at each time step. In this way, the parameter z will be the only control parameter of the model, and we shall refer to it as the growth parameter of the network.

Analytical results (BARABÁSI; ALBERT, 2002) show that, in fact, the Barabási-Albert model effectively produces a scale-free network with a power law degree distribution. In particular, scale-free networks built according to such algorithm are known to display a power law degree distribution with exponent $\gamma = 3$, irrespective of the growth parameter's value.

Furthermore, the connection process of Barabási-Albert networks, via the preferential attachment algorithm, facilitates the emergence of hubs—small number of nodes with a great number of connections. In this way, hubs play a crucial role in the effective connectedness of said network, as they essentially act as connection bridges between nodes in the system. As a result, scale-free networks built according to the Barabási-Albert algorithm display a smaller average path length than those observed in random networks.

Another critical feature displayed by Barabási-Albert networks is that they display a clustering coefficient approximately five times greater than the ones obtained in random networks. This is an interesting feat, as it shows that beyond the capability of displaying the small-world property and the emergence of hubs, these networks also show a tendency to form cliques, which are commonly present in real social networks. Results show that the clustering coefficient of Barabási-Albert networks scales with the number of nodes of the network as $C \sim N^{-0.75}$. Moreover, we remark that such networks are characterized by an average connectivity $\langle k \rangle \approx 2z$ for $N \gg 1$ (BARABÁSI; ALBERT, 2002).

Figure 4(a) displays a visual representation of a Barabási-Albert scale-free network with $N = 300$ nodes and a growth parameter $z = 5$. In this representation, the size of a node is proportional to its degree. Note that the figure shows a small number of hubs, displayed as larger circles, which are expected to be presented in such topological structures.

Moreover, Fig. 4(b) shows the degree distributions of Barabási-Albert networks with size $N = 10^4$ nodes and several values of the growth parameter z. Note that the degree distributions follow the expected behavior of scale-free networks, displaying a power law degree distribution with the expected exponent of $\gamma = 3$, as shown by the comparative dashed red line. Furthermore, note that this behavior is independent of the value of the growth parameter used.

Figure 4 – (a) Visual representation of Barabási-Albert scale-free networks with size $N = 300$ and a growth parameter $z = 5$. A node's size is proportional to its number of connections. Also displayed is (b) the degree distributions $P(k)$ for several values of $z = 4, 8, 10, 50$ and 100, and networks of size $N = 10^4$. The dashed red line corresponds to a power-law function with exponent $\gamma = 3$.

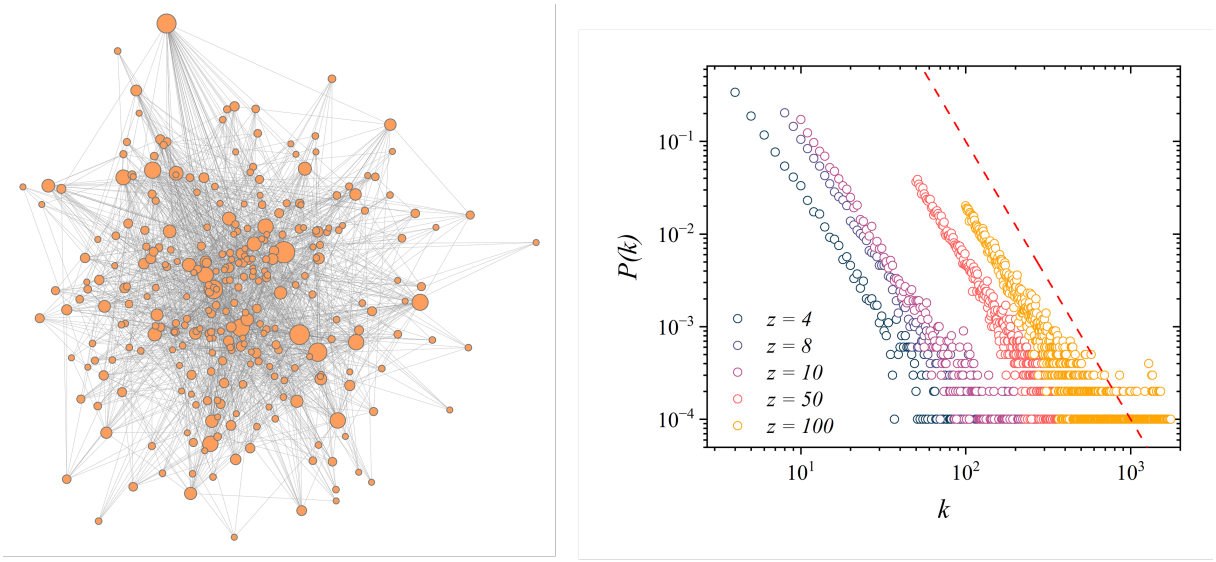

(a) (b)

Source: The author (2025).

Barabási-Albert networks provide a powerful substrate for the investigation of real-world complex systems due to their capability of displaying key features observed in modern socioeconomic networks. Its construction mechanisms are responsible for the natural emergence of hubs in the network, which play a crucial role in lowering its average path length. Hence, Barabási-Albert networks will be the primary focus of this work. We shall explore its impact on opinion dynamics and consensus formation in social systems, as well as on price formation and financial return distributions in modern economic systems.

3 STOCHASTIC PROCESSES AND MONTE CARLO SIMULATIONS

This chapter shall closely follow the discussion presented by Reichl (2016) and Tomé (2001) to introduce the formal treatment for stochastic processes. We shall obtain the master equation and introduce the foundations for Monte Carlo simulations, a widely implemented method for the simulation of random processes. Our objective is to establish the theoretical fundamentals that will be implemented in this work, in particular, the basis for Monte Carlo sampling, finite-size scaling relations and their implication in obtaining the system's critical points.

3.1 RANDOM VARIABLES

Picture a financial stock of a given company. Over time, the daily number of trades involving this stock can fluctuate significantly due to factors like market sentiment, breaking news, or strategic decisions by financial agents. While we can observe a discrete number of trades that occurred at the end of the day, the exact value remains unpredictable beforehand. This behavior exemplifies the nature of a *random variable*, a quantity whose outcome is determined by many other underlying random factors, making it impossible to predict its value. Moreover, the trading activity itself may be modeled as a *stochastic process* – a mathematical framework describing the evolution of a system through a set of time-dependent random variables.

In real-world scenarios, such mathematical representations are fundamental in modeling complex systems across diverse domains. In particular, the interdisciplinary field of sociophysics investigates how individual interactions and randomness crucially influence consensus dynamics or polarization in social subjects, where models such as the majority-vote (OLIVEIRA, 1992) play a key role. Furthermore, as mentioned previously, the price dynamics in stock markets is strongly impacted by individual strategies and external news, where stochastic models have confirmed the emergence of expectation bubbles and market crashes (LUX; MARCHESI, 1999; BORNHOLDT, 2001). Finally, crucial global events such as the COVID-19 pandemic are similarly driven by random factors such as individual interactions, transmission rates, and recovery times, where stochastic models such as the SIR framework are critical in understanding and managing global outbreaks (COOPER; MONDAL; ANTONOPOULOS, 2020).

Before delving into the mathematical details of stochastic processes, we shall first set the

foundations of random variables and some key properties, where, for simplicity, we will consider the discrete case. Let x be a random variable described by a distribution P_x, which relates each possible outcome of $x = x_i$ with a given probability $0 \leq P_{x_i} \leq 1$. Naturally, such probability distribution must obey the normalization condition, expressed as

$$\sum_i P_{x_i} = 1, \tag{3.1}$$

where the summation runs over all possible realizations of the variable $x = \{x_1, x_2, x_3, \ldots, x_n\}$.

3.2 STOCHASTIC PROCESSES

Suppose that we are investigating a system in which its state depends exclusively on a random variable x, which by itself evolves over time t. We shall consider that the variable x may adopt discrete integer values and the time t may adopt discrete non-negative integer values, for simplicity. In this framework, the evolutionary dynamics of the system is governed by a *stochastic process*, while the variable $x(t)$ is referred to as *stochastic variable*. Thus, such process at time $t = \ell$ will be described by the joint probability

$$P_\ell(x_0, x_1, x_2, \ldots, x_\ell). \tag{3.2}$$

Note that the expression describes the history preceding the present state of the system, where the variable x adopted values $x_0, x_1, \ldots, x_\ell$ at times $t = 0, t = 1, \ldots, t = \ell$ respectively. Naturally, the probability that the variable $x = x_{\ell+1}$ at time $t = \ell + 1$ is given by the conditional probability

$$P_{\ell+1}(x_{\ell+1}|x_0, x_1, x_2, \ldots, x_\ell). \tag{3.3}$$

A particular type of stochastic process is defined when such conditional probability of $x = x_{\ell+1}$ at $t = \ell+1$ depends exclusively on the previous state $x = x_\ell$ at time $t = \ell$, regardless of the previous values adopted by the stochastic variable $x_0, x_1, \ldots, x_{\ell-1}$. In this case, such process is termed a *Markovian process* in honor of the distinguished Russian mathematician Andreyevich Markov, who made significant contributions to the theory of stochastic systems. Thus, in a Markovian process, Eq. (3.3) can be simplified as

$$P_{\ell+1}(x_{\ell+1}|x_0, x_1, x_2, \ldots, x_\ell) = P_{\ell+1}(x_{\ell+1}|x_\ell). \tag{3.4}$$

In simpler terms, while Eq. (3.3) holds the entire history of the system, a Markovian process is inherently memoryless, as the future state of the system exclusively depends on its current state. Furthermore, Eq. (3.4) is known as the Markov property. In such systems, the joint probability expressed in Eq. (3.2) may be expressed as

$$P_\ell(x_0, x_1, x_2, \ldots, x_\ell) = P_\ell(x_\ell|x_{\ell-1})P_{\ell-1}(x_{\ell-1}|x_{\ell-2}) \cdots P_1(x_1|x_0)P_0(x_0). \tag{3.5}$$

The probability that the variable $x = x_\ell$ at time $t = \ell$, regardless of the values adopted previously is expressed as

$$P_\ell(x_\ell) = \sum_{x_0, x_1, \ldots, x_{\ell-1}} P_\ell(x_0, x_1, x_2, \ldots, x_\ell), \tag{3.6}$$

where the summation runs over all possible values adopted by the stochastic variable x at each time step except for the present state x_ℓ. Plugging Eq. (3.4) in the above expression, we obtain

$$P_\ell(x_\ell) = \sum_{x_{\ell-1}} P_\ell(x_\ell|x_{\ell-1})P_{\ell-1}(x_{\ell-1}), \tag{3.7}$$

in which the sum encapsulates all the possible paths linking states $x_{\ell-1}$ and x_ℓ. Note that knowledge of the initial condition of the system $P_0(x_0)$ allows us to determine future states $P_\ell(x_\ell)$ via the recursive relation above. Moreover, the conditional probability $P_\ell(x_\ell|x_{\ell-1})$ may be physically interpreted as the transition probability between subsequent states $x_{\ell-1}$ and x_ℓ. We remark that such transition probabilities are, in principle, time-dependent; nevertheless, through the course of this work, we shall only consider stationary Markovian processes. In this way, the transition probabilities may be expressed as

$$P_\ell(x_\ell|x_{\ell-1}) = T(x_\ell, x_{\ell-1}), \tag{3.8}$$

where $T(x_\ell, x_{\ell-1})$ represents the stationary transition probabilities. Thus, Eq. (3.7) may be adjusted as follows:

$$P_\ell(x_\ell) = \sum_{x_{\ell-1}} T(x_\ell, x_{\ell-1})P_{\ell-1}(x_{\ell-1}). \tag{3.9}$$

3.3 STOCHASTIC MATRIX

We may express Eq. (3.9) in simpler terms if we consider $T(n,m)$ as entries of a *stochastic matrix* $\mathbf{T}$. Thus, we write

$$P_\ell(n) = \sum_m T(n,m) P_{\ell-1}(m). \tag{3.10}$$

In a stochastic matrix, each element $T(n,m)$ relates to the transition probability from state m to state n. For all pairs (n,m), the elements of the stochastic matrix must be non-negative, $T(n,m) \geq 0$, as a consequence of their definition. Furthermore, the transition probabilities must obey the normalization condition expressed as

$$\sum_n T(n,m) = 1. \tag{3.11}$$

This is equivalent to stating that the probability that the state m transitions to any other state n is equal to unity.

In this matrix representation, let P_ℓ be understood as a column vector with components $P_\ell(n)$. Thus, Eq. (3.10) may be expressed in the matrix form as

$$P_\ell = T P_{\ell-1}. \tag{3.12}$$

As previously mentioned, with knowledge of the initial probabilities of the system P_0 and the transition probabilities, now expressed in terms of the stochastic matrix (T), we have access to the state of the system at any time $t = \ell$. In other words, we may rewrite Eq. (3.12) in terms of the initial probabilities as

$$P_\ell = T^\ell P_0. \tag{3.13}$$

Hence, we simplify the problem of determining the probability distribution of the system at time $t = \ell$ to the calculation of the $\ell-$th power of the stochastic matrix. Applying this condition to Eq. (3.10) we have, for state n:

$$P_\ell(n) = \sum_m T^\ell(n,m) P_0(m), \tag{3.14}$$

where $T^\ell(n,m)$ is the transition probability from state m to state n after ℓ time steps.

3.4 MASTER EQUATION AND EXPECTATION VALUES

Consider a Markovian stochastic process governed by a stochastic matrix $\mathbf{T}$. Suppose that the transitions between states m and n occur within a time scale τ and that the elements $T(n,m)$ of the stochastic matrix may be expressed as

$$T(m,n) = \tau W(m,n), \tag{3.15}$$

$$T(n,n) = 1 - \tau\Omega(n), \tag{3.16}$$

where Eq. (3.15) considers transitions for $n \neq m$ while Eq. (3.16) considers transitions for $n = m$.

Recall that the elements of the stochastic matrix must obey the normalization condition, which states that the sum of the transition probabilities from state n to any other state in the system must equate to unity. Thus, if we express such normalization condition in terms of Eq. (3.15) and Eq. (3.16), we have

$$1 = \sum_{n} T(m,n) = 1 - \tau\Omega(n) + \sum_{n\neq m} \tau W(m,n). \tag{3.17}$$

Simplifying the equation above, we obtain

$$\Omega(n) = \sum_{n\neq m} W(m,n), \tag{3.18}$$

independent of the time window τ. Note that $W(m,n)$ can be interpreted as the transition probability per unit time from state n to state m, whereas $\Omega(n)$ represents the transition probability per unit time from state n to any other state of the system except itself, as elucidated by the equation above.

We may interpret the probability that the system finds itself on state n at any given time $t = \ell + 1$ as the probability that the system, in the previous time $t = \ell$, does one of the following movements:

1. Being on state n and remaining on it;

2. Transitioning from any other state m to state n.

Mathematically, these conditions are expressed as follows:

$$P_{\ell+1}(n) = T(n,n)P_\ell(n) + \sum_{m\neq n} T(n,m)P_\ell(m). \tag{3.19}$$

Plugging Eq. (3.15) and Eq. (3.16) on the expression above, we find:

$$P_{\ell+1}(n) = [1 - \tau\Omega(n)]P_\ell(n) + \tau \sum_{m\neq n} W(n,m)P_\ell(m). \tag{3.20}$$

We now seek to investigate the time evolution of this quantity. Let $P(n,t) \equiv P_\ell(n)$ be defined as the probability that the system is on state n at time $t = \ell\tau$. Thus, substituting $P(n,t)$ on Eq. (3.20) and reorganizing the terms, we find:

$$\frac{P(n,t+\tau) - P(n,t)}{\tau} = \sum_{m\neq n} W(n,m)P(m,t) - \Omega(n)P(n,t) \tag{3.21}$$

If we apply the limit $\tau \to 0$, the left-hand side of the equation above becomes the time derivative of the probability $P(n,t)$. Thus, for continuous-time we have

$$\frac{d}{dt}P(n,t) = \sum_{m\neq n} W(n,m)P(m,t) - \Omega(n)P(n,t). \tag{3.22}$$

Recalling Eq. (3.18), we finally obtain

$$\frac{d}{dt}P(n,t) = \sum_{m\neq n} [W(n,m)P(m,t) - W(m,n)P(n,t)]. \tag{3.23}$$

Eq. (3.23) is known as the master equation, which describes the dynamics of Markovian stochastic processes with time-dependent transition rates $W(n,m)$. Such probabilities are elements of the *evolution matrix* of the system.

In this work, we will consider that the system is composed of N constituents, such as individuals in a voting system, each placed in the nodes of a complex network. We shall associate the state of site i with a stochastic variable that may assume one out of two values $\sigma_i = \pm 1$. In the social context, for example, state $+1$ could indicate voting for candidate A, while state -1 would suggest supporting candidate B. Collectively, the state of the system shall be defined by the $N-$tuple $\sigma = (\sigma_1, \sigma_2, \ldots, \sigma_N)$, where each combination of states relates to a *microstate* of the system. Naturally, there are 2^N accessible microstates in the system's configuration space.

If we consider σ and σ' as distinct microstate configurations, we may reorganize the master equation of the system as follows

$$\frac{d}{dt}P(\sigma,t) = \sum_{\sigma' \neq \sigma} [W(\sigma,\sigma')P(\sigma',t) - W(\sigma',\sigma)P(\sigma,t)]. \tag{3.24}$$

Note that the diagonal elements of the evolution matrix are excluded from this expression, which enables us to conveniently define them so that the condition below is satisfied:

$$\sum_{\sigma'} W(\sigma,\sigma') = 0. \tag{3.25}$$

Thus, the elements of the evolution matrix are related to the diagonal elements as

$$W(\sigma,\sigma) = -\sum_{\sigma' \neq \sigma} W(\sigma,\sigma'). \tag{3.26}$$

Plugging this expression in Eq. (3.24) allows the master equation to be expressed as

$$\frac{d}{dt}P(\sigma,t) = \sum_{\sigma'} W(\sigma,\sigma')P(\sigma',t), \tag{3.27}$$

where the sum in σ' is irrestricted and runs over all 2^N available microstates.

For the sake of simplicity, in this work, we shall only consider transitions between states that differ in only one site i. In this case, the transition rate $W(\sigma',\sigma)$ is written as

$$W(\sigma',\sigma) = \sum_i \delta(\sigma'_1,\sigma_1)\delta(\sigma'_2,\sigma_2)\ldots\delta(\sigma'_i,-\sigma_i)\ldots\delta(\sigma'_N,\sigma_N)w_i(\sigma), \tag{3.28}$$

where $\delta(i,j)$ is the Kronecker delta function and $w_i(\sigma)$ is the transition rate of the $i-$th site from state σ_i to state $-\sigma_i$. Using this notation, we may rewrite the master equation for this process as

$$\frac{d}{dt}P(\sigma,t) = \sum_{i=1}^{N}[w_i(\sigma^i)P(\sigma^i,t) - w_i(\sigma)P(\sigma,t)], \tag{3.29}$$

where σ^i represents the microstate obtained by flipping the state of the $i-$th site, from σ_i to $-\sigma_i$.

Expressing the master equation as Eq. (3.29) allows us to determine the time evolution of the expectation values of any given state function of the system $f(\sigma)$. In statistical mechanics, the expectation value of a state function is defined as

$$\langle f(\sigma)\rangle_c = \sum_{\sigma} f(\sigma)P(\sigma,t), \tag{3.30}$$

where $\langle \cdots \rangle_c$ represents configurational averages of the state function. Multiplying both sides of the master equation (3.29) by the state function $f(\sigma)$ and taking a sum over all possible system microstates σ, we obtain

$$\frac{d}{dt}\langle f(\sigma)\rangle_c = \sum_{\sigma}\sum_{i=1}^{N} f(\sigma)[w_i(\sigma^i)P(\sigma^i,t) - w_i(\sigma)P(\sigma,t)]. \tag{3.31}$$

Note that we can conveniently separate the two terms of the sum as

$$\frac{d}{dt}\langle f(\sigma)\rangle_c = \sum_{\sigma}\sum_{i=1}^{N} f(\sigma)w_i(\sigma^i)P(\sigma^i,t) - \sum_{\sigma}\sum_{i=1}^{N} f(\sigma)w_i(\sigma)P(\sigma,t). \tag{3.32}$$

Now consider the change of variables $\sigma \leftrightarrow \sigma^i$ in the first term on the right-hand side of the equation. Importantly, since the summation runs over all 2^N available microstates, the summation is invariant under this transformation. This allows us to rewrite the above equation in a much simpler fashion, as shown below:

$$\frac{d}{dt}\langle f(\sigma)\rangle_c = \sum_{i=1}^{N}\Big\langle [f(\sigma^i) - f(\sigma)]w_i(\sigma)\Big\rangle_c. \tag{3.33}$$

3.5 THEORETICAL FOUNDATIONS OF MONTE CARLO SAMPLING

The study of complex systems often involves dealing with intricate dynamics between the individual parts of the system and high-dimensional configuration spaces, rendering the analytical treatment of the system simply impractical. In this context, computational tools offer a pathway to model, simulate and analyze such systems. Within this framework, Monte Carlo methods stand out as a versatile alternative to investigating the statistical properties of complex phenomena, especially for systems comprised of several degrees of freedom. As suggested by Ulam, Metropolis and Teller, among other important collaborators, the idea was to explore the capability of pseudo-random number generation of computers in the simulation of the distinct stochastic trajectories available in the configuration space of a given system (METROPOLIS; ULAM, 1949; METROPOLIS et al., 1953). Such a walk through the system's phase space enables the determination of thermodynamic averages of macroscopic observables since the system displays the ergodic property.[1]

[1] Describes the tendency of a system to eventually explore all regions of its space uniformly. This property ensures that the average behavior of the system can be inferred from a sufficiently large sample.

For the purpose of this work, we shall focus our attention on the majority-vote model, which is known to display a stationary state after a thermalization time. Consider that in such a stationary regime, a given trajectory of the system may visit a total of $\mathscr{M}$ microstates, attainable via the transition probabilities $P(\sigma)$, which do not depend on time in the stationary state. The Monte Carlo framework allows us to estimate the time average of the state function $f(\sigma)$ upon visiting the $\mathscr{M}$ sampled microstates

$$\langle f \rangle_t = \frac{1}{\mathscr{M}} \sum_{i=1}^{\mathscr{M}} f(\sigma_i), \tag{3.34}$$

where $\langle \cdots \rangle_t$ represents time averages of the state function, σ_i represents the $i-$th microstate, and the sum runs over all $\mathscr{M}$ microstates in the stationary regime. Assuming ergodicity, time averages in the stationary state provide estimators for ensemble expectation values of macroscopic quantities

$$\langle f \rangle_t = \frac{1}{\mathscr{M}} \sum_{i=1}^{\mathscr{M}} f(\sigma_i) \approx \sum_{\sigma} f(\sigma) P(\sigma) = \langle f(\sigma) \rangle_c. \tag{3.35}$$

By macroscopic quantities, we are essentially referring to the system's *opinionization* $\mathcal{O}$ and *noise sensitivity* χ in the context of the majority-vote model. While the former acts as an order parameter, measuring the average consensus in the system, the latter is defined as the variance of the order parameter, quantifying the degree of fluctuations in the system. Within this framework, Monte Carlo simulations play a crucial role in enabling the calculation of the opinionization and noise sensitivity via the exploitation of time and ensemble averages within the system's configuration space. The quantities mentioned above are defined as

$$\mathcal{O} = \langle \mathscr{o}(\sigma) \rangle, \tag{3.36}$$

$$\chi = N \left[\langle \mathscr{o}^2(\sigma) \rangle - \langle \mathscr{o}(\sigma) \rangle^2 \right], \tag{3.37}$$

where $\mathscr{o}(\sigma)$ is the instantaneous order parameter of the system and shall be defined and explored in Chapter 4.

4 THE MAJORITY-VOTE MODEL

The following chapter presents the theoretical and probabilistic foundations of the majority-vote model, which implements Monte Carlo simulations to investigate opinion dynamics and consensus formation in societal scenarios. We shall define the macroscopic quantities investigated and their essential properties, addressing their relevance in determining the critical behavior of the system. We then introduce a modified version of the majority-vote model inspired by biased opinion algorithms commonly found in real-world social networks. Moreover, we introduce the global-vote model, an extension of the majority-vote framework to study price formation in financial markets.

As will be discussed through the course of this chapter, some of the thermodynamic quantities studied in the majority-vote model are size-dependent; thus, we shall also introduce the theoretical basis of finite-size scaling, a mathematical framework that allows the extrapolation of some properties of the system beyond the constraints of simulating finite systems. This scaling technique will enable us to estimate the critical exponents of the system, which are related to the behavior of physical quantities near criticality and are fundamental for identifying the universality class of the model.

4.1 THEORETICAL MODELING IN STATISTICAL PHYSICS

In recent years, computational models have emerged as crucial tools for investigating complex phenomena, especially when the dynamics involve many interacting constituents. These models offer insights into the fundamental principles governing systems where analytical solutions are infeasible, bridging theoretical formulations and experimental observations. Within this framework, a particularly relevant example of statistical mechanical modeling is the investigation of magnetic systems, where the Ising model (ONSAGER, 1944) stands out for its capability of capturing critical features of the system via a reasonably straightforward mathematical framework. Furthermore, it played a key role in fomenting similar models in statistical mechanics, such as the Heisenberg, Potts, and XY models (STANLEY, 1971; LANDAU; BINDER, 2021). The effectiveness of such physical models inspired scientists to extend them toward broader interdisciplinary areas, with applications ranging from social dynamics to economic systems (BORNHOLDT, 2001; STAUFFER, 2008).

These stochastic models can be divided into two categories regarding the processes involved in their dynamics: *microscopically reversible* and *microscopically irreversible* (TOMÉ, 2001).

The time evolution of reversible models is characterized by the presence of a Hamiltonian, which models the interaction between the many particles of the system. The statistical mechanics theory supposes that we may associate a partition function to this Hamiltonian, from which we may extract the transition probabilities between states based on the energetic configuration of the system and the energy involved in the transition process itself. Reversible systems naturally evolve toward stationary states of thermodynamic equilibrium; hence, the probability that the system goes through a sequence of microstates in one direction is the same as in the inverse direction, a feature known as *detailed balance*.

Conversely, irreversible models cannot be described via a Hamiltonian. Their time evolution does not involve an associated partition function yet is still governed by transition probabilities between states. As discussed in the previous chapter, they may evolve towards stationary states, but those are not thermodynamic states of equilibrium. Moreover, the lack of a Hamiltonian describing the system's dynamics implies that the evolution of irreversible models does not obey detailed balance.

In this work, we shall investigate the *majority-vote model*, a stochastic irreversible model designed to simulate opinion dynamics and consensus formations in modern societies. Possible applications of the majority-vote formulation range from investigating the effects of social networks in opinion propagation and collective decision-making processes in economic markets.

4.2 THE MAJORITY-VOTE MODEL

The majority-vote model with noise is one of the most simple yet powerful formulations of agent-based models within sociophysics (OLIVEIRA, 1992; OLIVEIRA; MENDES; SANTOS, 1993). It is designed as a social analogous to the Ising model, where individuals are represented as nodes (sites) in a network. For the purpose of this work, we shall associate a stochastic opinion variable σ_i to each individual i, which may assume one out of two values regarding some social issue. We remark that possible extensions of this framework include the generalization of the stochastic opinion variable, allowing it to assume more than two values, where the *three-state framework* (BRUNSTEIN; TOMÉ, 1999; TOMÉ; PETRI, 2002) stands out as one of the most relevant examples.

4.2.1 Two-state Majority-vote Model

Let us initially focus on the two-state configuration of the model's dynamics. In this case, we consider a group of N individuals who position themselves in one of two ways: *favorable* or *contrary* to some political debate, for example. In real-world scenarios, individuals' opinions are expected to change over time due to interactions with their closest acquaintances (neighbors). Social beings tend to follow the majoritarian opinion within their peer groups driven by social pressure, an effect known as *conformity*, which was well demonstrated in Asch's experiments (ASCH, 2016). Still, we implement a parameter q to model situations in which individuals might disagree with the majority of their friends (OLIVEIRA, 1992; OLIVEIRA; MENDES; SANTOS, 1993). This parameter is usually referred to as the *noise parameter*, and it measures a level of social anxiety inherently present in decision-making processes.

The majority-vote dynamics follows the master equation (3.29), with the single spin-flip probability being defined as

$$w_i(\sigma) = \frac{1}{2}\left\{1 - (1-2q)\sigma_i S\left(\sum_{\delta=1}^{k_i}\sigma_\delta\right)\right\}, \quad \text{with } S(x) = \begin{cases} -1, \text{ if } x < 0, \\ 0, \text{ if } x = 0, \\ +1, \text{ if } x > 0, \end{cases} \tag{4.1}$$

where the summation runs over all k_i nearest neighbors of site i and $S(x)$ is the sign function. We remark that the model displays inversion symmetry, i.e., flipping the states of all the network sites, we obtain an equivalent global state to the initial one.

The overall behavior of the system depends on the value of the noise parameter q. As the Ising model, its thermal analogous, the majority-vote model displays a second-order phase transition, where q acts as a social temperature of the system. Hence, just as there is a critical temperature T_c in the Ising model (Curie temperature), there is a critical value of the social anxiety parameter q_c that divides the systems into ordered (consensus) and disordered (dissensus) phases.

Consider a network of individuals where the links indicate social relations among them. Let us adopt the absolute consensus as the system's initial condition, i.e., all individuals in the network have the same opinion regarding some social issue. If we randomly visit sites in the network and flip their states with the probabilities defined in Eq. (4.1), we shall find that the system, after some time, lies in one of the following states:

1. For $q = 0$, all sites in the network will be in the same state;

2. For $0 < q < q_c$, the majority of the sites in the network will be in the same state ($+1$ or -1), while the rest will adopt the contrary state;

3. For $q \geq q_c$, half of the individuals will adopt one opinion and the other half the contrary one, on average. The system is polarized at this point, and we have transitioned to a dissensus phase.

To investigate the critical behavior of the system, let us define some macroscopic quantities of interest. The first of these quantities is the order parameter of the system, which we shall refer to as the *opinionization* $\mathcal{O}$. This quantity is a social analogous to the magnetization of spin systems and measures the average consensus in the network. Thus, the opinionization of the system is defined as

$$\mathcal{O}_N(q) = \langle\langle o \rangle_t\rangle_c, \quad \text{with} \quad o = \frac{1}{N}\left|\sum_{i=1}^{N}\sigma_i\right|, \tag{4.2}$$

where o is the instantaneous order parameter of the system, $\langle\cdots\rangle_c$ represents configurational averages and $\langle\cdots\rangle_t$ represents time averages of the quantity. Note that we consider the modulus of the summation over the individuals' states σ_i due to the inversion symmetry mentioned previously.

Furthermore, we are interested in investigating the fluctuations of the order parameter. Thus, we define the noise sensitivity χ as the variance of the order parameter, shown below

$$\chi_N(q) = N\left[\langle\langle o^2\rangle_t\rangle_c - \langle\langle o\rangle_t\rangle_c^2\right]. \tag{4.3}$$

Similarly to the behavior of magnetic systems, the noise sensitivity acts as a tool to indicate consensus-dissensus phase transitions in the system, displaying a peak in the vicinity of q_c. Notably, in the thermodynamic limit, values of χ would diverge at q_c.

Finally, we define another useful quantity, especially regarding the finite size limitations of the simulations, known as the *fourth-order Binder cumulant* (BINDER, 1981)

$$U_N(q) = 1 - \frac{\langle\langle o^4\rangle_t\rangle_c}{3\langle\langle o^2\rangle_t\rangle_c^2}. \tag{4.4}$$

The fourth-order Binder cumulant is a mathematical tool that allows us to identify the critical value of the noise parameter q_c. It is constructed in such a way that its value is independent

of the system size at the critical social temperature. Thus, if we simulate different system sizes and calculate the Binder cumulant for each one, we may extract the critical noise of the system via the intersection of the curves for different sizes.

4.2.2 Three-state Majority-vote Model

Another significant development of the majority-vote model's theory is considering more than two possible states for each individual in the system. In particular, consider that any agent may adopt one out of three possible opinions $s \in \{1, 2, 3\}$, such as voting for candidates A, B or C in a political election. Similar to the two-state case, individuals tend to follow the predominant opinion of their closest friends with probability $1 - q$ or disagree with them with chance q. Once again, q is referred to as the social anxiety parameter and models a non-conforming behavior in the system dynamics.

In the three-state majority-vote model (BRUNSTEIN; TOMÉ, 1999; TOMÉ; PETRI, 2002), we shall consider a set of probabilistic opinion update rules instead of single spin-flip probabilities. Let i represent an individual in the network of social connections and $k_{i,s}$ represent the number of neighboring sites of i occupying a given state $s \in \{1, 2, 3\}$. Below, we summarize the stochastic update rules for an agent to adopt the state $s = 1$:

$$
\begin{aligned}
&P\left(1|k_{i,1} > k_{i,2}; k_{i,3}\right) \quad = P\left(2|k_{i,2} > k_{i,3}; k_{i,1}\right) \quad = P\left(3|k_{i,3} > k_{i,1}; k_{i,2}\right) \quad = 1 - q, \\
&P\left(1|k_{i,1} = k_{i,2} > k_{i,3}\right) = P\left(2|k_{i,2} = k_{i,3} > k_{i,1}\right) = P\left(3|k_{i,3} = k_{i,1} > k_{i,2}\right) = (1 - q)/2, \\
&P\left(1|k_{i,1} < k_{i,2} = k_{i,3}\right) = P\left(2|k_{i,2} < k_{i,3} = k_{i,1}\right) = P\left(3|k_{i,3} < k_{i,1} = k_{i,2}\right) = q, \\
&P\left(1|k_{i,1}; k_{i,2} < k_{i,3}\right) \quad = P\left(2|k_{i,2}; k_{i,3} < k_{i,1}\right) \quad = P\left(3|k_{i,3}; k_{i,1} < k_{i,2}\right) \quad = q/2, \\
&P\left(1|k_{i,1} = k_{i,2} = k_{i,3}\right) = P\left(2|k_{i,2} = k_{i,3} = k_{i,1}\right) = P\left(3|k_{i,3} = k_{i,1} = k_{i,2}\right) = 1/3.
\end{aligned}
\tag{4.5}
$$

Note that the probabilities for the states follow from the symmetry operations of the $C_{3\nu}$ group: $1 \to 2$, $2 \to 3$ and $3 \to 1$. Furthermore, the probabilities must be normalized, i.e., $P(1|\{k_i\}) + P(2|\{k_i\}) + P(3|\{k_i\}) = 1$ for any global state configuration $\{k_i\} \equiv \{k_{i,1}, k_{i,2}, k_{i,3}\}$.

Once again, we remark that the global stationary state of the system is highly dependent on the social anxiety parameter q. As q increases, the system undergoes a second-order phase

transition at $q = q_c$. Thus, for $q < q_c$, the system finds itself in a consensus phase, with one of the opinions having the majority of the votes, whereas for $q > q_c$, dissensus dominates, and approximately $1/3$ of the individuals adopt each of the possible opinion states.

We shall investigate the system dynamics via the order parameter of the system, which, following the analogy with magnetic systems, will be defined as the magnitude of the average magnetization as in the three-state Potts model (WU, 1982). In this way, consider N_s as the number of individuals of the system that find themselves on state $s \in \{1, 2, 3\}$, where $N_1 + N_2 + N_3 = N$, naturally. In this way, the instantaneous opinionization of the three-state majority-vote model may be understood as the magnitude of a vector with components $\mathscr{o}_s$. Hence, the elements of the opinionization vector are defined as

$$\mathscr{o}_s = \sqrt{\frac{3}{2}} \left(\frac{N_s}{N} - \frac{1}{3} \right), \tag{4.6}$$

with the instantaneous opinionization being defined as follows

$$\mathscr{o} = \sqrt{\mathscr{o}_1^2 + \mathscr{o}_2^2 + \mathscr{o}_3^2}. \tag{4.7}$$

Furthermore, the statistical quantities of interest, namely the opinionization, the noise sensitivity and the fourth-order Binder cumulant, are defined in a similar fashion to the two-state case. Thus, below, we recall the mathematical expressions for the aforementioned quantities

$$\mathscr{O}_N(q) = \langle \langle \mathscr{o} \rangle_t \rangle_c, \tag{4.8}$$

$$\chi_N(q) = N \left[\langle \langle \mathscr{o}^2 \rangle_t \rangle_c - \langle \langle \mathscr{o} \rangle_t \rangle_c^2 \right], \tag{4.9}$$

$$U_N(q) = 1 - \frac{\langle \langle \mathscr{o}^4 \rangle_t \rangle_c}{3 \langle \langle \mathscr{o}^2 \rangle_t \rangle_c^2}, \tag{4.10}$$

where $\langle \cdots \rangle_c$ represents configurational averages, and $\langle \cdots \rangle_t$ represents time averages taken on the stationary regime.

4.3 VISIBILITY ALGORITHMS AND THE MAJORITY-VOTE DYNAMICS

In today's highly connected world, social media platforms have become powerful drivers of content dissemination and user engagement, with many companies profiting directly from these

interactions. To maximize revenue, these platforms deploy algorithms that operate behind the perception of average users, determining which content to promote based on user behavior. A key example of such algorithmic strategies is collaborative filtering, which recommends content by analyzing patterns of similarity between users' past interactions (KOREN; RENDLE; BELL, 2021). This phenomenon is commonly referred to as the *click economy*, highlighting the economic incentives that prioritize engagement metrics over content diversity, shaping how individuals consume information in the digital age.

Thus, social media algorithms are tuned to maximize clicks, often favoring content that triggers strong emotional responses as they tend to drive higher interaction rates. While effective for delivering personalized recommendations, these techniques also contribute to amplifying sensationalism, spreading misinformation, and forming filter bubbles, where curated content reinforces users' pre-existing beliefs. Such opinion echo chambers intensify polarization in public debates via the formation of artificial majorities. Thus, content algorithms have become crucial players in modern social platforms, and obtaining insights into how they operate is essential for understanding the influence of biased content sharing and its broader societal impacts.

The model investigated in this work draws inspiration from previous studies of opinion dynamics driven by algorithmic visibility, such as the work of (VILELA et al., 2021). Their approach considers an unbiased visibility model, where content may be hidden with a certain probability but without favoring converging opinions. While this framework provides valuable insights into the evolution of collective opinions under neutral conditions, it does not capture the inherent biases present in real-world social media algorithms. In contrast, our model explores the effects of an opinion-biased visibility algorithm fostered by the click economy, in which engagement-driven content curation is prioritized.

Similar to the standard majority-vote model (OLIVEIRA, 1992; OLIVEIRA; MENDES; SANTOS, 1993), our model represents a society of N individuals, each associated with a stochastic spin variable σ_i that can assume one of two possible states, ± 1. Individuals shall follow their near-neighbor majority with chance $1 - q$ while dissenting from it with chance q, where q is the noise parameter, as previously mentioned. Furthermore, we extend this framework by introducing a *biased visibility parameter* V, quantifying the probability that an agent is able to access the fraction of its neighborhood holding opposing opinions on a given social issue. The parameter V ranges from $0 \leq V \leq 1$, allowing us to tune the degree of strength of the bias algorithm. When $V = 0$, an individual exclusively considers like-minded neighbors, while when

$V = 1$, the visibility bias is removed, and the model reduces to the standard majority-vote formulation.

Let Λ_i denote the set of neighbors of site i that share the same opinion, and $\Lambda_i^\star$ represent the set of neighbors with opposing views in a given social debate. Moreover, we define a visibility index $I(V)$ as

$$I(V) = \begin{cases} 1, & \text{with probability } V; \\ 0, & \text{with probability } 1 - V, \end{cases} \tag{4.11}$$

where V is the visibility parameter. Once again, we remark that the majority-vote model evolves via the master equation (3.29), where the single-spin flip probability shall be rewritten as

$$w_i(\sigma) = \frac{1}{2}\left\{1 - (1-2q)\sigma_i S\left(\sum_{\delta\in\Lambda_i}\sigma_\delta + \sum_{\delta\in\Lambda_i^\star} I_\delta(V)\sigma_\delta\right)\right\}, \tag{4.12}$$

where $S(x) = +1, 0, -1$ for $x > 0, x = 0, x < 0$, respectively. We note that in the special case where all neighboring nodes of site i hold opposing opinions, i.e., $\Lambda_i^\star = \{1, 2, \cdots, k_i\}$, and the visibility index satisfies $I_\delta(V) = 0$ for all $\delta \in \Lambda_i^\star$, the spin of site i remains unchanged.

Furthermore, the critical behavior of the system shall be investigated via the aforementioned macroscopic quantities, namely the opinionization (4.2), the noise sensitivity (4.3) and the fourth-order Binder cumulant (4.4).

4.4 GLOBAL-VOTE MODEL FOR FINANCIAL MARKETS

In this section, we shall discuss one of the most critical applications of the majority-vote framework: investigating price formation and dynamics in financial markets. In this case, individuals in the network now represent financial agents in the market, and the possible opinion states σ_i relates to financial actions an agent may perform in the market. The global-vote model has been investigated both in its two-state (VILELA et al., 2019; GRANHA et al., 2022) and in its three-state configuration (ZUBILLAGA et al., 2022b), where they differ essentially in the number of actions that may be performed:

1. Two-state: considers individuals who may buy or sell a financial asset at each time step;

2. Three-state: models individuals who may buy, sell or remain inactive at each time step.

Furthermore, we still consider the presence of a noise parameter q, which models a level of socioeconomic anxiety present in the decision-making process of financial agents.

In such a complex environment as financial markets, we expect that an agent's decisions arise not only from rational strategies they may have but also from the psychological circumstances that define one's psiché. For instance, we have previously discussed how individuals may feel pressured to conform with their closest friends upon making a decision, an effect known as herding behavior. Such behavior is also present in financial market decision-making processes, where herding is often displayed as informational cascades, in which individuals base their decisions on the observed actions of others rather than on their private information, amplifying collective trends (CONT; BOUCHAUD, 2000; RAAFAT; CHATER; FRITH, 2009; HONG; KUBIK; STEIN, 2005; ZHAO et al., 2011; BIKHCHANDANI; HIRSHLEIFER; WELCH, 1992; GALAM, 2008).

The global-vote model (VILELA et al., 2019) considers two types of financial strategies that the financial agents may carry out in the system for their impact on price dynamics. The first of these strategies implements the effects of herding behavior, and individuals who adopt it will be referred to as *noise traders*. Such agents tend to follow the local majority of their acquaintances when deciding which action to perform and tend to overreact to the arrival of news in the market.

Conversely, the second type of agents comprised in the model tend to follow the global minority of the system as an investment strategy; essentially, they tend to buy (sell) when noise traders are selling (buying). Such agents are widely present in the literature, being referred to as *fundamentalists*, contrarians, sophisticated traders, or $\alpha-$investors (DAY; HUANG, 1990; VOIT, 2005; BORNHOLDT, 2001; KAIZOJI; BORNHOLDT; FUJIWARA, 2002; TAKAISHI, 2005; LUX; MARCHESI, 1999; LUX; MARCHESI, 2000; LONG et al., 1990). Fundamentalist agents guide their rational decision-making on analyzing the underlying fundamentals of assets, and their actions contribute to price movements that converge towards the assets' *fundamental* values.

4.4.1 Three-state Global-vote Model

For the purpose of this work, we shall focus exclusively on the three-state configuration of the global-vote model (ZUBILLAGA et al., 2022b). As previously mentioned, a noise trader agent tends to follow the behavior adopted by the majority of their closest friends. Thus, the time evolution of their option state will be described by the probabilistic prescriptions in Eq.

(4.5).

Conversely, fundamentalist agents interact globally with the market in order to determine their course of action in the following steps. As per their strategy, they tend to follow the global minority of the market, avoiding market trends and crowd movements. Hence, the state update rules for a fundamentalist agent to adopt the state $s = 1$ are described by the probabilistic prescription below

$$\begin{aligned}
&P\left(1|N_1 < N_2; N_3\right) \quad = P\left(2|N_2 < N_3; N_1\right) \quad = P\left(3|N_3 < N_1; N_2\right) \quad = 1 - q, \\
&P\left(1|N_1 = N_2 < N_3\right) = P\left(2|N_2 = N_3 < N_1\right) = P\left(3|N_3 = N_1 < N_2\right) = (1 - q)/2, \\
&P\left(1|N_1 > N_2 = N_3\right) = P\left(2|N_2 > N_3 = N_1\right) = P\left(3|N_3 > N_1 = N_2\right) = q, \\
&P\left(1|N_1; N_2 > N_3\right) \quad = P\left(2|N_2; N_3 > N_1\right) \quad = P\left(3|N_3; N_1 > N_2\right) \quad = q/2, \\
&P\left(1|N_1 = N_2 = N_3\right) = P\left(2|N_1 = N_2 = N_3\right) = P\left(3|N_1 = N_2 = N_3\right) = 1/3.
\end{aligned} \tag{4.13}$$

where N_s represents the total number of agents in the network within a given state $s \in \{1, 2, 3\}$, and $N = N_1 + N_2 + N_3$. Similarly to the noise trader case, the probabilities can be obtained from symmetry operations of the $C_{3\nu}$ group. Furthermore, the normalization condition, i.e. $P(1|\{N\}) + P(2|\{N\}) + P(3|\{N\}) = 1$, holds for any configuration of the system $\{N\} \equiv \{N_1, N_2, N_3\}$.

In the financial context, we shall relate fluctuations of the order parameter of the system with market volatility for their impact on asset price dynamics. We define the order parameter of the system as the three-state opinionization (4.7) in analogy to the Potts model, and it measures the market's stability. The global-vote formulation interprets opinionization as a measure of price in modern markets. It relates variations in the instantaneous order parameter $\mathscr{o}(t)$ to the logarithmic returns $r(t)$ of a financial asset. Thus, the logarithmic returns are defined as (BORNHOLDT, 2001; KAIZOJI; BORNHOLDT; FUJIWARA, 2002; TAKAISHI, 2005; CONT, 2007)

$$r(t) = \log\left[\mathscr{o}(t)\right] - \log\left[\mathscr{o}(t-1)\right]. \tag{4.14}$$

Another important quantity we shall investigate is the volatility, denoted by v, which measures the amplitude of price fluctuations in the time series. Hence, the volatility is defined as follows

$$v(t) \equiv |r(t)|. \tag{4.15}$$

4.5 FINITE-SIZE SCALING

As previously discussed, the thermodynamic functions defined to investigate the system's global behavior display a unique behavior near the phase transition. Formally, a second-order phase transition in the majority-vote formulation would only be displayed at the thermodynamic limit, $N \to \infty$, where we would observe a divergence of the noise sensitivity at $q = q_c$. This would pose a significant challenge to the numerical investigation of such systems since one would require access to infinite memory resources as well as an infinite simulation time. Hence, one is unable to computationally simulate the behavior of critical systems directly.

Within this context, finite-size scaling techniques are fundamental tools for the analysis of the statistical mechanical properties of complex systems near criticality. The reasoning is to simulate systems with finite sizes and extrapolate the results obtained to analyze the behavior of such complex systems near criticality. Moreover, from this mathematical analysis, we may extract the critical exponents of the system, which are related to the behavior of thermodynamic quantities at the phase transition. The set of critical exponent values defines the so-called *universality class*, which groups systems with distinct microscopic details but similar macroscopic behavior near their critical points, highlighting the shared underlying physics of phase transitions (STANLEY, 1971; CARDY, 1996).

For the majority-vote model, let us define an adimensional parameter ε as

$$\varepsilon = q - q_c, \tag{4.16}$$

which provides a measure of how distant the system is from the critical social temperature q_c. Hence, we may define the critical exponent related to a thermodynamic function in terms of the adimensional parameter ε

$$\lambda = \lim_{\varepsilon \to 0} \frac{\ln |f(\varepsilon)|}{\ln |\varepsilon|}, \tag{4.17}$$

where we assume the existence of the limit above. In such a limit, i.e., when we are sufficiently close to the critical social temperature of the system, it is more useful to express the relation above explicitly in terms of the thermodynamic function as

$$f(\varepsilon) \sim |\varepsilon|^{\lambda}. \tag{4.18}$$

For Ising-like systems, such as the majority-vote model, the scaling laws for the relevant macroscopic quantities, i.e., the opinionization and the noise sensitivity, are given by

$$\mathcal{O} \sim |\varepsilon|^{\beta}, \tag{4.19}$$

$$\chi \sim |\varepsilon|^{-\gamma}. \tag{4.20}$$

Furthermore, another crucial quantity in the investigation of the critical behavior of such systems is the correlation length ξ, as it measures the typical distance over which the opinion state of an individual affects other agents in the network. This quantity is known to diverge in the thermodynamic limit, and its associated scaling function is defined as:

$$\xi \sim |\varepsilon|^{-\nu}. \tag{4.21}$$

However, we are dealing with systems with finite size $N = L^d$, where d represents the dimension and L relates to the linear size of the system. In this case, the system becomes effectively ordered when the correlation length is of the order of L. Consequently, the thermodynamic functions also depend on the system size, as mentioned previously. Hence, we may rewrite the scaling function of the correlation length as

$$\xi \sim L \sim |\varepsilon|^{-\nu}. \tag{4.22}$$

Moreover, we may explicitly express the parameter ε in terms of the system size, as shown below:

$$|\varepsilon| \sim L^{1/\nu}. \tag{4.23}$$

Rewriting the scaling functions for the thermodynamic quantities, we obtain:

$$\mathcal{O}_L \sim L^{-\beta/\nu}, \tag{4.24}$$

$$\chi_L \sim L^{\gamma/\nu}. \tag{4.25}$$

Hence, the exponents β/ν and γ/ν determine the opinionization and the noise sensitivity, respectively, with the system size at the critical temperature of the system. Simulating the

majority-vote dynamics and calculating the aforementioned quantities for different system sizes enables us to obtain the critical exponents of the system.

Furthermore, as discussed previously, the Binder fourth-order cumulant is constructed so that it does not depend on the system size at the critical social temperature of the system. With that in mind, we may write the scaling relations for the investigated quantities in the limit $\varepsilon \to 0$ as

$$\mathcal{O}_L(q) = L^{-\beta/\nu}\ \widetilde{\mathcal{O}}(\varepsilon L^{1/\nu}), \tag{4.26}$$

$$\chi_L(q) = L^{\gamma/\nu}\ \widetilde{\chi}(\varepsilon L^{1/\nu}), \tag{4.27}$$

$$U_L(q) = \widetilde{U}(\varepsilon L^{1/\nu}), \tag{4.28}$$

where $\widetilde{\mathcal{O}}(x)$, $\widetilde{\chi}(x)$ and $\widetilde{U}(x)$ are the universal scaling functions. The set of equations above describes the so-called finite-size scaling relations of the majority-vote model.

We remark that we may obtain the exponent $1/\nu$ via the scaling relation for the Binder cumulant. Taking the derivative of Eq. (4.28) in terms of the noise parameter in the critical region, we find

$$\frac{dU_L(q)}{dq} = L^{1/\nu}\frac{d\widetilde{U}(\varepsilon L^{1/\nu})}{dq}. \tag{4.29}$$

Thus, at the critical temperature ($\varepsilon = 0$), the derivative of the Binder fourth-order cumulant behaves as:

$$U'_L(q_c) = L^{1/\nu}\ \widetilde{U}'(0). \tag{4.30}$$

Hence, determining the value of the derivative of the Binder fourth-order cumulant at the critical social temperature for different system sizes allows us to obtain the critical exponent $1/\nu$.

4.5.1 The Hyperscaling Relation

The underlying theory of renormalization groups connects the exponents related to the scaling functions of the opinionization (4.26) and noise sensitivity (4.27) with the critical dimension of the system. This is possible via a unique mathematical expression known as the

hyperscaling relation. Initially, let us recall the known result for the hyperscaling relation for many-body systems in regular arrays (STANLEY, 1971; CARDY, 1996):

$$2\frac{\beta}{\nu} + \frac{\gamma}{\nu} = d, \tag{4.31}$$

where d represents the dimension of the lattice. Thus, Eq. (4.31) displays the fundamental role played by the dimension of the system in its critical behavior.

Note that the expression above supposes that the system we are dealing with is regular, consisting of an array of dimension d. Conversely, real-world complex systems are rarely regular, exhibiting rich topologies, where complex networks rise as important substrates for their dynamics. In such structures, the concept of physical dimension becomes less clear, and recent developments generalized the hyperscaling relation for a broader range of network topologies—the unitary relation under volumetric scaling(VILELA et al., 2020).

4.5.2 The Unitary Relation

Note that the demonstration of the finite-size scaling relations considered a system of size $N = L^d$, where L represents the linear size and d is the dimension of the system. Nevertheless, when simulating complex network topologies, the concepts of physical dimension and linear size are unclear, which in part questions our initial assumption that the correlation length scales with the system's linear size at the critical region. Hence, considering a volumetric scaling of the correlation length, we write (BOTET; JULLIEN; PFEUTY, 1982; HONG; HA; PARK, 2007; VILELA et al., 2020)

$$\xi \sim N. \tag{4.32}$$

Following a similar mathematical formulation for the scaling relations of the thermodynamic functions under this new assumption, the finite-size scaling relations take the form:

$$\mathcal{O}_N(q) = N^{-\beta/\bar{\nu}}\ \widetilde{\mathcal{O}}(\varepsilon N^{1/\bar{\nu}}), \tag{4.33}$$

$$\chi_N(q) = N^{\gamma/\bar{\nu}}\ \widetilde{\chi}(\varepsilon N^{1/\bar{\nu}}), \tag{4.34}$$

$$U_N(q) = \widetilde{U}(\varepsilon N^{1/\bar{\nu}}), \tag{4.35}$$

where $\bar{\nu}$ highlights that we are now assuming a volumetric scaling for the correlation length.

Consider now a regular lattice of linear size L in d dimensions. In this case, the size of the system is $N = L^d$, and the scaling relations for the opinionization and noise sensitivity in terms of a volumetric scaling become:

$$\mathcal{O}_L(q) = L^{-d\beta/\bar{\nu}}\ \widetilde{\mathcal{O}}(\varepsilon N^{1/\bar{\nu}}), \tag{4.36}$$

$$\chi_L(q) = L^{d\gamma/\bar{\nu}}\ \widetilde{\chi}(\varepsilon N^{1/\bar{\nu}}). \tag{4.37}$$

Consequently, the hyperscaling relation will now be expressed as

$$2d\frac{\beta}{\bar{\nu}} + d\frac{\gamma}{\bar{\nu}} = d. \tag{4.38}$$

Simplifying the terms in the expression above, we find the *unitary relation for critical exponents* $\upsilon = 1$ (VILELA et al., 2020):

$$2\frac{\beta}{\bar{\nu}} + \frac{\gamma}{\bar{\nu}} \equiv \upsilon = 1, \tag{4.39}$$

which is independent of the dimension and topological complexities of the network. In this work, the unitary relation shall be used to confirm the accuracy and validity of the critical exponents estimated in our analysis.

4.6 OVERVIEW OF THE EXISTING LITERATURE

4.6.1 The Majority-Vote Model

The two-state majority-vote model with noise was proposed by Oliveira (1992) and Oliveira, Mendes and Santos (1993). In this work, he simulates a system of individuals that are represented as sites in a regular network (square lattice). Via Monte Carlo simulations, he obtains the critical social noise as $q_c = 0.075(1)$. Furthermore, he implements finite-size scaling to estimate the critical exponents of the system, where he obtains $\beta/\nu = 0.125(5)$, $\gamma/\nu = 1.73(5)$ and $1/\nu = 1.01(5)$. Oliveira thus confirmed the previous assumption that non-equilibrium models with inversion symmetry lie within the same universality class as the Ising model (GRINSTEIN; JAYAPRAKASH; HE, 1985).

The framework presented by Oliveira essentially involved two fundamental aspects: the topological structure of the network of social interactions and the nature of the social dynamics

within the system. From the standpoint of the dynamics, several authors investigated distinct effects on the system's overall behavior. Santos and Teixeira (1995) introduced anisotropic effects, while Vilela et al. (VILELA; MOREIRA, 2009; VILELA; MOREIRA; SOUZA, 2012) investigated the impacts of heterogeneous agents and bimodal social temperature distributions. Vieira and Crokidakis (2016) explored the role of different types of social noise, and Vilela et al. (VILELA; STANLEY, 2018; VILELA et al., 2021) examined the effects of opinion weight disparities and social visibility parameters. More recently, Oliveira et al. (2024) considered the influence of cooperative behavior on social order.

Additionally, inspired by the three-state Potts model (WU, 1982), Brunstein and Tomé (1999), and Tomé and Petri (2002) proposed the three-state majority-vote model on square lattices. Their numerical simulations display the presence of a second-order phase transition at a critical social parameter of $q_c \approx 0.118$ and critical exponent values $\beta/\nu = 0.134(5)$ and $\gamma/\nu = 1.74(2)$. Comparatively, simulations on the three-state Potts model obtained $\beta/\nu = 2/15$ and $\gamma/\nu = 26/15$ (WU, 1982), suggesting that both models lie within the same universality class.

Similarly, from the topological perspective, the majority-vote dynamics were implemented in several complex network structures. Within the two-state isotropic configuration, Campos, Oliveira and Moreira (2003) investigated the effects of long-range interactions via the small-world framework (WATTS; STROGATZ, 1998); Pereira and Moreira (2005) considered the implementation of random networks (ERDÖS; RÉNYI, 1960); and (LIMA, 2007) studied the impacts of scale-free networks via the Barabási-Albert algorithm of preferential attachment (BARABÁSI; ALBERT; JEONG, 2000). Furthermore, recent works also considered implementing the three-state majority-vote model on the complex network structures mentioned previously (MELO; PEREIRA; MOREIRA, 2010; VILELA et al., 2020; ZUBILLAGA et al., 2022a).

4.6.2 The Global-Vote Model for Financial Markets

Building on the majority-vote framework, Vilela et al. (2019) proposed the global-vote model to simulate price formation in modern financial markets. The model comprised two distinct financial strategies: a "follow the crowd" behavior, adopted by the so-called noise trader agents, and a "ride against the tide" strategy, taken by more experienced agents referred to as fundamentalists or noise contrarian traders. Each agent may adopt one out of two options related to buying or selling an asset for each time step. Furthermore, the system presents a finite socioeconomic anxiety parameter q that models a change of adrift financial actions. The

global-vote model on square lattice networks displays fundamental features of financial market time series, such as *volatility clustering* and *long-term memory of the volatility* (VILELA et al., 2019).

More recently, the two-state global-vote model has been extended to incorporate complex network structures, more specifically random networks (GRANHA et al., 2022). In this study, the authors explore how the connectivity patterns of agents' socioeconomic interactions influence price formation dynamics. Random graphs allow for the analysis of more realistic and heterogeneous interaction structures, providing insights into the effects of network topology on key financial market phenomena. Beyond the discussion on the numerical results of the model, the authors compared their results with crucial financial indices such as the S&P 500 and Dow Jones, displaying the outstanding capability of the model to reproduce real-world market stylized facts, despite its simplicity.

Another important contribution in this context considers applying a three-state global-vote model for financial markets, where agents may now adopt one out of three possible options regarding buying, selling, or neither (remaining inactive) at each time step. The three-state framework was originally considered on regular networks Zubillaga et al. (2022b). In this work, we present an extension of the discussion contained in (ZUBILLAGA, 2020), in which we show inaugural results for the three-state global-vote model in Barabási-Albert networks. These recent results are organized in a scientific paper submitted to an international peer-reviewed journal and found in Appendix A.

5 BIASED VISIBILITY AND SCALE-FREE EFFECTS ON THE TWO-STATE MAJORITY-VOTE MODEL

We shall now proceed to the main results of our study on biased algorithms in the majority-vote model. We consider the implementation of a visibility parameter V, which only impacts diverging opinions. Furthermore, the macroscopic behavior of the system shall be investigated via Monte Carlo simulations of the majority-vote dynamics.

Individuals shall be represented as nodes in a scale-free Barabási-Albert network, where links stand for social connections between agents. Hence, individuals may interact with each other in order to evolve their current stance in some social debate depending on the influence they receive from their closest acquaintances. The model's dynamics are governed by the single-spin flip probability, described by Eq. (4.12). We remark that the scale-free networks considered in this work are built via the Barabási-Albert algorithm described in Sec. 2.5, in which N and z represent the network's size and growth parameter, respectively.

In Monte Carlo simulations, a unit of time, named Monte Carlo Step (MCS), is defined as a total of N attempts to update the states of randomly selected individuals with probabilities according to Eq. (4.12). Note that, on average, each network site shall be visited at least once for each MCS.

We consider a fully ordered state as the initial condition of our system, i.e., $\sigma_i = +1, \forall i \in [1, N]$. For every Monte Carlo simulation, we allow the system to run for an initial 10^4 MCS as the thermalization time. As the system relaxes into the stationary state, we then proceed to calculate the thermodynamic quantities in the following 5×10^4 MCS, sampling over the configuration space. Furthermore, for every value of the noise parameter q, we perform 100 independent samples, averaging over network disorder. This process shall be repeated for every set of parameters (N, z, V, q) considered.

We recall that the thermodynamic quantities of interest in our simulations, namely the opinionization (4.2), the noise sensitivity (4.3) and the fourth-order Binder cumulant (4.4), were defined in Sec. 4.2.1.

5.1 NUMERICAL RESULTS AND BEHAVIOR OF THE MACROSCOPIC QUANTITIES

5.1.1 Overview of Biased Visibility Effects

Figure 5 displays the dependence of the system's average order on the visibility parameter V. Here we show (a) the opinionization $\mathcal{O}_N(q, z, V)$, (b) the noise sensitivity $\chi_N(q, z, V)$ and (c) the fourth-order Binder cumulant $U_N(q, z, V)$ and their dependence on the noise parameter q. The specific network parameters considered were $N = 12000$ and $z = 10$. In particular, note that Fig. 5(a) clearly displays two distinct phases concerning the behavior of the system: an ordered phase for lower values of q, where the system adopts a consensus macroscopic state, as reflected by $\mathcal{O}_N(q, z, V) = O(1)$; and a disordered phase for higher values of q, where on average half of the individuals adopt one opinion and the other half the opposing one, and, in this case, $\mathcal{O}_N(q, z, V) \sim 0$.

In this way, increasing the social noise parameter q reflects a consensus-dissensus phase transition in the system. Additionally, upon further analysis of Fig. 5(a), one may note that the phase transitions do not occur in a similar fashion for different values of the visibility parameter V. As we progressively decrease the visibility parameter from $V = 1.0$ to 0.1, thus enhancing opinion biases in the system, we observe that the phase transitions in the order parameter shift from smooth and continuous to sharp and discontinuous. Hence, for a fixed value of the growth parameter z, the system shall display both first-order (discontinuous) and second-order (continuous) phase transitions near a critical social temperature $q_c(z, V)$ depending on the value of the visibility parameter V.

Furthermore, note that Fig. 5 shows that the visibility parameter strongly impacts the system's ability to withstand the disorder promoted by the noise parameter q. In particular, as we decrease the visibility parameter, we observe that the system becomes less robust to social noise, as evidenced by the left shift in the order-disorder phase transitions of the order parameter $\mathcal{O}_N$. This behavior is further confirmed by the noise sensitivity curves χ_N, which display a maximum (pseudocritical noise) pointing towards the approximate location of the critical noise $q_c(z, V)$, and by the fourth-order Binder cumulants, which present a clear drop from their expected value in the fully ordered state $U_N = 2/3$. Hence, strongly biased opinion algorithms, modeled in our simulations by lower values of the visibility parameter V, exert a highly polarizing influence, making the system more prone to fragmentation as the individuals have less access to diverging opinions in social debates.

Figure 5 – Impacts of the biased visibility parameter V on the two-state majority-vote model in Barbási-Albert networks with $z = 10$ and $N = 12000$. Here, we display the behavior of (a) the order parameter, (b) the noise sensitivity and (c) the fourth-order Binder cumulant as a function of social temperature q. From left to right, the system slightly shifts from first-order to second-order phase transitions as V increases from 0.1 to 1.0. Lines represent visual guides.

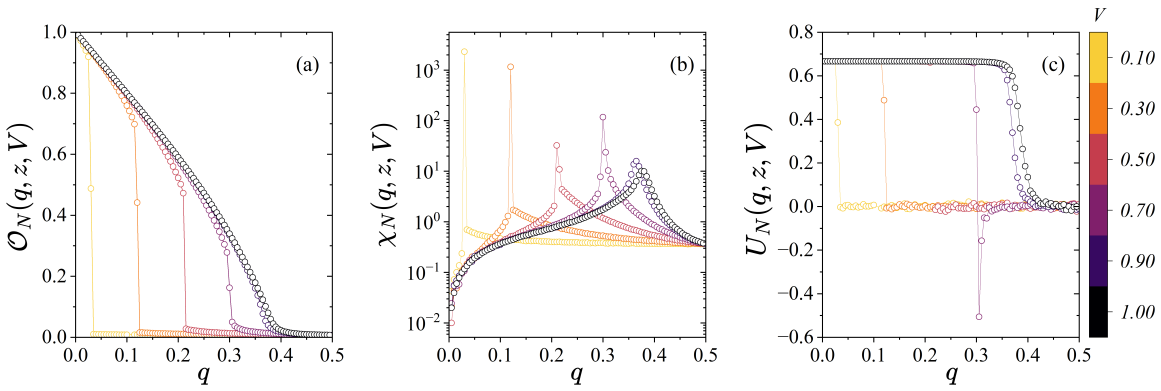

Source: The author (2025).

In Fig. 6, we investigate the effects of the growth parameter of Barbási-Albert networks z on the system's social order for a visibility parameter $V = 0.5$ and network size $N = 12000$. Here we plot (a) the order parameter $\mathcal{O}_N$, (b) the noise sensitivity χ_N and (c) the fourth-order Binder cumulant U_N as a function of the social noise q. We observe that increasing the growth parameter influences the behavior of the phase transition of the order parameter of the system, progressively shifting them from second-order to first-order. Similar to what was discussed previously, we further confirm this effect via the peaks in the noise sensitivity curves and the drop in the fourth-order Binder cumulants.

Furthermore, Fig. 6 highlights two interesting effects regarding the shape of the phase transitions of the system. Initially, the pseudocritical noise parameters for distinct values of the growth parameter z, related to the maxima of the noise sensitivity curves in Fig. 6(b), indicate that networks constructed with higher values of z display a higher resilience to social disorder. We remark that increasing z reflects an increase in the average connectivity of the network $\langle k \rangle \approx 2z$, which promotes higher robustness to the disorder effects fostered by the social temperature q (LIMA, 2007; PEREIRA; MOREIRA, 2005; VILELA et al., 2020; MELO; PEREIRA; MOREIRA, 2010). Conversely, more connected networks display a stronger sensitivity to biased visibility algorithms, as displayed by the sharper transitions in the order parameter for higher values of z. Thus, in our model, highly connected networks act as opinion amplifiers in social debates, fostering strong polarizing effects and intensively impacting the system's behavior

near the critical social temperature $q_c(z, V)$.

Figure 6 – Plots of (a) the opinionization, (b) the noise sensitivity, and (c) the fourth-order Binder cumulant for distinct values of Barabási-Albert network's growth parameter z. Here, we consider a fixed visibility parameter value $V = 0.5$ and networks of size $N = 12000$. As we increase the growth parameter z, from left to right, we observe that the phase transitions become sharper as they shift from second-order to first-order. Lines represent guides to the eyes.

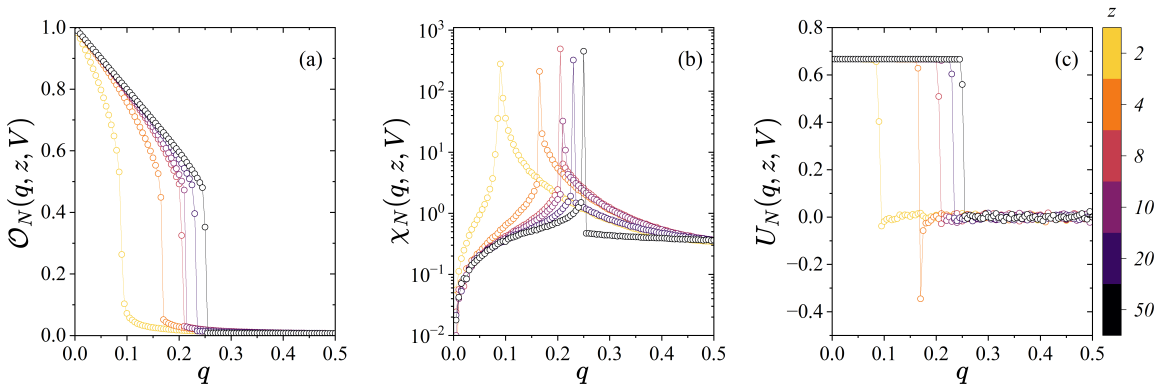

Source: The author (2025).

As it might have become clear by now, the implementation of the biased visibility parameter in our simulations introduces exuberant effects in the system's behavior. By tuning its strength, we not only modify the critical social noise threshold at which consensus dissolves but also influence the very nature of the phase transitions themselves. Given this distinct feature, we shall structure the following two sections of our analysis accordingly: firstly, we focus on first-order phase transitions, and secondly, we examine second-order phase transitions. In this way, we hope to provide a more precise framework for investigating our model under different regimes.

5.2 FIRST-ORDER PHASE TRANSITIONS OF THE TWO-STATE MAJORITY-VOTE MODEL WITH BIASED VISIBILITY

In Fig. 7, we extend our previous discussion by investigating the order parameter of the system $\mathcal{O}_N(q, z, V)$ for distinct values of the visibility V. In particular, we consider Barabási-Albert networks of size $N = 12000$ and growth parameter $z = 10$, and several values of the visibility parameter: $V = 1.0, 0.7, 0.5$ and 0.3, from (a) to (d). This plot compares the results obtained for forward and backward simulations of the majority-vote dynamics with limited

visibility. Forward simulations start with a fully ordered state and progressively increase the system's social temperature, while backward simulations begin with a fully disordered state and gradually decrease the social temperature. In both cases, the final configuration at each noise value will be used as the initial condition for the subsequent step. Both curves are expected to coincide for continuous phase transitions but diverge for first-order phase transitions. Thus, for discontinuous consensus-dissensus transitions, we shall observe the emergence of hysteresis loops in the order parameter, indicating the system's bistability regarding ordered and disordered states, depending on its initial condition (CHEN et al., 2017; HARUNARI; OLIVEIRA; FIORE, 2017; ENCINAS et al., 2018).

Figure 7 – Order parameter of the system $\mathcal{O}_N(q, z, V)$ as a function of the noise parameter q for distinct values of the visibility parameter: (a) $V = 1.0$, (b) $V = 0.7$, (c) $V = 0.5$ and (d) $V = 0.3$. Here, we consider networks of size $N = 12000$ and growth parameter $z = 10$. The green (blue) symbols relate to forward (backward) simulations. As we decrease the visibility parameter, a hysteresis loop emerges, indicating a shift in the nature of the phase transitions. Lines are included as visual guides only.

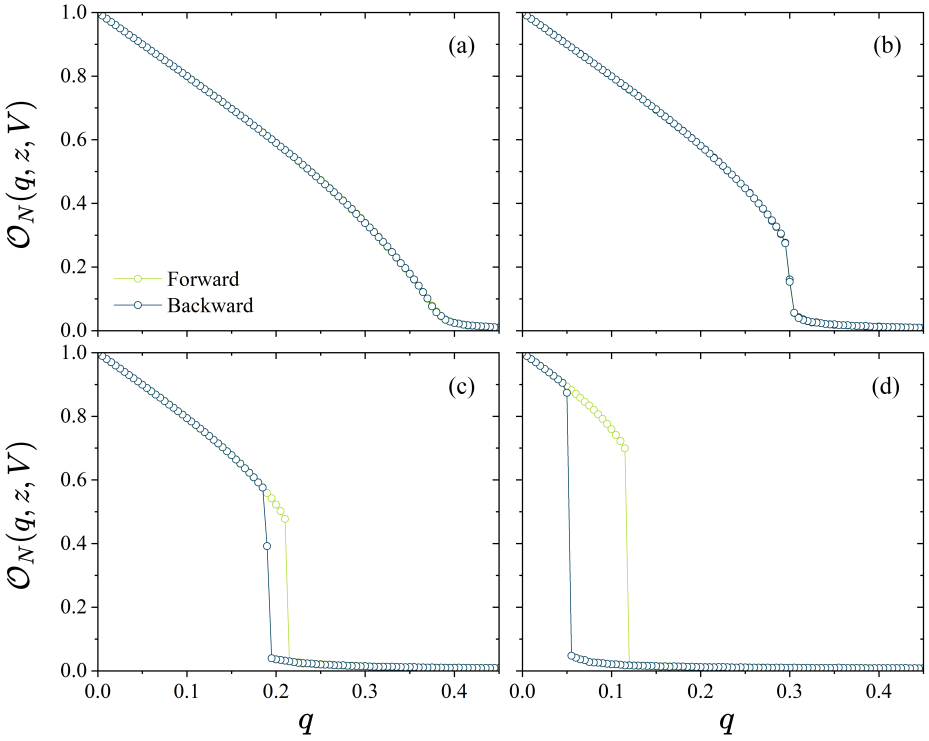

Source: The author (2025).

Thus, in Fig. 7(a), we observe the behavior of the order parameter of the system for $V = 1.0$. We remark that in such limit, we recall the standard two-state majority-vote model on Barabási-Albert networks, which is known to display second-order phase transitions irrespective of the growth parameter value adopted (LIMA, 2007). Our simulations confirm this

behavior, as the forward and backward paths coincide. For (b) $V = 0.7$, despite the transition becoming sharper, both paths still coincide, indicating a continuous regime. Further decreasing the visibility parameter, as in (c) $V = 0.5$ and (d) $V = 0.3$, we observe the emergence of hysteresis loops, with forward and backward simulations displaying sharp transitions at distinct critical social noise values $q_{c_F}(z, V) \neq q_{c_B}(z, V)$. Hence, we confirm that lower values of the visibility parameter V yield first-order consensus-dissensus phase transitions in the system.

Another hallmark of the system's behavior under discontinuous phase transitions is the multimodality of the probability distribution of the order parameter. This reflects the system's bistability between ordered and disordered states within the aforementioned hysteresis region. In contrast, second-order phase transitions are characterized by a single peaked probability distribution, whose position naturally depends on the value of social temperature q adopted (CHEN et al., 2017; HARUNARI; OLIVEIRA; FIORE, 2017).

Thus, Fig. 8 displays (a) the time series of $o_N(q, z, V)$ for $q = 0.102$. In this result, $o_N(q, z, V) = \sigma_1 + \sigma_2 + \cdots + \sigma_N$ to highlight the sign variations of the average opinion of the system. Also shown are the probability distributions of the $o_N(q, z, V)$ for different noise parameter values: $q = 0.098, 0.102$ and 0.106 from (b) to (d), respectively. In all cases, we consider Barabási-Albert networks of size $N = 500$ and growth parameter $z = 10$, as well as a visibility parameter of $V = 0.3$. From Fig. 7(d), we expect the system to lie within the hysteretic region for these parameter combinations.

Figure 8 – (a) Time series of the order parameter of the system $o_N(q, z, V) = \sigma_1 + \sigma_2 + \cdots + \sigma_N$ for a Barabási-Albert network of size $N = 500$ and growth parameter $z = 10$. Here, we consider a visibility $V = 0.3$ and a social noise $q = 0.102$. Also included are the probability distributions of the opinionization for (b) $q = 0.098$, (c) $q = 0.102$ and (d) $q = 0.106$. Within the hysteresis region, the system displays a bistable regime, as highlighted by the transitions between ordered and disordered states in the time series and the multimodal behavior of the probability distributions.

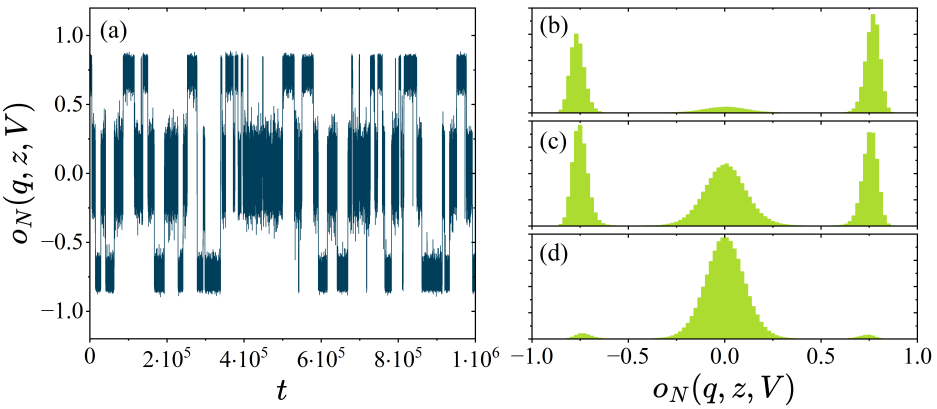

Source: The author (2025).

In fact, Fig. 8(a) displays a clear bistable behavior, showing multiple transitions between ordered and disordered states within the analyzed time frame. The probability distributions in Fig. 8(b)—(d) further confirm this feature, as highlighted by their multimodal shape. Note that for lower values of the noise parameter q, as we approach the non-hysteretic region, the ordered phase starts to dominate the distributions, as shown by the almost not visible peak around zero. Conversely, the disordered phase dominates for higher values of q, and the peaks at the ordered state become less apparent.

Finally, we briefly remark that the finite-size scaling techniques discussed in Sec. 4.5 are inadequate for investigating first-order phase transitions. Such tools suppose the divergence of the system's correlation length, a characteristic feature of continuous phase transitions. Furthermore, as mentioned previously, discontinuous phase transitions are characterized by a hysteretic loop, with forward and backward simulations diverging near the transition. Hence, for first-order phase transitions, we shall adopt the social noise values at which the system becomes fully disordered ($\mathcal{O}_N \sim 0$) as estimators of the critical social temperatures of the system q_{c_F} and q_{c_B}, for forward and backward simulations respectively (CHEN et al., 2017).

Figure 9 – Phase diagrams of the system under first-order phase transitions for several values of (a) visibility parameter and $z = 10$ and (b) several values of the growth parameter and $V = 0.3$. The green (blue) symbols relate to the critical noises found for forward (backward) simulations obtained for networks of size $N = 12000$.

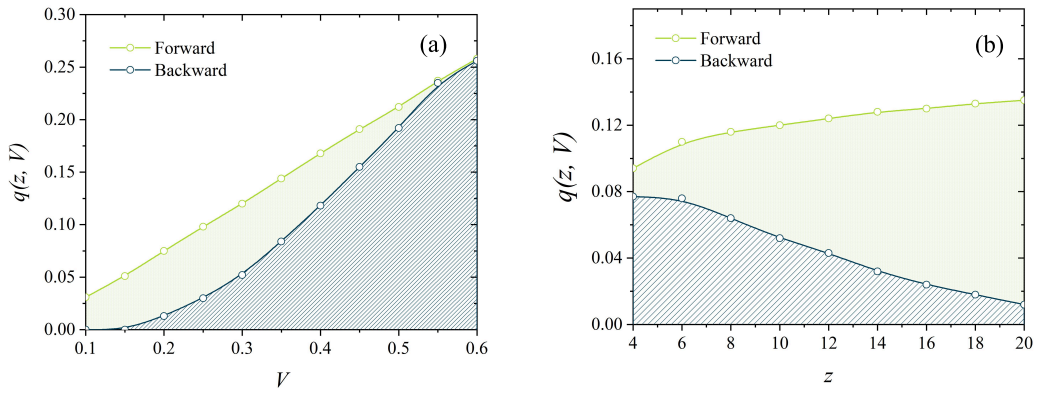

Source: The author (2025).

Thus, Fig. 9 displays the phase diagrams for first-order transitions in the system, highlighted by the diverging critical social noises between forward and backward simulations. The critical social noises were obtained from numerical simulations of social systems with $N = 12000$ individuals. In the figures, the regions above the green data points reflect the disordered state, while the blue regions define the ordered state of the system. Additionally, the green region determines the metastable region, where the order parameter of the system is bistable,

reflecting the aforementioned hysteretic behavior. Furthermore, in Fig. 9(a), we observe that by increasing the visibility parameter, the system gradually shifts towards continuous phase transitions, as shown by the forward and backward critical social noises slowly gravitating toward each other. In contrast, Fig. 9(b) shows that increasing the growth parameter of the network leads to an opposite effect, further pushing the system towards discontinuous order-disorder phase transitions.

5.3 SECOND-ORDER PHASE TRANSITIONS OF THE TWO-STATE MAJORITY-VOTE MODEL WITH BIASED VISIBILITY

Figure 10 – Plots of (a) the opinionization, (b) the noise sensitivity, and (c) the fourth-order Binder cumulant for several network sizes N. Here, we consider a visibility parameter $V = 0.7$ and a growth parameter $z = 8$. The opinionization and noise sensitivity curves display a size-dependent behavior at the critical region, while the fourth-order Binder cumulant is independent of size at the critical social temperature. Lines are just guides to the eyes.

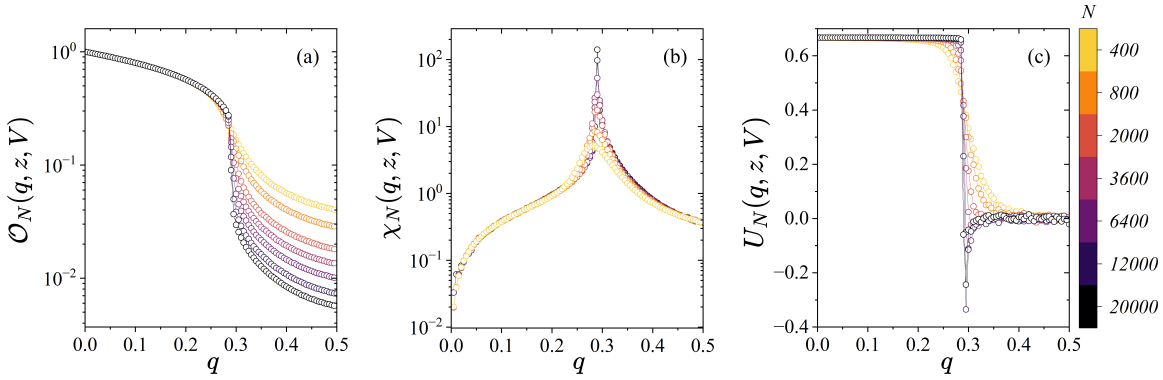

Source: The author (2025).

In Fig. 10, we observe the behavior of the macroscopic quantities of the system, namely (a) the opinionization $\mathcal{O}$, (b) the noise sensitivity χ_N and (c) the fourth-order Binder cumulant U_N for a growth parameter $z = 8$ and visibility $V = 0.7$. As mentioned in Sec. 4.2.1, we expect the order parameter of the system and the noise sensitivity to display a size-dependent behavior near the critical region. In fact, we observe that before the phase transitions take place, the order parameter curves for different system sizes are essentially superposed. In contrast, as we approach the critical melting point of the system, their behavior diverges. This behavior is further observed in the pseudocritical social temperature values, extracted from the maxima of the noise sensitivity curves, which also demonstrate to depend on the system

size. More importantly, we observe that the fourth-order Binder cumulants in Fig. 10(c) are indeed size-independent at the critical temperature, showing a clear crossing at $q = q_c(z, V)$.

Furthermore, Fig. 11 displays a closer detail of the behavior of the fourth-order Binder cumulant U_N near the critical region, for $z = 8$ and $V = 0.7$. Here we consider five distinct system sizes $N = 1000, 2000, 3600, 6400,$ and 12000. Indeed, we observe that curves for different system sizes intersect each other, allowing us to estimate the critical social temperature of the system near the thermodynamic limit $N \to \infty$. Here we obtain $q_c(z = 8, V = 0.7) = 0.2889(1)$.

Figure 11 – Fourth-order Binder cumulant near the critical social temperature for a growth parameter $z = 8$ and a visibility $V = 0.7$. The crossing of the curves for different system sizes indicates the critical social temperature of the system. Lines correspond to B-spline interpolations of the data points.

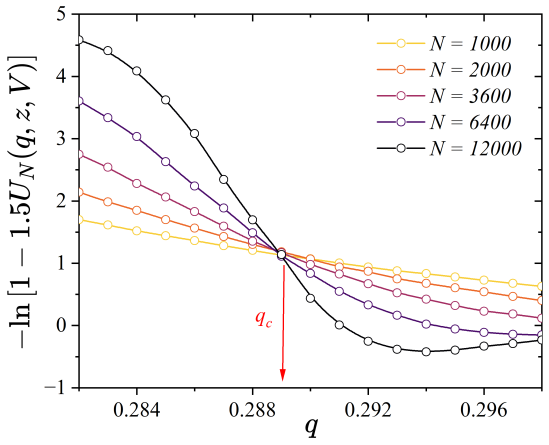

Source: The author (2025).

Following the discussion contained in Sec. 4.5, we expect the order parameter of the system and the noise sensitivity to follow volumetric scaling relations of the form:

$$\mathcal{O}_N(q, z, V) = N^{-\beta/\bar{\nu}}\ \widetilde{\mathcal{O}}(\varepsilon N^{1/\bar{\nu}}), \tag{5.1}$$

$$\chi_N(q, z, V) = N^{\gamma/\bar{\nu}}\ \widetilde{\chi}(\varepsilon N^{1/\bar{\nu}}). \tag{5.2}$$

Hence, by plotting $\ln[\mathcal{O}_N(q_c, z, V)]$ versus $\ln[N]$ and $\ln[\chi_N(q_c, z, V)]$ versus $\ln[N]$, we may extract their corresponding critical exponents $\beta/\bar{\nu}$ and $\gamma/\bar{\nu}$, via a linear fit of the data in a log-log plot. We remark that these exponents relate themselves in a unique fashion, known as the unitary relation of critical exponents (VILELA et al., 2020). Below we recall the result for the unitary relation

$$2\frac{\beta}{\bar{\nu}} + \frac{\gamma}{\bar{\nu}} \equiv \upsilon = 1. \tag{5.3}$$

Furthermore, such mathematical relation acts as a confirmation tool for the accuracy of the calculated critical exponents, regardless of the topological structure adopted.

Thus, Fig. 12 displays the numerical results for (a) the opinionization $\mathcal{O}_N$ and (b) the noise sensitivity χ_N at the critical social temperature for $q = q_c(z, V)$ for $z = 8$ and limited visibility $V = 0.7$. Furthermore, we perform a linear fit for the data, from which we extract $\beta/\bar{\nu} = 0.0371(4)$ and $\gamma/\bar{\nu} = 0.96(2)$. Thus, for the unitary relation, we have:

$$2\frac{\beta}{\bar{\nu}} + \frac{\gamma}{\bar{\nu}} = 1.03(2). \tag{5.4}$$

Hence, our model shows considerable agreement with the unitary relation within the error bars.

Figure 12 – Plots of (a) $\ln[\mathcal{O}_N(q_c, z, V)]$ and (b) $\ln[\chi_N(q_c, z, V)]$ versus $\ln[N]$ for a growth parameter $z = 8$ and a visibility $V = 0.7$. Data points correspond to simulations of different system sizes at the corresponding critical temperature $q_c(z, V)$. Lines relate to linear fits for the data, and their slope corresponds to the respective critical exponents.

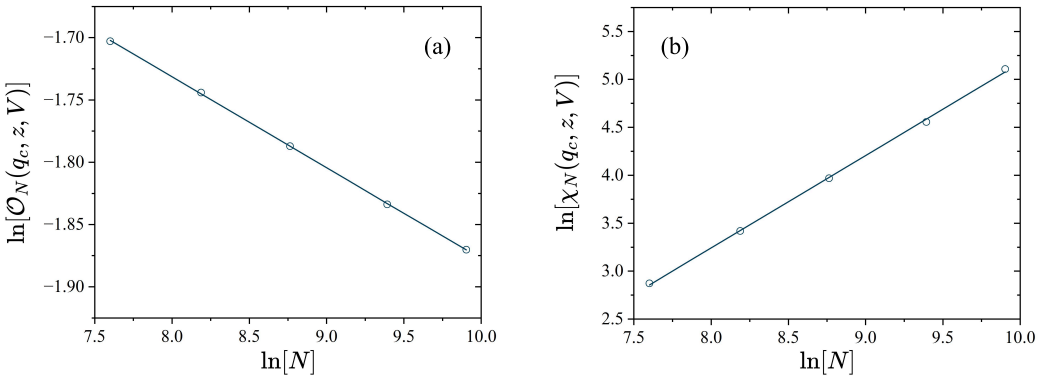

Source: The author (2025).

5.4 DISCUSSIONS AND FUTURE PERSPECTIVES

In the current highly connected status of social media platforms, algorithms tuned for the so-called *click economy* have become important drivers of opinion spreading. Within this context, individuals are often restricted from accessing diverging opinions, being artificially led into fake majorities. Such a scenario has crucial impacts on modern social debates, contributing to the amplification of sensationalism and the formation of echo chambers.

In this context, we investigate an extension of the two-state majority-vote dynamics (OLIVEIRA, 1992; OLIVEIRA; MENDES; SANTOS, 1993) by incorporating biased visibility effects. In our model, we consider a biased visibility parameter V that impacts the individuals' ability to perceive opposing views in some social debate. Hence, individuals shall always be presented

with converging opinions while only viewing distinct ones with probability V. When $V = 0$, an individual shall only consider like-minded neighbors, while for $V = 1$, the visibility bias is effectively removed, and our model reduces to the standard majority-vote formulation.

We place individuals in the nodes of a Barabási-Albert network of social connections, with links representing social connections between them. Furthermore, individuals shall adopt the opinion of the majority of their acquaintances with chance $1 - q$ while following the opposing stance with probability q. The parameter q is termed the social temperature of the system, and it measures the level of social unrest in decision-making processes.

Our simulations display both first-order (discontinuous) and second-order (continuous) order-disorder phase transitions for a critical value of the social temperature $q = q_c(z, V)$ depending on the growth parameter and visibility adopted. Regarding first-order phase transitions, we confirm the presence of a hysteretic behavior near the phase transition as a reflection of the bistability between order and disorder displayed in such systems. Additionally, for second-order phase transitions, we obtain the critical social temperature and the critical exponents for $z = 8$ and $V = 0.7$, confirming the unitary relation (VILELA et al., 2020).

Based on the results presented in this Chapter, we expect to expand our analysis by investigating the behavior of the system under distinct configurations of the control parameters of the system, namely the growth parameter of the system z and the visibility parameter V, furthering our understandings of first and second-order critical phase transitions in biased emergent phenomena of social systems.

6 THREE-STATE GLOBAL-VOTE MODEL ON SCALE-FREE NETWORKS

We now discuss the main results of our investigation on the extension of the three-state majority-vote model to study price formation in financial markets. Our work expands on the current status of the three-state global-vote framework by implementing scale-free network topologies and analyzing their impact on the system's macroscopic observables. We perform Monte Carlo simulations on Barabási-Albert networks of size $N = 10^4$ and distinct values of the growth parameter z.

Within a complex network structure, financial agents are represented as nodes, with links representing socioeconomic connections between them. We consider a financial market comprised of two types of individual strategies for their impact on price dynamics: *noise traders* and *fundamentalists*. The former acts based on the majority of their closest friends, while the latter is influenced by the global behavior of the market. Furthermore, we randomly assign a fraction $1 - f$ as noise traders and the remaining, f, as fundamentalist agents.

We map the agents' financial options at any time t via stochastic variables, which may assume one out of three possible states $s \in \{1, 2, 3\}$, regarding buying, holding, or selling an asset, for example. Moreover, noise traders and fundamentalists shall update their financial options according to the probability prescriptions given by Eq. (4.5) and Eq. (4.13), respectively. Nevertheless, we introduce a noise parameter q that models a level of socioeconomic anxiety present in the market, which shall impact both noise trader and fundamentalist actions.

We recall that in Monte Carlo simulations, N attempts to update the states of randomly selected financial agents define a unit of time—Monte Carlo steps (MCS). In our simulations, we consider a randomized initial state, assigning to each agent any of the three possible states with equal probability. In each simulation, we discard the initial 10^4 MCS as the thermalization time, performing our analysis in the subsequent 10^4 MCS. Additionally, for every pair (q, f), we consider 100 independent Monte Carlo simulations to average over topological disorder. Hence, an effective 10^6 MCS were recorded for every set of parameters (q, f) analyzed.

Based on previous studies of the global-vote model, we expect essential market features to be present when the system is near its socioeconomic melting point $q \approx q_c$ in the absence of contrarian individuals $f = 0$ (VILELA et al., 2019; ZUBILLAGA et al., 2022b; GRANHA et al., 2022). Thus, we shall focus our investigation on systems built near criticality, where fluctuations in the order parameter are more expressive. We shall extract the critical noise values $q_c(z)$ for each

value of the growth parameter considered from previous studies on the three-state majority-vote model on Barabási-Albert networks (VILELA et al., 2020).

In the financial context, we relate time variations of the instantaneous opinionization (4.7) of the system with a financial asset's logarithmic returns (4.14). We remark these quantities were defined in Sec. 4.2.2 and 4.4.1, respectively.

6.1 TIME SERIES OF LOGARITHMIC RETURNS

In Fig. 13, we show the logarithmic returns of NYSE Composite's daily closing values in US dollars from May 28, 1985, to February 03, 2025[1]. Here we highlight that the price dynamics of the NYSE Composite is mainly driven by market supply and demand, similar to any other economic asset. The imbalance between these two economic forces leads to periods of intense price fluctuations, as observed in several time windows in the plot. The curious detail is that such periods of strong volatility tend to be compressed over the time series, an effect known as *volatility clustering* (LUX; MARCHESI, 2000; KRAWIECKI; HOLYST; HELBING, 2002; CONT, 2007). This is an essential feature of real-world financial markets and may be understood via Maldelbrot's observation that "large changes tend to be followed by large changes—of either sign—and small changes tend to be followed by small changes" (MANDELBROT, 1963).

Figure 14 displays the time series of logarithmic returns obtained in our model for two distinct socioeconomic network compositions: (a) $z = 6$ and $q = 0.4550$, and (b) $z = 50$ and $q = 0.5918$. Furthermore, we consider in each case two concentrations of market strategies, $f = 0.20$ and $f = 0.50$. Here we aim to understand the impacts of the growth parameter z and the concentration of fundamentalists f on the market behavior near the critical point.

Thus, Fig. 14(a) illustrates two clearly distinct market phases regarding the concentration of fundamentalist agents in the market: a *strong market phase* for $f = 0.20$, where the time series of log-returns are characterized by several events of high volatility, as depicted by the large spikes in the plot; and a *weak market phase* for $f = 0.50$, where such events are attenuated, as the market becomes stabilized. This observation agrees with previous investigations in the global-vote framework, in which a higher presence of fundamentalist agents drives market stability (VILELA et al., 2019; ZUBILLAGA et al., 2022b; GRANHA et al., 2022).

Conversely, Fig. 14(b) shows that for higher values of the network growth parameter, the log-returns display an intensively volatile behavior for both values of f considered. As a

[1] Data provided by Yahoo Finance

Figure 13 – Time series of the logarithmic returns of NYSE Composite's daily closing values in US dollars. Here we analyzed dates ranging from May 28, 1985, to February 03, 2025, comprising a time window of approximately 10^4 market trading days.

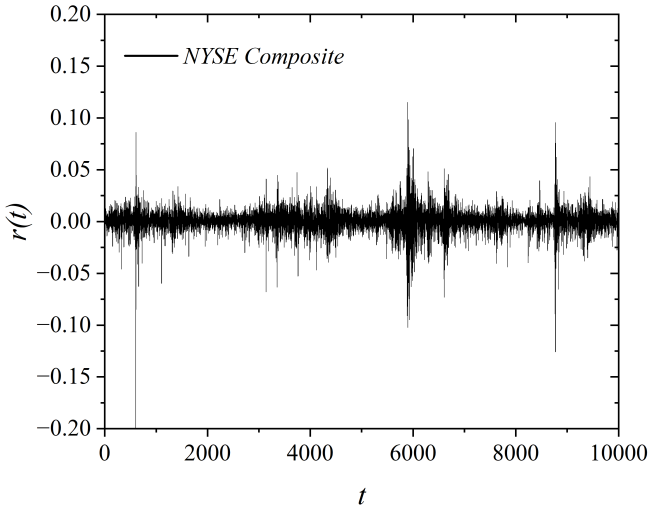

Source: The author (2025).

reflection, the presence of clustered volatility becomes less clear as the system deviates from the expected behavior of real-world financial markets. Hence, we focus our investigation on lower values of the growth parameter z, i.e., lower values of the average connectivity of the network $\langle k \rangle \approx 2z$, for their ability to reproduce key market features (GRANHA et al., 2022).

Figure 14 – Time series of the logarithmic returns $r(t)$ for two sets of network growth and social noise parameters: (a) $z = 6$ and $q = 0.4550$, and (b) $z = 50$ and $q = 0.5918$. Greater concentrations of fundamentalist agents ($f = 0.50$) tend to stabilize log-return fluctuations, as highlighted by the lower spikes in the plot. In contrast, increasing the growth parameter of the network reduces clustered volatility, deviating from real-world market behavior.

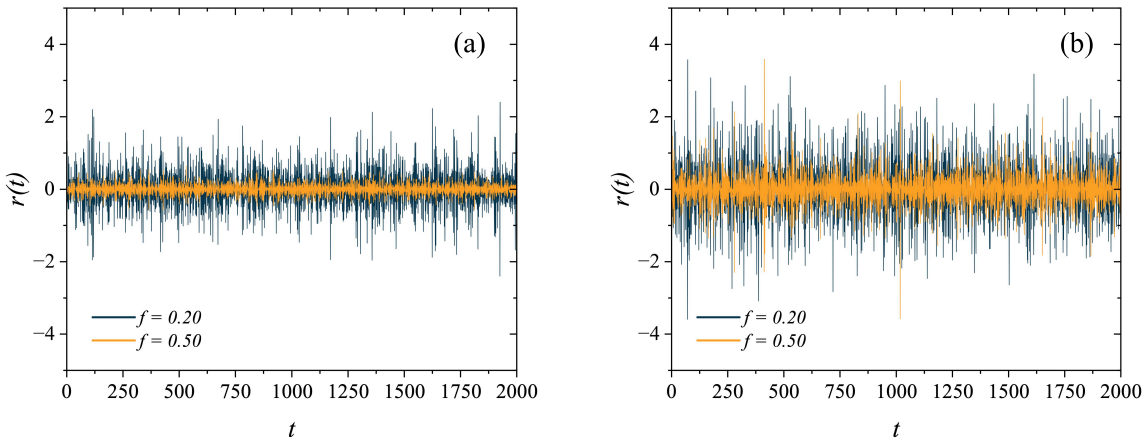

Source: The author (2025).

6.2 VOLATILITY CLUSTERING AND TIME CORRELATIONS

In real-world financial time series, we expect the returns of any given asset to display a short-term memory with a fast correlation decay. This feature is consistent with the efficient market hypothesis, which states the statistical independence of returns in time (PEIRIS; HUNT, 2023; TIMMERMANN; GRANGER, 2004; MALKIEL, 1989). In contrast, correlations in the volatilities tend to persist on much longer time scales as a reflection of volatility clustering effects (MANDELBROT, 1963). Hence, to quantify correlations in the time series of the financial observables, we define the autocorrelation functions of the logarithmic returns and volatility, respectively, as

$$C_{ret}(\tau) = \frac{\sum_{t=\tau+1}^{T} [r(t) - \bar{r}]\,[r(t-\tau) - \bar{r}]}{\sum_{t=1}^{T} [r(t) - \bar{r}]^2}, \tag{6.1}$$

$$A(\tau) = \frac{\sum_{t=\tau+1}^{T} [|r(t)| - |\bar{r}|]\,[|r(t-\tau)| - |\bar{r}|]}{\sum_{t=1}^{T} [|r(t)| - |\bar{r}|]^2}. \tag{6.2}$$

Here, $1 \leq \tau \leq 10^4$ MCS is the time-step difference between observations, $T = 10^4$ MCS is the time of simulation for each network sample, $r(t)$ is the return at a time t and $\bar{r}$ the average return value.

We remark that the function defined in Eq. (6.2) measures non-linear correlations in the volatility time series, and we expect such quantity to be strongly correlated in time. In other words, we empirically anticipate that the volatility autocorrelation functions should display a power law regime for at least two orders of magnitude (MANTEGNA; STANLEY, 2000; VOIT, 2005). Furthermore, due to the finite size of the data, an exponential decay for longer time scales is also expected (BORNHOLDT, 2001; TAKAISHI, 2005).

In Fig. 15, we display (a) the autocorrelation of the volatilities $|r(t)|$ for several market compositions regarding the fraction of fundamentalist agents f and the daily closing values of the NYSE composite. We include financial data comprising approximately 10^4 market trading days from May 28, 1985, to February 03, 2025. Additionally, we present the outcomes for the autocorrelation functions of (b) the volatilities and (c) the returns $r(t)$, averaged over 100 distinct network realizations. In our simulations, we consider a growth parameter $z = 6$ and a socioeconomic noise value $q = 0.4550$.

Thus, Fig. 15(a) displays a qualitative comparison between our simulations and real-world financial time series regarding time correlations of the volatilities. As previously mentioned,

Figure 15 – (a) Qualitative comparison of the autocorrelation function of the volatility $|r(t)|$ for several values of the fraction of fundamentalist agents f, and daily closing values of the NYSE Composite. Here, we consider dates ranging from May 28, 1985, to February 03, 2025, for an average of 10^4 market trading days. The dashed red lines correspond to power-law data fits. Also included are the averaged autocorrelation functions of (b) the volatilities and (c) logarithmic returns $r(t)$, with the red dots representing an exponential fit of the data.

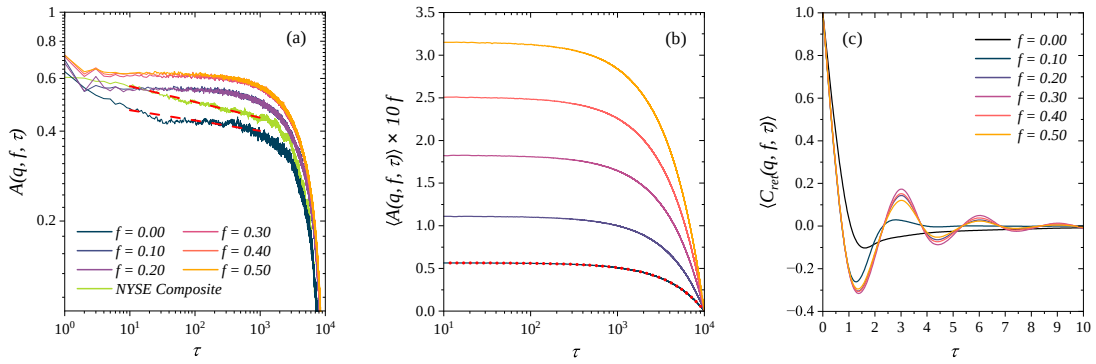

Source: The author (2025).

we expect the autocorrelation of the volatilities to display a power-law behavior for at least two orders of magnitude. Hence, we perform power-law fits for the autocorrelation functions, $A(\tau) \sim \tau^{-\eta}$, over the same time periods $10^1 \leq \tau \leq T^3$. The numerical simulations and empirical data display a quantitative agreement in the order of the decay rate, with power-law exponents $\eta \sim 0.04(1)$ for our simulations with $f = 0.0$ and $\eta_{NYSE} \sim 0.083(1)$ for the NYSE Composite (BORNHOLDT, 2001; TAKAISHI, 2005; ZUBILLAGA et al., 2022b).

In Figure 15(b), we display the average autocorrelation of the volatilities $|r(t)|$ for several values of the fraction of fundamentalists f and 100 market simulations. As expected, results display a persistent correlation in time, presenting a slow exponential decay that spans several orders of magnitude. We confirm this effect via an exponential fit of the data $\langle A(q, f, \tau)\rangle \sim \exp(-\tau/\tau_0)$ for $f = 0.10$, in which we obtain $\tau_0 \approx 7\times10^7$ MCS, with other values of f yielding similar results. We highlight that this behavior is consistent with the expected exponential cut-off due to finite size effects of the available data (GOPIKRISHNAN et al., 1999; MANTEGNA; STANLEY, 2000; BORNHOLDT, 2001; KAIZOJI; BORNHOLDT; FUJIWARA, 2002; TAKAISHI, 2005; VOIT, 2005). Figure 15(a) also exhibits such finite size effect and exponential long-time decay.

Moreover, Fig. 15(c) presents the autocorrelation function C_{ret} for the returns time series $r(t)$ obtained in our simulations for several values of the fundamentalist fraction f, and averaged over 100 network realizations. For enhanced plot visualization, we connect data points

via B-spline curves that interpolate between those, resulting in a smooth, continuous curve. Our results display an excellent agreement with the expected behavior of financial observables, showing that returns are essentially uncorrelated in time as $C_{ret} \to 0$ on a short-time scale of $\tau \sim O(1)$, especially for lower values of f. Hence, our model is in accordance with the efficient market hypothesis (PEIRIS; HUNT, 2023; TIMMERMANN; GRANGER, 2004; MALKIEL, 1989). Yet, for larger fractions of contrarians, C_{ret} displays diminishing anti-persistent oscillations in the short term. This stems from the cyclical behavior of the system, primarily driven by a large fraction of noise contrarians consistently seeking to occupy the instantaneous global minority state (ZUBILLAGA et al., 2022b).

6.3 DISTRIBUTIONS OF LOGARITHMIC RETURNS AND VOLATILITIES

Figure 16 displays the histogram of the log-returns in 10^6 MCS for a growth parameter $z = 6$, noise parameter $q = 0.4550$ and several values of the fraction of fundamentalist agents f. Following our previous discussion, we observe that higher values of the fraction of contrarians are associated with a stabilization of the system. In contrast, for lower values of f, the distributions display fat tails as a reflection of the high number of intense volatility events. Increasing the values of f, distributions' tails become less heavy as they gradually shift towards a Gaussian regime.

Figure 16 – Distribution of logarithmic returns in 10^6 MCS for a growth parameter $z = 6$, socioeconomic anxiety level $q = 0.4550$ and several values of the fraction of fundamentalists f. Increasing the presence of contrarian agents leads to a progressive loss of the distribution tails.

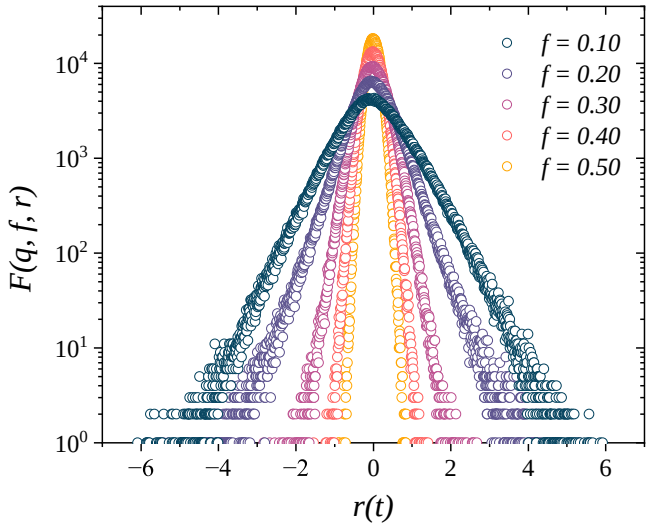

Source: The author (2025).

We quantify the return distributions via a statistical analysis of the data obtained in our simulations. In particular, we calculate the kurtosis $K(z, f)$ for the distributions at distinct market phases, and we obtain $K(6, 0.10) = 4.48$ in the strong market phase and $K(6, 0.50) = 3.12$ in the weak market phase. We remark that for a Gaussian distribution, $K = 3$. Thus, increasing the fraction of contrarian agents f shifts the system's behavior from a leptokurtic regime ($K > 3$) to a mesokurtic regime ($K \approx 3$), deviating from the expected results of real-world financial markets.

For further qualification of the distributions displayed in Fig. 16, we perform comparative quantile-quantile (Q–Q) plots. These plots provide a visual means to assess how well a given distribution aligns with an expected theoretical distribution. If the data points closely follow the theoretical reference line, shown in red, this suggests a strong agreement between the distributions. Thus, Fig. 17 displays comparative Q–Q plots (a) of the logarithmic returns against a normal distribution and (b) of the volatility against an exponential distribution.

In Fig. 17(a), lower values of the fraction of contrarians f (specifically $f \leq 0.30$) show significant nonlinearity, indicating the aforementioned fat-tailed behavior, typical of real-world financial data. As f increases, the distribution tails are lost, as those approaches a Gaussian behavior, as indicated by the close alignment between data points and the reference line. Furthermore, Fig. 17(b) shows that the distributions display deviations in higher quantiles, revealing a slower decay than expected for an exponential distribution. Such behavior implies a higher probability of large values than an exponential distribution would predict, confirming the heavy-tailed regime (MANDELBROT, 1963; GOPIKRISHNAN et al., 1999; CONT, 2001).

We may also quantify the transition observed in the logarithmic return distributions—from a heavy-tailed (leptokurtic) regime into a Gaussian (mesokurtic) regime—as we progressively increase the fraction of contrarians in the system via the coupled exponential family of distributions $P_{\mu,\sigma,\kappa,\alpha}(r)$ (NELSON; UMAROV; KON, 2017; NELSON; KON; UMAROV, 2019). Within this family of functions, we shall refer to the shape parameter κ as the *nonlinear statistical coupling* and to σ as the scale parameter in an interpretation of non-extensive statistical mechanics of complex systems (TSALLIS et al., 2003; QUEIRÓS et al., 2007; NELSON; UMAROV; KON, 2017; NELSON; KON; UMAROV, 2019; BIONDO; PLUCHINO; RAPISARDA, 2015). Moreover, the scale parameter σ measures the spread of the distribution.

We adopt the mean value of the distributions of logarithmic returns as zero for all values of the fraction of fundamentalist agents considered, in agreement with Fig. 19. In this way, we fit the distributions via the symmetric coupled exponential family $P_{\mu,\sigma,\kappa,\alpha}(r) = P_{\sigma,\kappa,\alpha}(r)$,

Figure 17 – Quantile–quantile plots of the distributions of (a) normal versus logarithmic returns $r(t)$ and (b) exponential versus volatility $|r(t)|$. Our simulations consider a growth parameter $z = 6$ and noise parameter $q = 0.4550$ for a time series of 10^6 MCS long. The red line displays the theoretically expected results for each distribution.

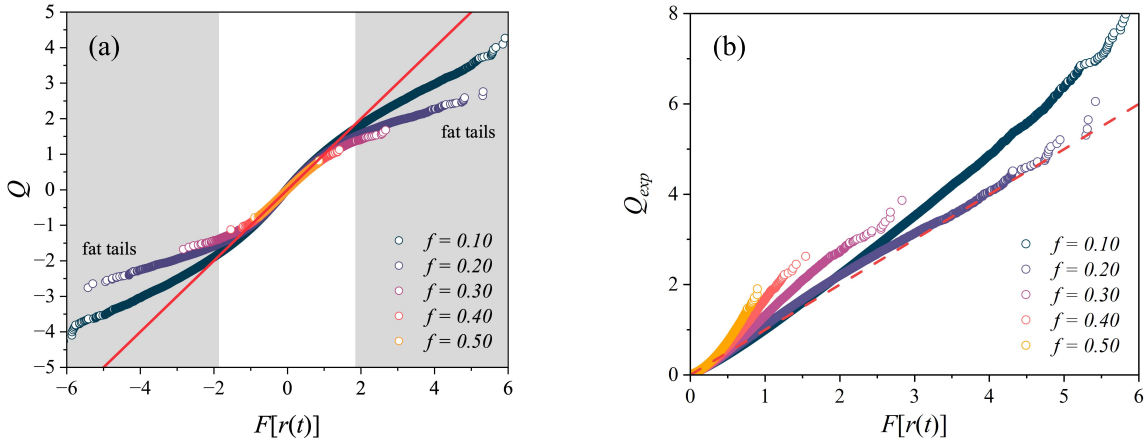

Source: The author (2025).

defined as

$$P_{\sigma,\kappa,\alpha}(r) \equiv \left[Z(\sigma,\kappa,\alpha) \left(1 + \kappa \left| \frac{r}{\sigma} \right|^{\alpha} \right)_{+}^{\frac{1+\kappa}{\alpha\kappa}} \right]^{-1}, \tag{6.3}$$

where $(x)_+ \equiv \max(0, x)$.

We remark that the coupled exponential family of distributions is able to accommodate a wide variety of statistical distributions upon varying its control parameters. In particular, by setting the parameter $\alpha = 2$, we recall the coupled Gaussian distribution: for $\kappa = 0$, we obtain the Gaussian distribution; and for $\kappa > 0$, we have the Student's t distribution. Moreover, in the latter, the degree of freedom ν is related to the shape parameter as $\nu = 1/\kappa$. Thus, the shape parameter κ provides a quantitative measure for the transition between distribution regimes (TSALLIS et al., 2003; QUEIRÓS et al., 2007; BIONDO; PLUCHINO; RAPISARDA, 2015; NELSON; UMAROV; KON, 2017; NELSON; KON; UMAROV, 2019).

Hence, Fig. 18 shows the probability distribution of the volatilities $|r(t)|$ for several values of the fraction of fundamentalists f in 10^6 MCS. Here we consider a network growth parameter $z = 6$ and a noise parameter $q = 0.4550$. The lines correspond to symmetric coupled exponential fits for the data, and the values obtained for the nonlinear coupling parameter κ and scale σ are displayed in Table 1. Our results support the aforementioned behavior shift in the system as we increase the fraction of contrarian agents f. More specifically, it provides a quantitative measure of said shift: as we progressively increase f, we observe that

Figure 18 – Distributions of the volatility $|r(t)|$ for a growth parameter $z = 6$ and socioeconomic noise $q = 0.4550$ in 10^6 MCS. The lines correspond to symmetric coupled exponential fits for the data.

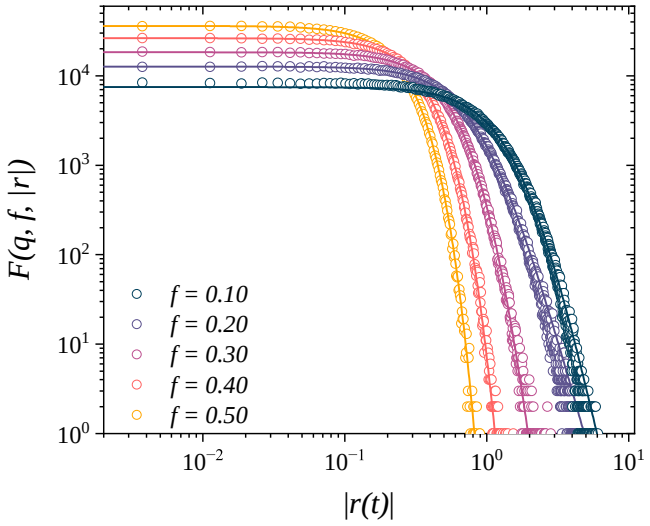

Source: The author (2025).

the nonlinear coupling parameter κ is pushed towards zero, indicating that distributions are indeed transitioning to a Gaussian regime; simultaneously, the scale σ is progressively reduced, indicating smaller spreads as the system becomes more stable. Thus, the coupled exponential fits performed provide an effective numerical measure of the transition from a heavy-tailed (leptokurtic) regime to a Gaussian (mesokurtic) as we increase the presence of fundamentalist agents in the system.

Figure 19 displays the cumulative distribution of logarithmic returns Φ for $z = 6$ and $q = 0.4550$ in 10^6 MCS. The inset shows an approximation of the plot around zero. As previously mentioned, we observe that the mean of the distributions remains zero, irrespective of the fraction of contrarian agents f present in the market.

Table 1 – Values obtained for the scale σ and shape κ parameters in the coupled exponential fits for the data. Here we consider a network growth parameter $z = 6$, a socioeconomic anxiety level $q = 0.4550$ and several values of the fraction of fundamentalists f.

Fraction f	0.10	0.20	0.30	0.40	0.50
Shape κ	0.16(3)	0.205(2)	0.070(2)	0.024(2)	0.017(1)
Scale σ	0.74(1)	0.4499(4)	0.3204(3)	0.2258(3)	0.1651(1)

Source: The author (2025).

Figure 19 – Cumulative distribution of logarithmic returns Φ in 10^6 MCS for $z = 6$, $q = 0.4550$ and several values of the fraction of contrarians f. In the inset, we show the behavior of Φ for $r(t)$ near zero. We confirm that for all values of f considered the mean of the distributions remains zero.

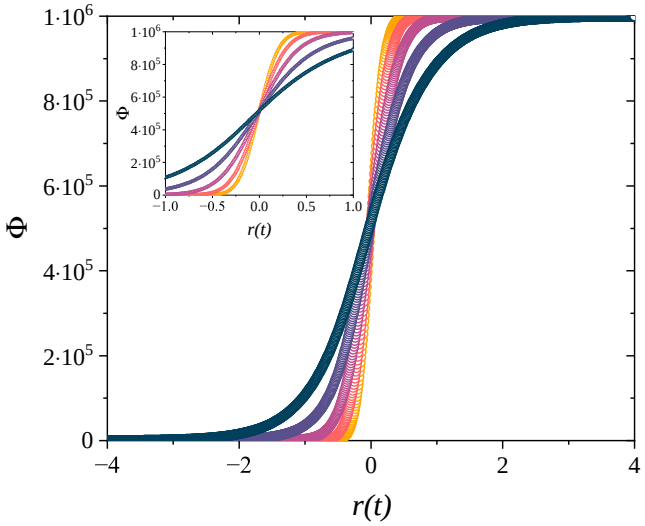

Source: The author (2025).

We also extensively investigate the model's behavior under several market configurations, which depend on the network growth parameter z, the socioeconomic anxiety level q and the fraction of fundamentalists f. In Fig. 20, we show a multi-plot table of the histograms of logarithmic returns for such micro-state configurations defined by (q, f, z) triplets, all of which investigated near the criticality of the system $q \approx q_c(z)$ for each value of z considered. Columns correspond to values of q, below criticality (left), at criticality (center), and above criticality (right), while rows investigate the effects of different growth parameter z values. We remark that the selected noise values above and below criticality are $q = q_c(z) \pm 0.1$.

Moving vertically (from top to bottom) in the plot along a column, we observe the strong effects of increasing the growth parameter of the network in the return distributions. In particular, as we increase z, we note that the spreads and tails of the distributions tend to increase slightly, suggesting broader return distributions. Nevertheless, increasing f leads to the usual progressive loss of tails in the return distributions. We remark that this behavior may be observed for most cells in the grid, highlighting the model's robustness over a wide range of scale-free networks near criticality.

Nevertheless, we highlight critical outliers of this behavior, especially for noise parameter values that deviate from criticality. For instance, the distributions for $f = 0.10$ below criticality for $z \geq 4$, which do not display the expected fat-tailed behavior, become highly peaked around

$r = 0$. Similarly, the distributions for $z = 8$ and 10 above criticality show that higher fractions of contrarians still display a heavy-tailed behavior instead of the expected transition to a Gaussian regime. Hence, this result conforms with our choice for the growth parameter z and noise parameter $q = q_c$ values used throughout our analysis.

Figure 20 – Distributions of logarithmic returns $r(t)$ in 10^6 MCS for different combinations of network growth and noise parameter values (z, q) in the vicinity of $q_c(z)$ and several values of the fraction of fundamentalists: $f = 0.10, 0.20, 0.30, 0.40$, and 0.50 in dark blue, purple, pink, orange, and yellow, respectively. Rows depict distinct values of the growth parameter $z = 2, 4, 6, 8$, and 10, from top to bottom, while columns correspond, respectively, to values of q below, at and above criticality for each value of z considered.

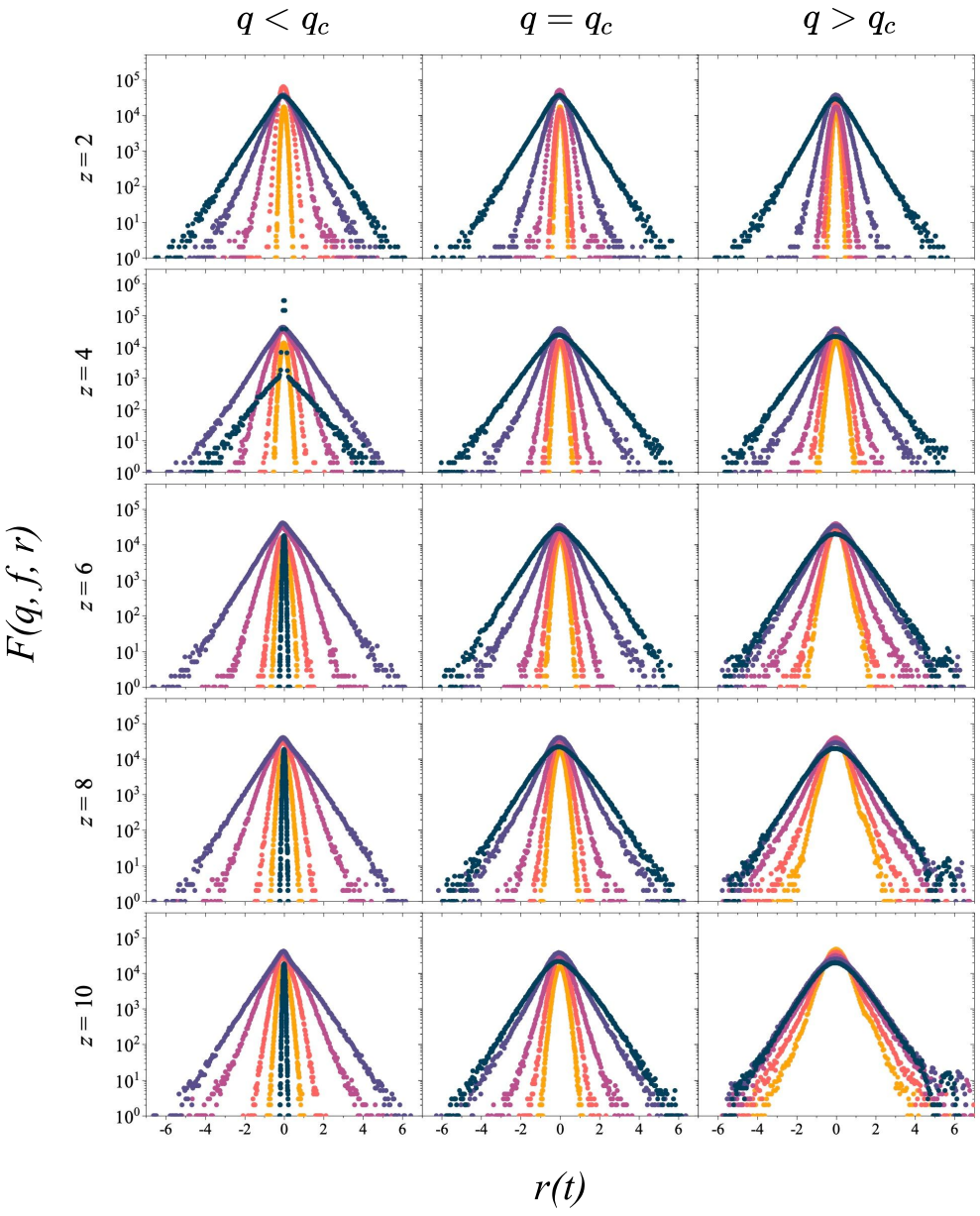

Source: The author (2025).

6.4 DISCUSSIONS AND CONCLUDING REMARKS

The three-state global-vote framework proposes to investigate price formation in economic systems through the lens of social psychology (ZUBILLAGA et al., 2022b). In particular, it considers a microscopic stochastic model in which agents may adopt three financial options regarding buying, selling or remaining inactive at any given time. Furthermore, as an agent-based model, it introduces two distinct financial strategies in the market: noise traders who perform financial actions based on local interactions with their nearest neighbors and tend to agree with the state of the *local majority* with probability $1 - q$; and fundamentalists, or contrarian traders, whose decisions are based on the financial index, and thus tend to follow the state of the *global minority* of the system with probability $1-q$. The parameter q quantifies a level of socioeconomic anxiety inherent to stock markets.

In this work, we extend the previous results on the three-state global-vote model (ZUBILLAGA et al., 2022b) by considering the implementation of Barabási-Albert networks. Within such structures, individuals are represented as nodes, with links regarding socioeconomic relations among them. Effectively, this work investigates how the control parameter of Barabási-Albert networks, namely the growth parameter z, impacts the macroscopic financial observables.

By relating changes in the instantaneous order parameter of this system to price fluctuations in stock markets, our model is able to reproduce the main stylized facts of real-world financial markets (BORNHOLDT, 2001; KAIZOJI; BORNHOLDT; FUJIWARA, 2002; TAKAISHI, 2005). In particular, our results demonstrate key features such as fat-tailed distributions of returns, volatility clustering, and long-term memory of the volatility, consistent with the efficient market hypothesis and previous investigations (VILELA et al., 2019; ZUBILLAGA et al., 2022b; GRANHA et al., 2022).

Hence, our model considers three main factors as drivers of the macroscopic behavior of financial observables: a heterogeneous composition of agents with different strategies, a scale-free network of economic interactions, and a finite level of socioeconomic uncertainty near consensus-dissensus criticality. We highlight that despite the model's simplicity, it is remarkably capable of shedding light on the underlying mechanisms at play in such complex systems as financial markets.

7 CONCLUSION AND FINAL REMARKS

This work aims to explore the underlying mechanisms that drive emergent behaviors in social and economic systems. At the center of this study lies the premise that large-scale collective phenomena—such as consensus formation in public debates or price fluctuations in financial markets—arise from local interactions between individuals. To capture the effects of micro-level interactions, we adopted agent-based models, which offer a robust framework for linking microscopic decision-making processes to macroscopic observables.

Within this context, two key research areas constitute the fundamental backbone of our work: statistical mechanics and network science. The theoretical foundations of statistical physics provide a natural framework for analyzing systems composed of a large number of interacting individuals by shifting the focus from individual components to macroscopic properties. Similarly, networks are a natural feature of human interactions, in which network science provides an essential tool for assessing how these underlying structures fundamentally shape individual decisions. Hence, statistical mechanics and complex networks constitute crucial elements in our analysis as we aim to explore how local interactions propagate through large-scale systems, influencing consensus formation, market stability, and information diffusion.

This thesis focuses on two central problems: the role of biased visibility algorithms in opinion formation and the impact of distinct financial strategies on price dynamics. In the first part, we introduce a variant of the two-state majority-vote model incorporating a visibility parameter V, which restricts an individual's exposure to opposing viewpoints. This modification is inspired by the urgent need to assess the possible side effects of algorithmic filtering on modern social media platforms that foster polarization and opinion echo chambers. The second part of the study extended the three-state global-vote model to investigate how financial decisions evolve within a complex network of socioeconomic relations.

Real-world networks are rarely regular. Their structures are typically heterogeneous, composed of a mixture of sparsely and densely connected nodes within a wide variety of complex systems. One of the most striking features observed in many of these networks is the presence of hubs—nodes with an exceptionally high number of connections. This is a hallmark of scale-free networks, a topological structure that underlies systems as diverse as social media platforms, financial markets, and even neural connections in the brain. Hence, we implement scale-free networks built with the Barabási-Albert algorithm as the substrate for the socioeco-

nomic interactions in our investigation.

For the opinion dynamics model, our findings revealed strikingly different behaviors depending on the degree of visibility bias. As the visibility parameter V decreases, phase transitions in the system shift from continuous (second-order) to abrupt and discontinuous (first-order). In this regime, we confirmed the presence of hysteresis loops, indicating bistable behavior where the system fluctuates between ordered and disordered states. Furthermore, within the second-order transition region, our results remained consistent with the unitary relations of critical exponents, validating the robustness of our simulations.

In the context of financial modeling, our results demonstrate that the three-state global-vote model successfully reproduces key stylized facts of real-world markets, including fat-tailed return distributions and volatility clustering. We identify three primary factors driving market behavior: the fraction of contrarian traders, the level of socioeconomic anxiety, and the network's topological structure. Our results suggest that real-world market fluctuations arise in systems with lower fractions of fundamentalist traders and networks with relatively low average connectivity. These findings not only align with previous studies on the global-vote model but also extend its applicability to a broader class of network structures, offering new insights into the role of connectivity in financial dynamics.

Ultimately, this work investigates the influence of social psychology in shaping critical social and economic emergent behavior. The majority-vote and global-vote frameworks offer a simple yet powerful approach to the study of real-world complex systems in which individual actions lead to exuberant collective phenomena. Our results shed light on the possible mechanisms that shape socioeconomic phenomena, allowing us to enrich the current knowledge of such complex systems without using an extensive number of variables.

REFERENCES

ALBERT, R. Scale-free networks in cell biology. *Journal of cell science*, Company of Biologists, v. 118, n. 21, p. 4947–4957, 2005.

ASCH, S. E. Effects of group pressure upon the modification and distortion of judgments. In: *Organizational influence processes*. [S.l.]: Routledge, 2016. p. 295–303.

BALL, P. The physical modelling of society: a historical perspective. *Physica A: Statistical Mechanics and its Applications*, Elsevier, v. 314, n. 1-4, p. 1–14, 2002.

BARABÁSI, A. L. *Network Science*. Cambridge University Press, 2016. ISBN 9781107076266. Available at: <https://networksciencebook.com/>.

BARABÁSI, A.-L.; ALBERT, R. Statistical mechanics of complex networks. *Reviews of Modern Physics*, v. 74, p. 47–97, 2002.

BARABÁSI, A.-L.; ALBERT, R.; JEONG, H. Scale-free characteristics of random networks: the topology of the world-wide web. *Physica A: Statistical Mechanics and its Applications*, Elsevier, v. 281, n. 1-4, p. 69–77, 2000.

BASSETT, D. S.; BULLMORE, E. Small-world brain networks. *The neuroscientist*, Sage Publications Sage CA: Thousand Oaks, CA, v. 12, n. 6, p. 512–523, 2006.

BIKHCHANDANI, S.; HIRSHLEIFER, D.; WELCH, I. A theory of fads, fashion, custom, and cultural change as informational cascades. *Journal of Political Economy*, v. 100, n. 5, p. 992–1026, 1992.

BINDER, K. Finite size scaling analysis of ising model block distribution functions. *Zeitschrift für Physik B Condensed Matter*, Springer, v. 43, p. 119–140, 1981.

BIONDO, A. E.; PLUCHINO, A.; RAPISARDA, A. Modeling financial markets by self-organized criticality. *Physical Review E*, APS, v. 92, n. 4, p. 042814, 2015.

BORNHOLDT, S. Expectation bubbles in a spin model of markets: Intermittency from frustration across scales. *International Journal of Modern Physics C*, World Scientific, v. 12, n. 05, p. 667–674, 2001.

BOTET, R.; JULLIEN, R.; PFEUTY, P. Size scaling for infinitely coordinated systems. *Physical Review Letters*, APS, v. 49, n. 7, p. 478, 1982.

BRUNSTEIN, A.; TOMÉ, T. Universal behavior in an irreversibe model with C_{3v} symmetry. *Physical Review E*, v. 60, n. 4, p. 3666–3669, 1999.

CAMPOS, P. R. A.; OLIVEIRA, V. M. de; MOREIRA, F. G. B. Small-world effects in the majority-vote model. *Physical Review E*, APS, v. 67, n. 2, p. 026104, 2003.

CARDY, J. *Scaling and renormalization in statistical physics*. [S.l.]: Cambridge university press, 1996.

CASTELLANO, C.; MUÑOZ, M. A.; PASTOR-SATORRAS, R. Nonlinear q-voter model. *Physical Review E—Statistical, Nonlinear, and Soft Matter Physics*, APS, v. 80, n. 4, p. 041129, 2009.

CHAKRABORTI, A.; TOKE, I. M.; PATRIARCA, M.; ABERGEL, F. Econophysics review: Ii. agent-based models. *Quantitative Finance*, Taylor & Francis, v. 11, n. 7, p. 1013–1041, 2011.

CHEN, H.; SHEN, C.; ZHANG, H.; LI, G.; HOU, Z.; KURTHS, J. First-order phase transition in a majority-vote model with inertia. *Physical Review E*, APS, v. 95, n. 4, p. 042304, 2017.

CONT, R. Empirical properties of asset returns: stylized facts and statistical issues. *Quantitative finance*, IOP Publishing, v. 1, n. 2, p. 223, 2001.

CONT, R. Volatility clustering in financial markets: empirical facts and agent-based models. In: *Long memory in economics*. [S.l.]: Springer, 2007. p. 289–309.

CONT, R.; BOUCHAUD, J.-P. Herd behavior and aggregate fluctuations in financial markets. *Macroeconomic dynamics*, Cambridge University Press, v. 4, n. 2, p. 170–196, 2000.

COOPER, I.; MONDAL, A.; ANTONOPOULOS, C. G. A sir model assumption for the spread of covid-19 in different communities. *Chaos, Solitons & Fractals*, Elsevier, v. 139, p. 110057, 2020.

DAY, R. H.; HUANG, W. Bulls, bears and market sheep. *Journal of Economic Behavior & Organization*, v. 14, p. 299–329, 1990.

DEFFUANT, G.; NEAU, D.; AMBLARD, F.; WEISBUCH, G. Mixing beliefs among interacting agents. *Advances in Complex Systems*, World Scientific, v. 3, n. 01n04, p. 87–98, 2000.

ENCINAS, J. M.; HARUNARI, P. E.; OLIVEIRA, M. de; FIORE, C. E. Fundamental ingredients for discontinuous phase transitions in the inertial majority vote model. *Scientific reports*, Nature Publishing Group UK London, v. 8, n. 1, p. 9338, 2018.

ERDÖS, P.; RÉNYI, A. On random graphs i. *Publ. math. debrecen*, v. 6, n. 290-297, p. 18, 1959.

ERDÖS, P.; RÉNYI, A. On the evolution of random graphs. *Publications of the Mathematical Institute of the Hungarian Academy of Sciences*, Citeseer, v. 5, n. 1, p. 17–60, 1960.

FELDHOFF, J. H.; LANGE, S.; VOLKHOLZ, J.; DONGES, J. F.; JÜRGEN, J. K.; GERSTENGARBE, F.-W. Complex networks for climate model evaluation with application to statistical versus dynamical modeling of south american climate. *Climate Dynamics*, Springer, v. 44, n. 5-6, p. 1567–1581, 2015.

GALAM, S. Majority rule, hierarchical structures, and democratic totalitarianism: A statistical approach. *Journal of Mathematical Psychology*, Elsevier, v. 30, n. 4, p. 426–434, 1986.

GALAM, S. Social paradoxes of majority rule voting and renormalization group. *Journal of Statistical Physics*, Springer, v. 61, p. 943–951, 1990.

GALAM, S. Application of statistical physics to politics. *Physica A: Statistical mechanics and its applications*, Elsevier, v. 274, n. 1-2, p. 132–139, 1999.

GALAM, S. Real space renormalization group and totalitarian paradox of majority rule voting. *Physica A: Statistical Mechanics and its Applications*, Elsevier, v. 285, n. 1-2, p. 66–76, 2000.

GALAM, S. Minority opinion spreading in random geometry. *The European Physical Journal B-Condensed Matter and Complex Systems*, Springer, v. 25, p. 403–406, 2002.

GALAM, S. Sociophysics: A review of galam models. *International Journal of Modern Physics C*, v. 19, p. 409, 2008.

GALAM, S. *Sociophysics: A Physicist's Modeling of Psycho-political Phenomena*. New York: Springer, 2012. 449 p.

GALAM, S. Modeling the forming of public opinion: an approach from sociophysics. *Global Economics and Management Review*, Elsevier, v. 18, n. 1, p. 2–11, 2013.

GALAM, S. The invisible hand and the rational agent are behind bubbles and crashes. *Chaos, Solitons & Fractals*, Elsevier, v. 88, p. 209–217, 2016.

GALAM, S.; GEFEN, Y.; SHAPIR, Y. Sociophysics: A new approach of sociological collective behaviour. i. mean-behaviour description of a strike. *Journal of Mathematical Sociology*, Taylor & Francis, v. 9, n. 1, p. 1–13, 1982.

GANDHMAL, D. P.; KUMAR, K. Systematic analysis and review of stock market prediction techniques. *Computer Science Review*, Elsevier, v. 34, p. 100190, 2019.

GOPIKRISHNAN, P.; PLEROU, V.; AMARAL, L. A. N.; MEYER, M.; STANLEY, H. E. Scaling of the distribution of fluctuations of financial market indices. *Physical Review E*, v. 60, p. 5305, 1999.

GRANHA, M. F. B.; VILELA, A. L. M.; WANG, C.; NELSON, K. P.; STANLEY, H. E. Opinion dynamics in financial markets via random networks. *Proceedings of the National Academy of Sciences*, National Acad Sciences, v. 119, n. 49, 2022.

GRINSTEIN, G.; JAYAPRAKASH, C.; HE, Y. Statistical mechanics of probabilistic cellular automata. *Physical review letters*, APS, v. 55, n. 23, p. 2527, 1985.

HARUNARI, P. E.; OLIVEIRA, M. de; FIORE, C. E. Partial inertia induces additional phase transition in the majority vote model. *Physical Review E*, APS, v. 96, n. 4, p. 042305, 2017.

HONG, H.; HA, M.; PARK, H. Finite-size scaling in complex networks. *Physical review letters*, APS, v. 98, n. 25, p. 258701, 2007.

HONG, H.; KUBIK, J. D.; STEIN, J. C. Thy neighbor's portfolio: word-of-mouth effects in the holdings of trades of money managers. *The Journal of Finance*, LX, n. 6, p. 2801–2824, 2005.

JIANG, W. Applications of deep learning in stock market prediction: recent progress. *Expert Systems with Applications*, Elsevier, v. 184, p. 115537, 2021.

KAIZOJI, T.; BORNHOLDT, S.; FUJIWARA, Y. Dynamics of price and trading volume in a spin model of stock markets with heterogeneous agents. *Physica A: Statistical Mechanics and its Applications*, Elsevier, v. 316, n. 1-4, p. 441–452, 2002.

KAUFFMAN, S. A. *The origins of order: Self-organization and selection in evolution*. [S.l.]: Oxford University Press, 1993.

KIMOTO, T.; ASAKAWA, K.; YODA, M.; TAKEOKA, M. Stock market prediction system with modular neural networks. In: IEEE. *1990 IJCNN international joint conference on neural networks*. [S.l.], 1990. p. 1–6.

KOREN, Y.; RENDLE, S.; BELL, R. Advances in collaborative filtering. *Recommender systems handbook*, Springer, p. 91–142, 2021.

KRAWIECKI, A.; HOLYST, J. A.; HELBING, D. Volatility clustering and scaling for financial time series due to attractor bubbling. *Physical Review Letters*, v. 89, n. 15, p. 158701, 2002.

LANDAU, D.; BINDER, K. *A guide to Monte Carlo simulations in statistical physics*. [S.l.]: Cambridge university press, 2021.

LIMA, F. W. S. Majority-vote on undirected barabási-albert networks. *Commun. Comput. Phys*, v. 2, p. 358–366, 2007.

LIMA, F. W. S.; SOUSA, A. O.; SUMUOR, M. A. Majority-vote on directed erdős–rényi random graphs. *Physica A: Statistical Mechanics and its Applications*, Elsevier, v. 387, n. 14, p. 3503–3510, 2008.

LONG, J. B. D.; SHLEIFER, A.; SUMMERS, L. H.; WALDMANN, R. J. Noise trader risk in financial markets. *Journal of Political Economy*, v. 98, n. 4, p. 703–738, 1990.

LUX, T.; MARCHESI, M. Scaling and criticality in a stochastic multi-agent model of a financial market. *Nature*, Nature Publishing Group UK London, v. 397, n. 6719, p. 498–500, 1999.

LUX, T.; MARCHESI, M. Volatility clustering in financial markets: a microsimulation of interacting agents. *International Journal of Theoretical and Applied Finance*, v. 3, n. 4, p. 675–702, 2000.

MALKIEL, B. G. Efficient market hypothesis. In: *Finance*. [S.l.]: Springer, 1989. p. 127–134.

MANDELBROT, B. The Variation of Certain Speculative Prices. *The Journal of Business*, v. 36, p. 394–394, 1963.

MANTEGNA, R. N.; STANLEY, H. E. *An Introduction to Econophysics: Correlations and Complexity in Finance*. Cambridge (United Kingdom): Cambridge University Press, 2000. 148 p.

MELO, D. F.; PEREIRA, L. F.; MOREIRA, F. B. The phase diagram and critical behavior of the three-state majority-vote model. *Journal of Statistical Mechanics: Theory and Experiment*, IOP Publishing, v. 2010, n. 11, p. P11032, 2010.

METROPOLIS, N.; ROSENBLUTH, A. W.; ROSENBLUTH, M. N.; TELLER, A. H.; TELLER, E. Equation of state calculations by fast computing machines. *The journal of chemical physics*, American Institute of Physics, v. 21, n. 6, p. 1087–1092, 1953.

METROPOLIS, N.; ULAM, S. The monte carlo method. *Journal of the American statistical association*, Taylor & Francis, v. 44, n. 247, p. 335–341, 1949.

MILGRAM, S. The small world problem. *Psychology today*, New York, v. 2, n. 1, p. 60–67, 1967.

MITCHELL, M. *Complexity: A guided tour*. [S.l.]: Oxford University Press, 2009.

NELSON, K. P.; KON, M. A.; UMAROV, S. R. Use of the geometric mean as a statistic for the scale of the coupled gaussian distributions. *Physica A: Statistical Mechanics and its Applications*, Elsevier, v. 515, p. 248–257, 2019.

NELSON, K. P.; UMAROV, S. R.; KON, M. A. On the average uncertainty for systems with nonlinear coupling. *Physica A: Statistical Mechanics and its Applications*, v. 468, p. 30–43, 2017.

NEWMAN, M. E. J. The structure and function of complex networks. *Society for Industrial and Applied Mathematics Review*, v. 45, p. 167–256, 2003.

OLIVEIRA, I. V.; WANG, C.; DONG, G.; DU, R.; FIORE, C. E.; VILELA, A. L.; STANLEY, H. E. Entropy production on cooperative opinion dynamics. *Chaos, Solitons & Fractals*, Elsevier, v. 181, p. 114694, 2024.

OLIVEIRA, M. J. de. Isotropic majority-vote model on a square lattice. *Journal of Statistical Physics*, Springer, v. 66, p. 273–281, 1992.

OLIVEIRA, M. J. de; MENDES, J. F. F.; SANTOS, M. A. Nonequilibrium spin models with ising universal behaviour. *Journal of Physics A: Mathematical and General*, IOP Publishing, v. 26, n. 10, p. 2317, 1993.

ONSAGER, L. Crystal statistics. i. a two-dimensional model with an order-disorder transition. *Physical Review*, APS, v. 65, n. 3-4, p. 117, 1944.

PEIRIS, S.; HUNT, R. Revisiting the autocorrelation of long memory time series models. *Mathematics*, MDPI, v. 11, n. 4, p. 817, 2023.

PEREIRA, L. F. C.; MOREIRA, F. G. B. Majority-vote model on random graphs. *Physical Review E*, APS, v. 71, n. 1, p. 016123, 2005.

QUEIRÓS, S.; MOYANO, L. G.; SOUZA, J. de; TSALLIS, C. A nonextensive approach to the dynamics of financial observables. *The European Physical Journal B*, v. 55, n. 2, p. 161–167, 2007.

QUETELET, A. Recherches sur le penchant au crime aux différens ages. *Mémoires de l'Académie royale de Belgique*, Persée-Portail des revues scientifiques en SHS, v. 7, n. 1, p. 1–87, 1832.

RAAFAT, R. M.; CHATER, N.; FRITH, C. Herding in humans. *Trends in Cognitive Sciences*, v. 13, n. 10, p. 420–428, 2009.

REICHL, L. E. *A modern course in statistical physics*. [S.l.]: John Wiley & Sons, 2016.

REIJNEVELD, J. C.; PONTEN, S. C.; BERENDSE, H. W.; STAM, C. J. The application of graph theoretical analysis to complex networks in the brain. *Clinical neurophysiology*, Elsevier, v. 118, n. 11, p. 2317–2331, 2007.

SANTOS, M. A.; TEIXEIRA, S. Anisotropic voter model. *Journal of statistical physics*, Springer, v. 78, n. 3-4, p. 963–970, 1995.

SOOD, V.; REDNER, S. Voter model on heterogeneous graphs. *Physical review letters*, APS, v. 94, n. 17, p. 178701, 2005.

SPORNS, O.; TONONI, G.; KÖTTER, R. The human connectome: a structural description of the human brain. *PLoS computational biology*, Public Library of Science San Francisco, USA, v. 1, n. 4, p. e42, 2005.

STANLEY, H. E. *Phase transitions and critical phenomena*. [S.l.]: Clarendon Press, Oxford, 1971.

STAUFFER, D. Social applications of two-dimensional ising models. *American Journal of Physics*, AIP Publishing, v. 76, n. 4, p. 470–473, 2008.

STAUFFER, D.; SOUSA, A. O.; OLIVEIRA, S. M. D. Generalization to square lattice of sznajd sociophysics model. *International Journal of Modern Physics C*, World Scientific, v. 11, n. 06, p. 1239–1245, 2000.

STROGATZ, S. H. Exploring complex networks. *Nature*, v. 410, p. 268–276, 2001.

SZNAJD-WERON, K.; SZNAJD, J. Opinion evolution in closed community. *International Journal of Modern Physics C*, World Scientific, v. 11, n. 06, p. 1157–1165, 2000.

SZNAJD-WERON, K.; WERON, R. A simple model of price formation. *International Journal of Modern Physics C*, World Scientific, v. 13, n. 01, p. 115–123, 2002.

TAKAISHI, T. Simulations of financial markets in a potts-like model. *International Journal of Modern Physics C*, World Scientific, v. 16, n. 08, p. 1311–1317, 2005.

TIMMERMANN, A.; GRANGER, C. W. Efficient market hypothesis and forecasting. *International Journal of forecasting*, Elsevier, v. 20, n. 1, p. 15–27, 2004.

TOMÉ, T. *Dinâmica Estocástica e Irreversibilidade Vol. 35*. [S.l.]: Edusp, 2001.

TOMÉ, T.; PETRI, A. Cumulants of the three-state potts model and of nonequilibrium models with C_{3v} symmetry. *Journal of Physics A: Mathematical and General*, v. 35, p. 5379–5390, 2002.

TRAVERS, J.; MILGRAM, S. An experimental study of the small world problem. In: *Social networks*. [S.l.]: Elsevier, 1977. p. 179–197.

TSALLIS, C.; ANTENEODO, C.; BORLAND, L.; OSORIO, R. Nonextensive statistical mechanics and economics. *Physica A: Statistical Mechanics and its Applications*, Elsevier, v. 324, n. 1-2, p. 89–100, 2003.

VIEIRA, A. R.; CROKIDAKIS, N. Phase transitions in the majority-vote model with two types of noises. *Physica A: Statistical Mechanics and its Applications*, Elsevier, v. 450, p. 30–36, 2016.

VILELA, A. L.; ZUBILLAGA, B. J.; WANG, C.; WANG, M.; DU, R.; STANLEY, H. E. Three-state majority-vote model on scale-free networks and the unitary relation for critical exponents. *Scientific Reports*, Nature Publishing Group UK London, v. 10, n. 1, p. 8255, 2020.

VILELA, A. L. M.; MOREIRA, F. G. B. Majority-vote model with different agents. *Physica A: Statistical Mechanics and its Applications*, v. 388, p. 4171, 2009.

VILELA, A. L. M.; MOREIRA, F. G. B.; SOUZA, A. J. F. de. Majority-vote model with a bimodal distribution of noises. *Physica A: Statistical Mechanics and its Applications*, Elsevier, v. 391, n. 24, p. 6456–6462, 2012.

VILELA, A. L. M.; PEREIRA, L. F. C.; DIAS, L.; STANLEY, H. E.; da Silva, L. R. Majority-vote model with limited visibility: An investigation into filter bubbles. *Physica A: Statistical Mechanics and its Applications*, Elsevier, v. 563, p. 125450, 2021. ISSN 0378-4371.

VILELA, A. L. M.; STANLEY, H. E. Effect of strong opinions on the dynamics of the majority-vote model. *Scientific reports*, Nature Publishing Group, v. 8, n. 1, p. 1–8, 2018.

VILELA, A. L. M.; WANG, C.; NELSON, K. P.; STANLEY, H. E. Majority-vote model for financial markets. *Physica A: Statistical Mechanics and its Applications*, Elsevier, v. 515, p. 762–770, 2019.

VOIT, J. *The Statistical Mechanics of Financial Markets*. Third. Berlin (Germany): Springer, 2005. ISBN 3540009787 (softcover : alk. paper).

WATTS, D. J.; DODDS, P. S. Influentials, networks, and public opinion formation. *Journal of consumer research*, The University of Chicago Press, v. 34, n. 4, p. 441–458, 2007.

WATTS, D. J.; STROGATZ, S. H. Collective dynamics of 'small-world' networks. *nature*, Nature Publishing Group, v. 393, n. 6684, p. 440–442, 1998.

WU, F.-Y. The potts model. *Reviews of modern physics*, APS, v. 54, n. 1, p. 235, 1982.

YAO, Z.; HU, B.; XIE, Y.; MOORE, P.; ZHENG, J. A review of structural and functional brain networks: small world and atlas. *Brain informatics*, Springer, v. 2, p. 45–52, 2015.

ZHAO, L.; YANG, G.; WANG, W.; CHEN, Y.; HUANG, J. P.; OHASHI, H.; STANLEY, H. E. Herd behavior in a complex adaptive system. *Proceedings of the National Academy of Sciences*, National Academy of Sciences, v. 108, n. 37, p. 15058–15063, 2011. ISSN 0027-8424.

ZUBILLAGA, B. J. *The statistical mechanics of societies: opinion formation dynamics and financial markets*. Phd Thesis (PhD Thesis), 2020.

ZUBILLAGA, B. J.; VILELA, A. L.; WANG, M.; DU, R.; DONG, G.; STANLEY, H. E. Three-state majority-vote model on small-world networks. *Scientific Reports*, Nature Publishing Group UK London, v. 12, n. 1, p. 282, 2022.

ZUBILLAGA, B. J.; VILELA, A. L. M.; WANG, C.; NELSON, K. P.; STANLEY, H. E. A three-state opinion formation model for financial markets. *Physica A: Statistical Mechanics and its Applications*, Elsevier, v. 588, p. 126527, 2022.

APPENDIX A – SUBMITTED PAPER: THREE-STATE OPINION DYNAMICS FOR FINANCIAL MARKETS ON COMPLEX NETWORKS

Three-state Opinion Dynamics for Financial Markets on Complex Networks

Bernardo J. Zubillaga

Center for Theoretical Biological Physics and Department of Physics, Northeastern University, Boston, MA 02115, USA and Center for Polymer Studies and Department of Physics, Boston University, Boston, MA 02215, USA

Mateus F. B. Granha

Departamento de Física, Universidade Federal de Pernambuco, Recife, PE 50670-901, Brazil and Física de Materiais, Universidade de Pernambuco, Recife, PE 50720-001, Brazil

Chao Wang*

College of Economics and Management, Beijing University of Technology, Beijing, 100124, China

Kenric P. Nelson

Photrek, LLC, Watertown, MA 02472, USA

André L. M. Vilela

Data Science and Analytics, SUNY Polytechnic Institute, Utica, NY 13502, USA Física de Materiais, Universidade de Pernambuco, Recife, PE 50720-001, Brazil and Departamento de Física, Universidade Federal de Pernambuco, Recife, PE 50670-901, Brazil

(Dated: February 5, 2025)

Abstract

This work investigates the effects of complex networks on the collective behavior of a three-state opinion formation model in economic systems. Our model considers two distinct types of investors in financial markets: noise traders and fundamentalists. Financial states evolve via probabilistic dynamics that include economic strategies with local and global influences. The local majoritarian opinion drives noise traders' market behavior, while the market index influences the financial decisions of fundamentalist agents. We introduce a level of market anxiety q present in the decision-making process that influences financial action. In our investigation, nodes of a complex network represent market agents, whereas the links represent their financial interactions. We investigate the stochastic dynamics of the model on three distinct network topologies, including scale-free networks, small-world networks and Erdös-Rényi random graphs. Our model mirrors various traits observed in real-world financial return series, such as heavy-tailed return distributions, volatility clustering, and short-term memory correlation of returns. The histograms of returns are fitted by coupled Gaussian distributions, quantitatively revealing transitions from a leptokurtic to a mesokurtic regime under specific economic heterogeneity. We show that the market dynamics depend mainly on the average agent connectivity, anxiety level, and market composition rather than on specific features of network topology.

Keywords: Econophysics, Sociophysics, Monte Carlo simulation, Phase transitions, Complex networks

* Correspondence email address: chaowanghn@vip.163.com

I. INTRODUCTION

Network science has become an essential tool for the study and analysis of complex systems such as financial markets. The structure of connections and dependencies intrinsic to commercial activities critically influences the economic landscape. As a complex system, financial markets can be modeled as networks, in which nodes represent individual investors and connections stand for interactions between them related to the purchase, sale or holding of financial assets. The convergence of individual decisions between different economic agents has repercussions on the behavior of the financial market observables, yielding essential collective behaviors, such as financial contagion and herd movements, speculative pricing, and crashes [1–4].

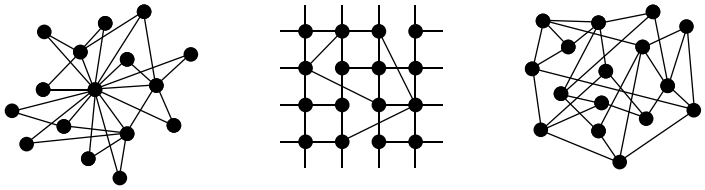

Figure 1: Illustration of distinct architectures of three complex networks with $N = 16$, and the average connectivity $\langle k \rangle = 4$: from the hubs of (a) scale-free networks, (b) to the clusters and shortcuts of small-world networks and (c) the randomness of random networks.

In the context of a society, two connected nodes may represent the fact that a pair of individuals know each other and may talk, trade, and exert influence on one another, for example. Different socioeconomic relations and organizational networks have a unique pattern of connectivity and structure. Figure 1 describes the visualization of three different complex networks with $N = 16$ nodes and average connectivity of $\langle k \rangle = 4$ and highlights their fundamental properties. We illustrate (a) a scale-free network and its hub-like structure, (b) a small-world network characterized by the presence of clusters and shortcuts and (c) a random network with disordered connectivity [5–7]. From network representation, we can infer fundamental principles that underlie complex systems and their collective critical behavior.

The dynamics of financial markets emerge from, among other factors, investors' rational and emotional activity, driven by the complex social dynamics and influences between agents

in a network of economic investors. An example of such a phenomenon is herding, whereby individuals tend to follow the opinion or behavior of their neighbors. Buying, selling, or holding an asset is an agent's decision taken in a social environment with which he interacts. In this context, herding behavior has been suggested to play an essential role in finance, where often coherence in social and economic imitation manifests as informational cascades [8–13].

In financial markets, behavioral finance has identified herding as a key to understanding the collective irrationality of investors [14]. An important class of economic agents is called *noise traders*, who typically follow their neighbors' trends and tend to overreact to the arrival of news when buying or selling. Another essential group of agents seems to follow the trends of the global minority as an investment strategy. They tend to buy when noise traders drive prices down and sell when they move prices up. We shall refer to these agents as *fundamentalists*, but they are also known as contrarians, sophisticated traders, or $\alpha-$investors [15–22]. For fundamentalist agents, the analysis of the fundamentals of an asset, based on financial data, guides their rational decision-making, and their action promotes price movements toward more realistic or *fundamental* values.

Over the years, several agent-based models capable of reproducing statistical features of real economic time series have been proposed as frameworks for understanding the dynamics of financial systems, with applications inspired by Ising systems and sociophysics models, such as the majority-vote dynamics [16–28]. Bornholdt proposed a spin model inspired by market dynamics, where local interactions and a competing global coupling create frustration, leading to metastable states, intermittency, and chaotic phases [17]. Kaizoji et al. expanded this Ising framework, linking log-returns to magnetization and finding correlations with trading volume, as well as scaling behavior in log-return distributions [18].

Takaishi designed a three-state Potts model for financial markets, in which agents can buy, sell, or remain inactive, reproducing key stylized facts such as fat-tailed return distributions and long-term correlations, with inactivity levels influencing the emergence of exponential return distributions [19]. Krawiecki et al. proposed a microscopic spin-based financial market model with coupled agents and randomly changing interactions, which exhibits chaotic bursts, attractor bubbling, and on-off intermittency, representing volatility clustering in financial markets [24]. Another spin-based model for price formation was proposed by K. Sznajd-Weron et al., in which the influence spreads outward from a central

agent to neighbors, emulating the spread of opinions among traders [23]. Bartolozzi et al. [25], modeled model opinion formation as a stochastic process in which agents respond to local social influences and global feedback on a scale-free Barabási-Albert network, exhibiting intermittent dynamics for certain parameter ranges.

Vilela et al. proposed a majority-vote dynamics model linking herding behavior and investment strategy to price formation, demonstrating strong agreement with several real-world financial time series [27]. The agent-based majority-vote model enables the investigation of the time evolution of opinion in society using an opinion variable and social anxiety noise. Similar to the Ising model, it also exhibits second-order phase transitions in several network topologies for a critical noise level [27–40].

The inherent complexity of collective human behavior is subject to interdisciplinary considerations. However, microscopic models of opinion formation attempt to simplify group dynamics to essential interaction mechanisms. The majority-vote consensus dynamics capture critical social phenomena, inspiring scientists to expand it further to model group behavior and financial market evolution. In this context, the *global-vote model* frames opinion dynamics as the foundation of agent decisions in financial markets [26–28]. The three-state model supports four essential features: individuals' strategies regarding market decisions, influence networks connecting agents in a market, a socioeconomic anxiety level, and agent financial action space. The latter is represented by a three-state stochastic variable standing for their opinion on a market decision, e.g., buying, selling, or holding an asset.

An extensive number of studies have explored agent-based interactive dynamics to model price formation in financial markets, often focusing on agent behavior and market features. In this work, we investigate the effects of the social connectivity structure in financial markets, which plays a crucial role in shaping collective behavior, opinion propagation, and market fluctuations. We examine emergent phenomena in a three-state opinion model on three distinct complex network topologies: scale-free, small-world, and random networks, and compare the outcomes [5–7]. We reveal insights into network topology's potential impact on market behavior by investigating how opinions propagate and evolve within these diverse network structures. Through our analysis, we seek to uncover valuable information about the interplay between market dynamics and network architecture, shedding light on the factors that may influence the formation and spread of financial opinions across different network types.

This work is organized as follows. Sec. II presents the main characteristics of the three-state global-vote model modeling for financial markets. Sec. III exhibits our Monte Carlo numerical results on scale-free networks, small-world networks, and random graphs. In Sec. IV, we present our concluding remarks, briefly synthesizing the results of this work.

II. FINANCIAL DYNAMICS

We map the agent's financial decision at a given time t by a stochastic variable, which may assume one of three states $s \in \{1, 2, 3\}$, which may represent buying, holding, or selling an asset. Financial market dynamics is driven by a heterogeneous composition of agents, randomly distributed in a network of social connections: a fraction $1-f$ of noise traders and the remaining fraction f of fundamentalist agents, also called noise contrarian traders. The former acts based on their nearest neighbors' decisions, whereas the latter on the behavior of the market as a whole. The total number of agents defines network size and equals N.

Financial markets often reflect the socioeconomic stability of nations. Critical worldwide events may lead to economic anxiety and uncertainty, impacting stock market volatility. To model the level of economic anxiety present in a financial market, we introduce the socioeconomic noise parameter q. We assume that q impacts both noise contrarians and noise traders' decisions and q represents the probability of an agent not following its standard strategy when negotiating in the financial market [26–28].

A noise trader agent updates its financial option according to the probabilistic prescription in Eq. (1), following the three-state dynamics [28–33]. A noise trader tends to follow the local majority, i.e., it agrees with the state of the majority of its nearest neighbors with probability $1-q$ or dissents from it with probability q. Let i represent a noise trader agent and $k_{i,s}$ represent the number of near-neighbors of i occupying a given state $s \in \{1, 2, 3\}$. Below, we summarize the stochastic update rules for the state of a noise trader. The probability for an agent to adopt state $s = 1, 2$ or 3 is given by

$$
\begin{aligned}
&P\left(1|k_{i,1} > k_{i,2}; k_{i,3}\right) \quad = P\left(2|k_{i,2} > k_{i,3}; k_{i,1}\right) \quad = P\left(3|k_{i,3} > k_{i,1}; k_{i,2}\right) \quad = 1-q,\\
&P\left(1|k_{i,1} = k_{i,2} > k_{i,3}\right) = P\left(2|k_{i,2} = k_{i,3} > k_{i,1}\right) = P\left(3|k_{i,3} = k_{i,1} > k_{i,2}\right) = (1-q)/2,\\
&P\left(1|k_{i,1} < k_{i,2} = k_{i,3}\right) = P\left(2|k_{i,2} < k_{i,3} = k_{i,1}\right) = P\left(3|k_{i,3} < k_{i,1} = k_{i,2}\right) = q,\\
&P\left(1|k_{i,1}; k_{i,2} < k_{i,3}\right) \quad = P\left(2|k_{i,2}; k_{i,3} < k_{i,1}\right) \quad = P\left(3|k_{i,3}; k_{i,1} < k_{i,2}\right) \quad = q/2,\\
&P\left(1|k_{i,1} = k_{i,2} = k_{i,3}\right) = P\left(2|k_{i,2} = k_{i,3} = k_{i,1}\right) = P\left(3|k_{i,3} = k_{i,1} = k_{i,2}\right) = 1/3.
\end{aligned}
\tag{1}
$$

Note that the probabilities for the states follow from the symmetry operations of the $C_{3\nu}$ group: $1 \to 2$, $2 \to 3$ and $3 \to 1$. Furthermore, the probabilities must be normalized, i.e., $P(1|\{k_i\}) + P(2|\{k_i\}) + P(3|\{k_i\}) = 1$ for any global state configuration $\{k_i\} \equiv \{k_{i,1}, k_{i,2}, k_{i,3}\}$.

By contrast, a noise contrarian trader updates its financial option according to the probabilistic description in Eq. (2). Fundamentalist agents tend to follow the global minority with probability $1-q$ or dissent from it with probability q. Let N_s represent the total number of agents in the network within a given state $s \in \{1,2,3\}$, where $N = N_1 + N_2 + N_3$. Below, we summarize the update rules for the state of a fundamentalist agent. The probability of adopting state $s = 1, 2$ or 3 is

$$
\begin{aligned}
&P\left(1|N_1 < N_2; N_3\right) \quad = P\left(2|N_2 < N_3; N_1\right) \quad = P\left(3|N_3 < N_1; N_2\right) \quad = 1-q,\\
&P\left(1|N_1 = N_2 < N_3\right) = P\left(2|N_2 = N_3 < N_1\right) = P\left(3|N_3 = N_1 < N_2\right) = (1-q)/2,\\
&P\left(1|N_1 > N_2 = N_3\right) = P\left(2|N_2 > N_3 = N_1\right) = P\left(3|N_3 > N_1 = N_2\right) = q,\\
&P\left(1|N_1; N_2 > N_3\right) \quad = P\left(2|N_2; N_3 > N_1\right) \quad = P\left(3|N_3; N_1 > N_2\right) \quad = q/2,\\
&P\left(1|N_1 = N_2 = N_3\right) = P\left(2|N_1 = N_2 = N_3\right) = P\left(3|N_1 = N_2 = N_3\right) = 1/3.
\end{aligned}
\tag{2}
$$

Once more, the probabilities for the states follow from the symmetry operations of the $C_{3\nu}$ group. The normalization condition, i.e. $P(1|\{N\}) + P(2|\{N\}) + P(3|\{N\}) = 1$ also holds for any global state configuration $\{N\} \equiv \{N_1, N_2, N_3\}$.

Moreover, we remark that economic stability fundamentally impacts market volatility. Thus, the order parameter M is defined in analogy to the three-state Potts model, and it measures the average market opinion, revealing the economic order

$$
M = \sqrt{M_1^2 + M_2^2 + M_3^2}. \tag{3}
$$

The order parameter M will be referred to as the opinionization in analogy to the magnetization of physical spins. The opinionization measures the uniformity of opinion in the market. If all the agents share the same opinion, then $M = 1$. If the opinions are split evenly between the three states, then $M = 0$. We express M as the magnitude of a vector with components

$$M_s = \sqrt{\frac{3}{2}} \left(\frac{N_s}{N} - \frac{1}{3} \right), \tag{4}$$

with $s \in \{1, 2, 3\}$.

In the market context, we shall interpret the order parameter of the system M as proportional to the price of a given asset [17–19]. We relate the time variations of the instantaneous opinionization $M(t)$ to a financial asset's logarithmic returns $r(t)$. Our model assumes that the investors' demands drive prices to update instantaneously. We define the logarithmic return at time t as follows:

$$r(t) = \log\left[M(t)\right] - \log\left[M(t-1)\right]. \tag{5}$$

The log-return measures the relative price changes of a financial asset between two instants of time. As such, it is a measure of the efficiency or performance of an investment. The volatility v of a financial asset estimates the risk of investment in such an asset. A usual measure of volatility, locally in time, is the absolute value of the returns, since it quantifies the amplitudes of price variations as measures of fluctuations in the time series $v(t) \equiv |r(t)|$.

III. NUMERICAL RESULTS

We perform Monte Carlo simulations on distinct complex network topologies with $N = 10^4$ nodes. We extensively investigate several network parameters: the growth parameter z for scale-free networks, the rewiring parameter p for small-world networks, and the average connectivity $\langle k \rangle$ for random graphs. We build the network of financial interactions by considering a fraction f of fundamentalist agents and the remaining fraction $1 - f$ as noise traders. From previous investigations [26–28], we expect essential market features to emerge in the noise region near criticality $q \simeq q_c$, when contrarians are absent $f = 0$ for all networks investigated [31–33].

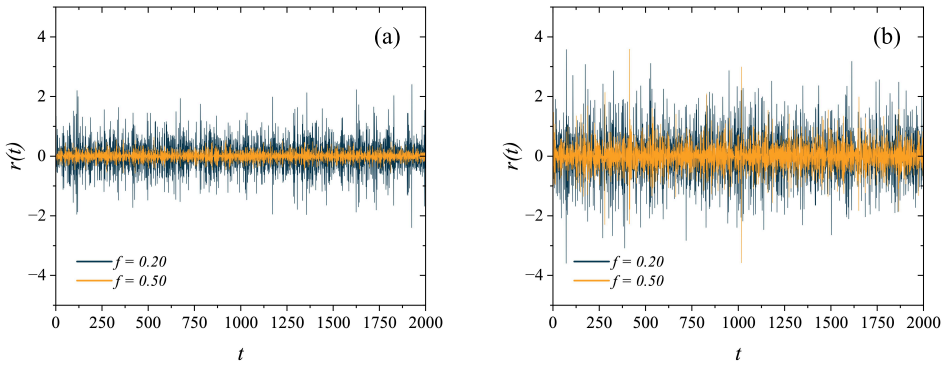

Figure 2: Time series of the logarithmic returns for (a) $z = 6$ and $q = 0.4550$, (b) $z = 50$ and $q = 0.5918$.

At each instant or Monte Carlo step (MCS), we perform N attempts to update the state of randomly selected individuals. Once selected, a financial agent updates his opinion accordingly with the probabilities given by Eqs. (1) or (2) for a noise trader or a fundamentalist agent, respectively. We randomize the initial state of the system, assigning to each agent any of the three available states with equal probability. We allow the dynamics to run during 10^4 MCS to discard the transient regime and perform our analysis in the subsequent 10^4 MCS. For every set of parameters (q, f), we perform 100 Monte Carlo simulations for each network topology considered, averaging over network disorder. Therefore, a total of 10^6 MCS was recorded for each pair of parameters (q, f) and network topology from all the runs. In this way, the statistics gathered many realizations of the disorder caused by the random allocation of contrarians and the disorder from the network construction models.

In our investigation, we place N agents on the nodes of three distinct network topologies: scale-free networks, small-world networks, and random graphs. Several network properties differentiate between each complex network topology [5–7]. The following sections detail the mechanisms for constructing the complex networks implemented in this work and the main results obtained for each topology considered. We aim to understand the socioeconomic dynamics under the effects of different network structures and compare our results with the observations made in behavioral economics and finance.

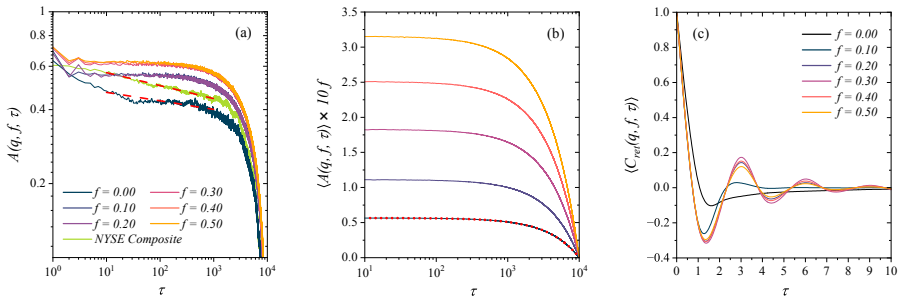

Figure 3: Autocorrelation function of volatility $|r(t)|$ for $z = 6$, $q = 0.4550$, and varying values of f from 0 to 0.5. Also included is the volatility autocorrelation of daily closing values for the NYSE Composite, covering 10^4 trading days from May 28, 1985, to February 2, 2025. The red dashed lines indicate power-law fits. Averaged autocorrelation functions for (b) volatility and (c) logarithmic returns $r(t)$, with the red dots representing an exponential fit.

A. Financial Markets on Scale-free Networks

Upon analyzing the topology of social networks, airline networks, or the World Wide Web, we observe the presence of *hubs* – highly connected nodes – a feature displayed by several other real-world networks. Such networks are frequently referred to as scale-free networks. The Barabási-Albert model is a well-known method for building scale-free networks via two fundamental mechanisms: growth, where we consider that nodes are iteratively added, and preferential attachment, which describes the "rich–get–richer" effect, in which nodes with a high degree of connectivity have a higher chance of obtaining new connections [5, 41, 42].

To generate scale-free networks, we use the Barabási-Albert model and start with a fully connected core of z nodes, where z is the growth parameter. According to the preferential attachment algorithm, a new node adds z new links to the existing network at each step of network growth. In this way, such networks present an average degree of $\langle k \rangle = 2z$. We remark that the degree distribution of Barabási-Albert scale-free networks display a power-law decay with exponent $\lambda \sim 3$ [5].

We focus the study of the financial dynamics near criticality $q \simeq q_c$ when there is an

absence of contrarians since we expect opinionization fluctuations to be more significant in that region of the phase diagram. We collect the respective critical noise values, $q_c(z)$, from previous studies of the three-state majority-vote model on Barabási-Albert networks [32].

In Fig. 2, we show the influence of the growth parameter z and the concentration of fundamentalist agents f on the market behavior at the critical point. Fig. 2(a) illustrates two distinct market phases for $q = 0.4550$ and $z = 6$: a *strong market phase* or *turbulent phase* for $f = 0.20$, where the system presents several events of considerable volatility, as depicted by the large spikes in the plot; and a *weak market phase* or *laminar phase* for $f = 0.50$, where returns fluctuations are attenuated. This finding agrees with previous investigations in which increasing the number of contrarian agents drives market stability [26–28]. Furthermore, Fig. 2(b) shows that for $q = 0.5918$ and $z = 50$, the frequency of high volatility events for both values of f increases with higher z, appearing in an uncorrelated form, indicating a deviation from the expected behavior of real-world financial markets.

Fig. 2(a) also demonstrates that periods of considerable return fluctuations are compressed for lower values of f, indicating the real-world market feature known as volatility clustering [21, 24, 43]. This financial phenomenon can be comprehended by Mandelbrot's observation that "large changes tend to be followed by large changes – of either sign – and small changes tend to be followed by small changes" [44]. To quantify the effects of volatility clustering, we define the autocorrelation function of the absolute returns as follows:

$$A(\tau) = \frac{\sum_{t=\tau+1}^{T} \left[|r(t)| - |\bar{r}|\right] \left[|r(t-\tau)| - |\bar{r}|\right]}{\sum_{t=1}^{T} \left[|r(t)| - |\bar{r}|\right]^2}, \tag{6}$$

where $1 \leq \tau \leq 10^4$ MCS is the time-step difference between observations, $T = 10^4$ MCS is the time of simulation for each network sample, $r(t)$ is the return at a time t and $\bar{r}$ the average return value.

The function defined by Eq. (6) measures non-linear correlations in a given time series, namely the autocorrelation function of the absolute value of log-returns, as a function of the time delay between observations. Many real-world studies demonstrate a strong positive correlation in the volatility $|r(t)|$ over extended periods such as days, weeks or months, consistent with the presence of volatility clustering in the data [27]. Figure 3(a) illustrates the autocorrelation function of the absolute values of log-returns for different fractions of fundamentalist agents, considering $z = 6$, $q = 0.4550$ and a simulation time of $T = 10^4$

MCS. For comparison, we also present the autocorrelation function of the daily volatility of the NYSE Composite's closing values, spanning from May 28, 1985, to February 2, 2025, covering a total of 10^4 trading days[1]. We explore power-law fits for the autocorrelation functions, $A(\tau) \sim \tau^{-\eta}$, over the same time periods, and the simulations and empirical data exhibit a quantitative agreement in the order of the rate of decay, with power-law exponents $\eta \sim 0.04(1)$ for the simulations and $\eta_{NYSE} \sim 0.083(1)$ for the closing values of the NYSE Composite [28].

In Figure 3(b), we display the average autocorrelation of the absolute value of log-returns for several values of f and 100 network samples and market simulations. Results show the persistent correlation between high-volatility events and a slow exponential decay in time spanning over several orders of magnitude. We also exhibit an exponential fit of the data $\langle A(q, f, \tau)\rangle \sim \exp(-\tau/\tau_0)$ for $f = 0.10$, in which we obtain $\tau_0 \approx 7 \times 10^7$ MCS [4, 16, 18, 45]. Other values of f yield similar results. We highlight that the observation of an exponential cut-off near 10^4 time steps for our averaged autocorrelation is to be expected. Since our simulations are 10^4 MCS long, the exponential decay is a reflection of the finite size of the data samples presented for the time series, agreeing with previous investigations [17, 19, 26, 28]. Figure 3(a) also exhibits such finite size effect and exponential long-time decay.

Figure 3(c) presents the autocorrelation function C_{ret} for the returns time series $r(t)$ generated by the model for several values of the fundamentalist fraction f, and averaged over 100 network realizations. We connect data points using B-spline curves that smoothly interpolate between the control points, resulting in a continuous curve. As expected from real-world markets, returns are uncorrelated in time as $C_{ret} \to 0$ on a short-time scale of $\tau \sim O(1)$, reflecting that our model lacks long-term memory, agreeing with the efficient market hypothesis [47–49]. For large fractions of contrarians, C_{ret} displays diminishing anti-persistent oscillations in the short term. This oscillation stems from the cyclical dynamics of the system, primarily driven by a substantial portion of noise contrarians consistently striving to inhabit the instantaneous global minority state [28].

Figure 4 displays the histogram of the log-returns in 10^6 MCS for $z = 6$ and several values of f. As previously discussed, we observe increased market stability for increasing fractions of contrarians in the network. Our results show that for lower values of the fraction f, the

[1] Data provided by Yahoo Finance.

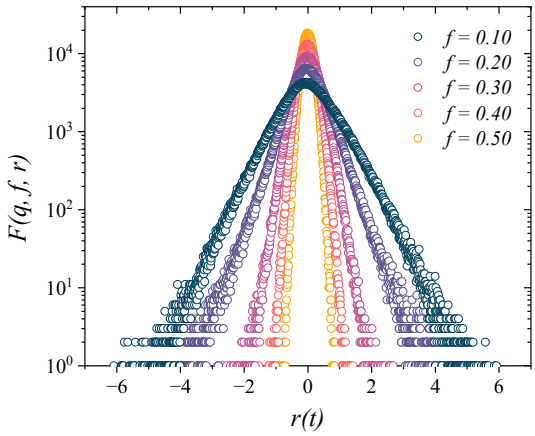

Figure 4: Distribution of logarithmic returns in 10^6 MCS for $z = 6$ and $q = 0.4550$ and several values of the fraction of noise contrarians.

distributions display fat tails as a reflection of the high number of intense volatility events. As we increase the values of f, distributions' tails become less heavy as they gradually shift towards a Gaussian regime. To quantify the return distributions, we perform a statistical analysis of the data. We calculate the kurtosis $K(z, f)$ for the distributions and obtain $K(6, 0.10) = 4.48$ in the strong market phase and $K(6, 0.50) = 3.12$ in the weak market phase. Thus, increasing the fraction of contrarian agents f shifts the system's behavior from a leptokurtic regime ($K > 3$) to a mesokurtic regime ($K \approx 3$).

To further qualify the distributions in Fig. 4, we compute comparative quantile-quantile (Q–Q) plots. In such plots, the reference line, depicted in red, represents the expected results of a theoretical distribution and, should data points align with it, would indicate a match to the distribution. Fig. 5 displays Q–Q plots (a) of the log-returns against a normal distribution and (b) of the volatility against an exponential distribution. In Fig. 5(a), lower values of the fraction of contrarians f (specifically $f \leq 0.30$) show significant nonlinearity, indicating fat-tailed, non-Gaussian behavior typical of real-world financial data. As f increases, the distributions approach Gaussian behavior, with data points aligning closer to the reference line. Additionally, Fig. 5(b) shows that deviations in higher quantiles reveal a slower decay than the expected for an exponential distribution, confirming the

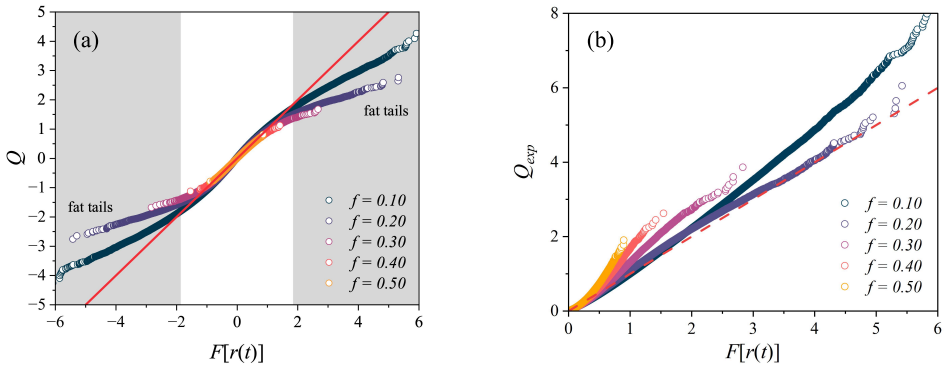

Figure 5: Quantile–quantile plots of the distributions of (a) normal versus logarithmic returns and (b) exponential versus volatility in 10^6 MCS for $z = 6$ and $q = 0.4550$. The red line displays the theoretically expected results for each distribution.

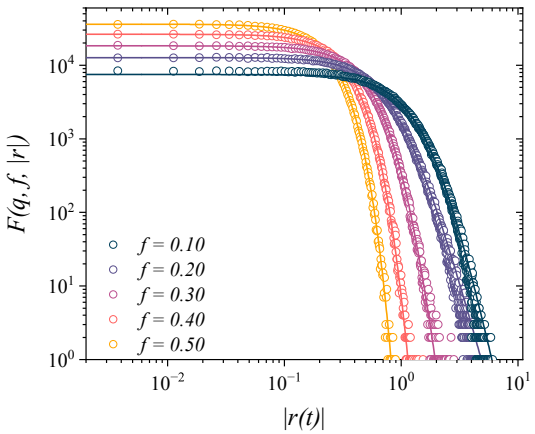

Figure 6: Distributions of the volatility for $z = 6$ and $q = 0.4550$ in 10^6 MCS. The lines correspond to symmetric coupled exponential fits for the data.

heavy-tailed regime [44–46]. Such behavior implies a higher probability of extreme values than an exponential distribution would predict, further highlighting the complex nature of the data.

To quantify the transition of the log-return distributions from a heavy-tailed (leptokurtic)

regime into a Gaussian (mesokurtic) regime, we consider the coupled exponential family of distributions $P_{\mu,\sigma,\kappa,\alpha}(r)$, where μ is the mean value, σ, κ and α are the parameters of the function [46]. We shall refer to the shape parameter κ as the *nonlinear statistical coupling* and to σ as the scale parameter in an interpretation of non-extensive statistical mechanics of complex systems [50–54]. Considering the mean value of the distributions as zero, in agreement with Fig. 7, we fit the distributions via the symmetric coupled exponential family $P_{\mu,\sigma,\kappa,\alpha}(r) = P_{\sigma,\kappa,\alpha}(r)$, defined as follows.

$$P_{\sigma,\kappa,\alpha}(r) \equiv \left[Z(\sigma,\kappa,\alpha) \left(1 + \kappa \left|\frac{r}{\sigma}\right|^{\alpha}\right)_{+}^{\frac{1+\kappa}{\alpha\kappa}} \right]^{-1}, \tag{7}$$

where $(x)_+ \equiv \max(0, x)$. Furthermore, if we set the parameter $\alpha = 2$, we obtain the coupled Gaussian distribution: for $\kappa = 0$, we recover the Gaussian distribution; and for $\kappa > 0$, we have the Student's t distribution, where the degree of freedom ν is related to the shape parameter as $\nu = 1/\kappa$. Thus, the shape parameter κ yields a quantitative measure for the transition between distribution regimes [50–54].

Table I: Correlation between the scale σ and shape κ as a function of the fraction of contrarian agents f, growth parameter z and noise q.

Fraction f	0.10	0.20	0.30	0.40	0.50
Shape κ	0.16(3)	0.205(2)	0.070(2)	0.024(2)	0.017(1)
Scale σ	0.74(1)	0.4499(4)	0.3204(3)	0.2258(3)	0.1651(1)

Figure 6 displays the probability distribution of the volatilities for several values of the fraction of fundamentalists f in 10^6 MCS. The lines correspond to symmetric coupled exponential fits for the data, and the values obtained for the nonlinear coupling parameter κ and scale σ are portrayed in Table I. The results provide a quantitative measurement of the gradual regime shift depending on the fraction of contrarians f: increasing f pushes the nonlinear coupling parameter κ towards zero, indicating the loss of fat tails as distributions become Gaussian; simultaneously, the scale σ is progressively reduced, as the higher presence of fundamentalists tends to stabilize market dynamics. Thus, the coupled exponential fits

performed provide a numerical measure of the transition from a heavy-tailed (leptokurtic) regime to a Gaussian (mesokurtic) regime depending on the fraction of contrarians f.

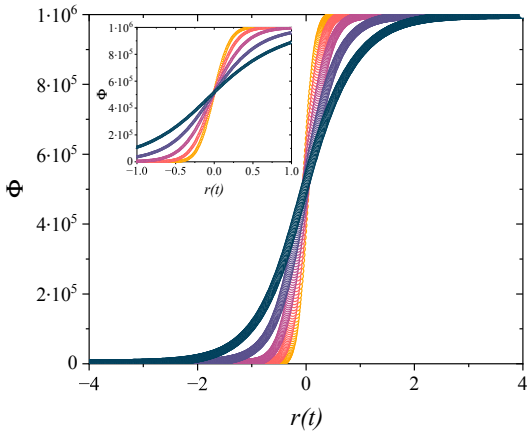

Figure 7: Cumulative distribution of logarithmic returns in 10^6 MCS for $z = 6$ and $q = 0.4550$. The inset displays the behavior of Φ for $r(t)$ near zero.

Figure 7 displays the cumulative distribution of logarithmic returns Φ for $z = 6$ in 10^6 MCS. As previously stated, we observe that the mean of the distributions remains zero for all investigated values of f.

We also extensively investigate the model's behavior for several micro-state configurations, depending on the growth parameter z, the fraction of contrarians f, and the noise parameter q. Figure 8 displays a multi-plot table of the histograms of logarithmic returns for several (q, f, z) triplets investigated near the criticality of the system $q \approx q_c(z)$. Columns correspond to values of q, below criticality (left), at criticality (center), and above criticality (right). The selected noise values above and below criticality are $q = q_c(z) \pm 0.1$.

As one moves vertically (from top to bottom) in the grid along a column, one observes the topological effect of increasing the growth parameter of the network, especially in the center column. Increasing z reveals that the spreads and tails of the return distributions tend to increase slightly, suggesting broader return distributions. Furthermore, shifting towards higher values of f leads to a progressive loss of tails in the return distributions. In contrast, this behavior is lost for noise parameter values that deviate from criticality, as observed in

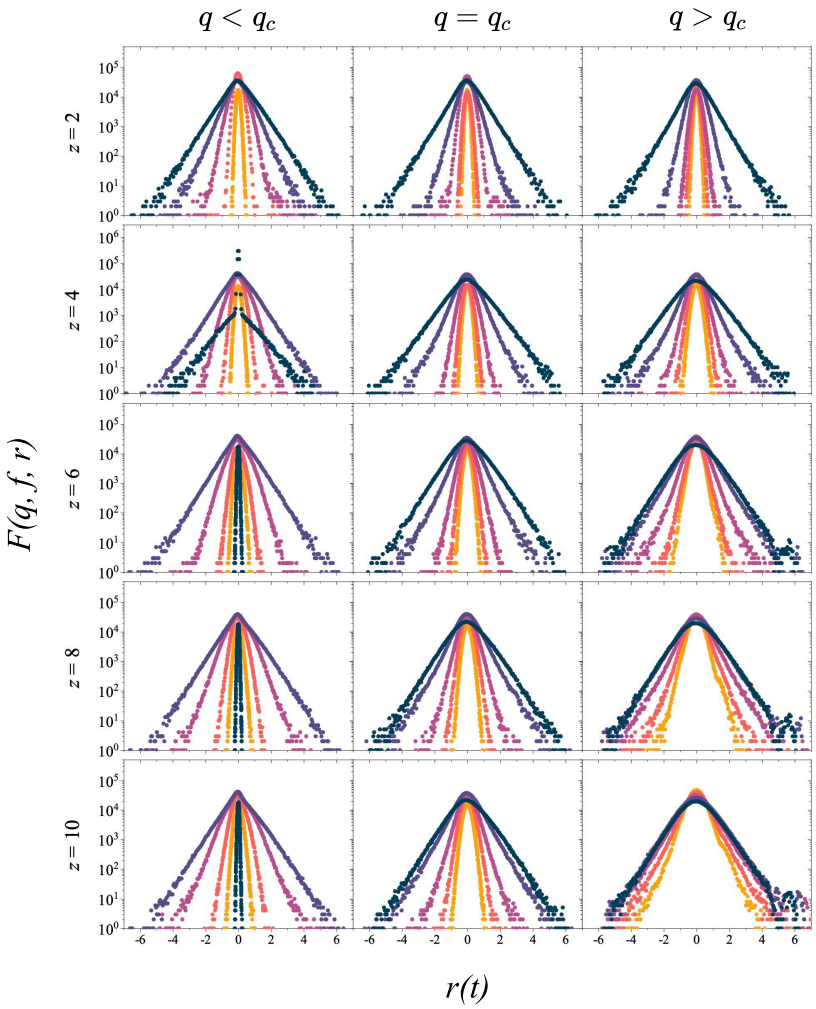

Figure 8: Distributions of logarithmic returns in 10^6 MCS for different combinations of parameter values (z, q) in the vicinity of $q_c(z)$ with $f = 0.10,\ 0.20,\ 0.30,\ 0.40$, and 0.50 in dark blue, purple, pink, orange, and yellow, respectively.

particular by the distributions for $f = 0.10$ below criticality, which becomes highly peaked around $r = 0$ for higher values of z, as well as the distributions for $z = 8$ and 10 above criticality, where higher fractions of contrarians still display a heavy-tailed behavior. Hence, this result conforms with our choice for the growth parameter z and noise parameter $q = q_c$ values.

Furthermore, we consider a quantitative approach to the distributions shown in Fig. 8, focusing exclusively on the system's behavior at the critical point $q = q_c(z)$. We perform fits for the volatility distributions of the system for different growth parameter values at their corresponding critical points according to the symmetric coupled exponential family of distributions Eq. (7) with $\alpha = 2$. Thus, Fig. 9 displays a heat map of the fitting parameters obtained for the nonlinear coupling κ and the scale parameter σ for several values of z. The rows correspond to different average connectivity values, each at their own critical noise parameter. Along the rows, we explore the effect of the different values of the fraction of contrarians f.

Figure 9(a) displays the heat map for κ where we observe the usual transition from a leptokurtic to a mesokurtic regime with increasing fractions of contrarians, evidence of the loss of heavy tails tending toward a Gaussian distribution for high values of f. For large enough values of f, this transition occurs in a universal-like way for Barabási-Albert networks. Nevertheless, we observe the effect of the topology on the tails of the distributions for small values of f. Indeed, the distributions for $z = 2$ display considerably heavier tails when compared with higher values of z.

Furthermore, Fig. 9(b) displays the heat maps for the scale parameter σ. We note that the scale parameter is small for $f \approx 0$. It rapidly grows with f, reaching a peak around the same value of f, decaying for larger fractions of contrarians as a reflection of the aforementioned transition between leptokurtic and mesokurtic regimes. Furthermore, we observe the effects of the topology on the volatility distributions as the peaks shift slightly to higher values of f as z increases.

We now proceed to investigate the influence of small-world networks and Erdös-Rényi random graphs on the behavior of the system's dynamics. For these topologies, the lack of correlations in the time series of log-returns is still present, consistent with the efficient market hypothesis. Anti-persistence emerges for large values of contrarians. Long-term correlation is still a feature of the volatilities as a reflection of the volatility clustering effect. Therefore, in the following subsections, we shall explore the effects of the topology on the histograms of log-returns.

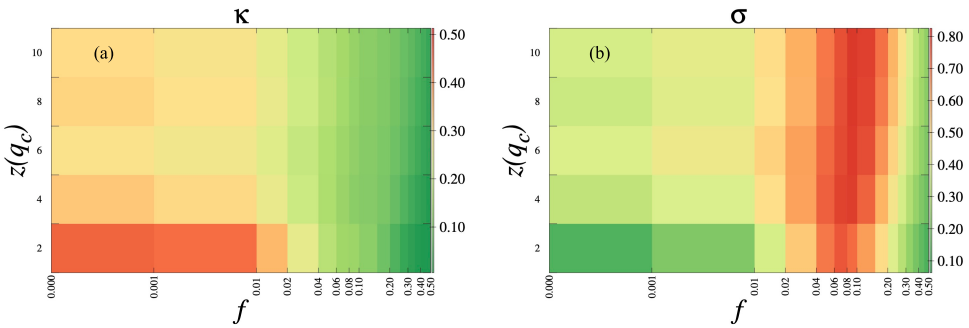

Figure 9: Heat map of (a) the nonlinear statistical coupling κ and (b) the scale parameter σ as a function of the critical noise parameter $q_c(z)$ at each corresponding value of z and the percentage of contrarians f.

B. Small-world Effects on Financial Dynamics

The term small-world effect alludes to the fact that most pairs of nodes in many real-world networks connect their elements by paths of short lengths, even though the sizes of complex networks are typically very large [6]. Furthermore, small-world networks encompass two essential features of real-world networks: short average path lengths and many network cliques.

Inspired by the Watts-Strogatz model, we build our networks by rewiring the links that connect the $N = L \times L$ nodes of bidimensional square lattices with probability p, while forbidding rewiring to the original nearest neighbors and double connections [6, 28, 33, 34]. We refer to p as the rewiring parameter, which also relates to the degree of randomness of the rewired network. When $p = 0$, we recover the standard square lattice, whereas we obtain a random network for $p = 1$. We remark that the rewiring process does not affect the original average connectivity of the square network. Thus, for small-world networks built via rewiring square lattices, $\langle k \rangle = 4$ for all values of p [6, 28].

We examine the return distributions and shall focus our investigation on the region around the critical points $q_c(p)$ for each corresponding value of the rewiring parameter p to investigate distinct system configurations near criticality. In this case, we also reference the critical social anxiety level $q_c(p)$ in market dynamics, with values obtained from previous investigations of the three-state majority-vote model on small-world networks [28].

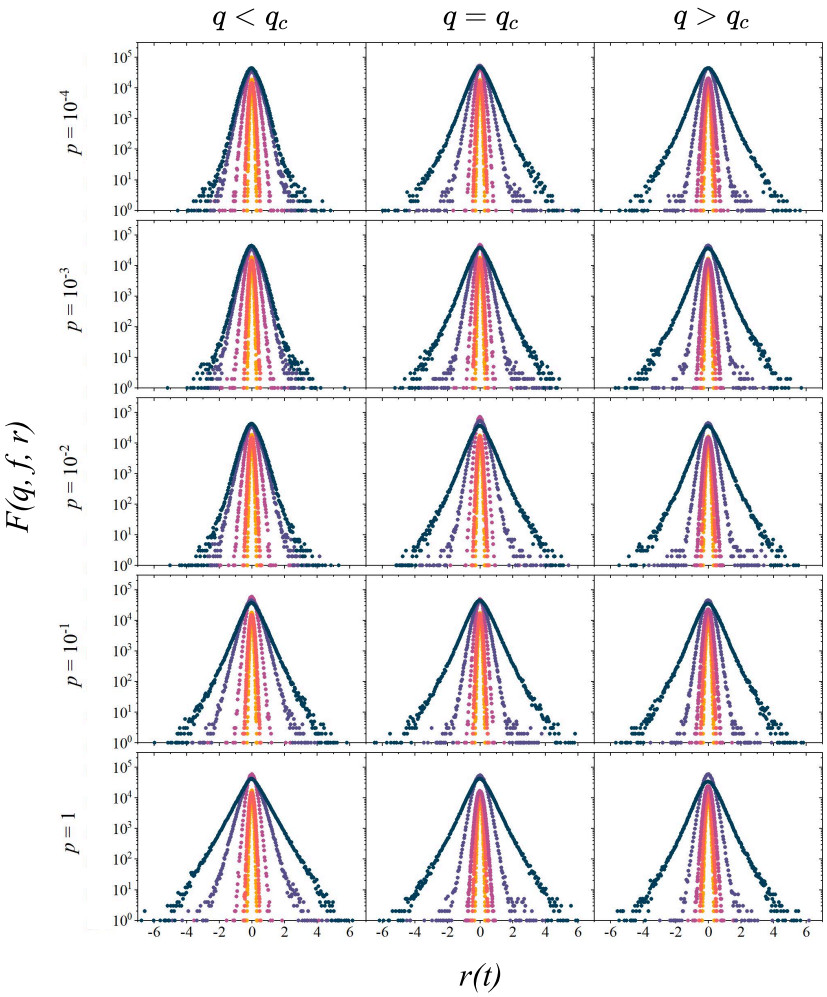

Figure 10: Distributions of logarithmic returns for various noise parameters q and rewiring probability p in the vicinity of $q_c(p)$ for several values of the fraction of contrarians: $f = 0.10,\ 0.20,\ 0.30,\ 0.40$, and 0.50 (dark blue, purple, pink, orange, and yellow, respectively).

In Fig. 10, we present a multi-plot table with the logarithmic return distributions for several (q, f, p) triplets. In analogy to the previously performed investigation, the rows correspond to distinct rewiring probabilities p, whereas the columns correspond to noise values below criticality, at criticality and above criticality for each value of p considered.

Hence, each cell in the grid depicts a (p, q) pair and shows several distributions corresponding to different concentrations of contrarians. The values of noise above and below criticality are taken to be $q \equiv q_c \pm 0.07$.

We observe that for macroscopically relevant fractions of contrarians, an increase in f leads to a progressive loss of tails in the return distributions, suggesting a similar transition between a leptokurtic regime and a mesokurtic regime. This feature is displayed in all the cells in the grid, i.e., for a broad spectrum of small-world networks at criticality or in its vicinity. Thus, the model shows evident robustness for these networks over different topologies and social temperatures q (above and below the critical point). Furthermore, moving vertically (from top to bottom) in the grid along a column displays the topological effect of increasing the rewiring probability of the system. In particular, for $q < q_c$, increasing p reveals that the spreads and tails of the return distributions also tend to increase, especially for low values of f. In contrast, the behavior along the $q = q_c$ and $q > q_c$ columns suggests that not much variation (if any) is present as one varies p, suggesting a universal-like behavior.

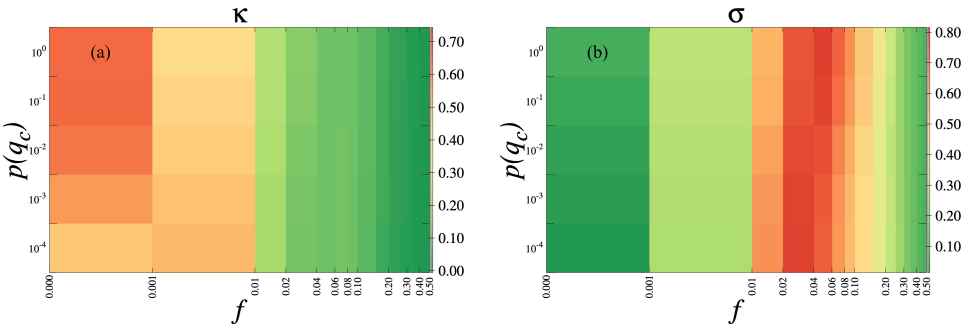

Figure 11: Heat map of (a) the nonlinear statistical coupling κ and (b) the scale parameter σ as a function of the critical noise parameter $q_c(p)$ at each corresponding rewiring probability p and the fraction of contrarians f.

We follow the above discussion with a quantitative approach, focusing on the volatility distributions for different values of p at their corresponding critical points $q = q_c(p)$. We perform fits for the data according to the symmetric coupled exponential family of distributions Eq. (7) with $\alpha = 2$. In Fig. 11, we display the fitting parameters corresponding to the

nonlinear coupling (a) κ and the scale parameter (b)n σ by means of heat maps. The rows correspond to distinct values of p, and along the rows, we explore the effects of different values of the fraction of contrarians f.

Once more, Fig. 11(a) displays the clear transition from a leptokurtic to a mesokurtic regime, i.e., the loss of tails due to the increasing fractions of contrarians. As previously remarked, for large enough values of f, this transition takes place universally for small-world networks built according to the link rewiring scheme. Fig. 11(b) shows the heat map corresponding to the scale parameter σ. Following the discussion regarding random networks, the scale parameter is small for $f \approx 0$, rapidly increasing with f, reaching a peak and then decaying similarly for macroscopically large fractions of contrarians. This indicates that the tails are lost in this regime as the distributions approach a Gaussian behavior.

C. Random Interacting Networks

A random network connects pairs of nodes with chance $0 < w \leq 1$, having an expected number of links equal to $\langle L \rangle = wN(N-1)/2$ out of the maximum number of links $L_{max} = N(N-1)/2$ as $w \to 1$. We adopt the Erdös-Rényi method for enabling random graphs on computers. This method adds $wN(N-1)/2$ links to the N initially isolated nodes, forbidding double connections. Such networks display a Poisson degree distribution for large values of N, with an average degree of connectivity $\langle k \rangle = 2\langle L \rangle / N = w(N-1)$ or $\langle k \rangle \approx wN$ [7, 42, 55]. We study market evolution under a socioeconomic network of randomly connected opinions and average connectivity $\langle k \rangle$ as a function of the anxiety level q and the fraction f of fundamentalist agents.

In Fig. 12, we present a multi-plot table with a set of logarithmic return distributions for several $(q, f, \langle k \rangle)$ triplets. In the plot, rows correspond to simulations done on random networks with different values of $\langle k \rangle$, whereas the three columns represent values of the noise parameter q below criticality, at criticality, and above criticality for each studied value of $\langle k \rangle$. In this way, each cell in the grid relates to a pair of values $(\langle k \rangle, q)$ and investigates several system micro-states regarding the fraction of contrarians f. The noise values above and below criticality are $q \equiv q_c \pm 0.1$, as we explore the model dynamics near criticality.

As in the other topologies explored thus far, it is clear from Fig. 12 that an increase in f leads to the aforementioned loss of tails in the return distributions, indicating the

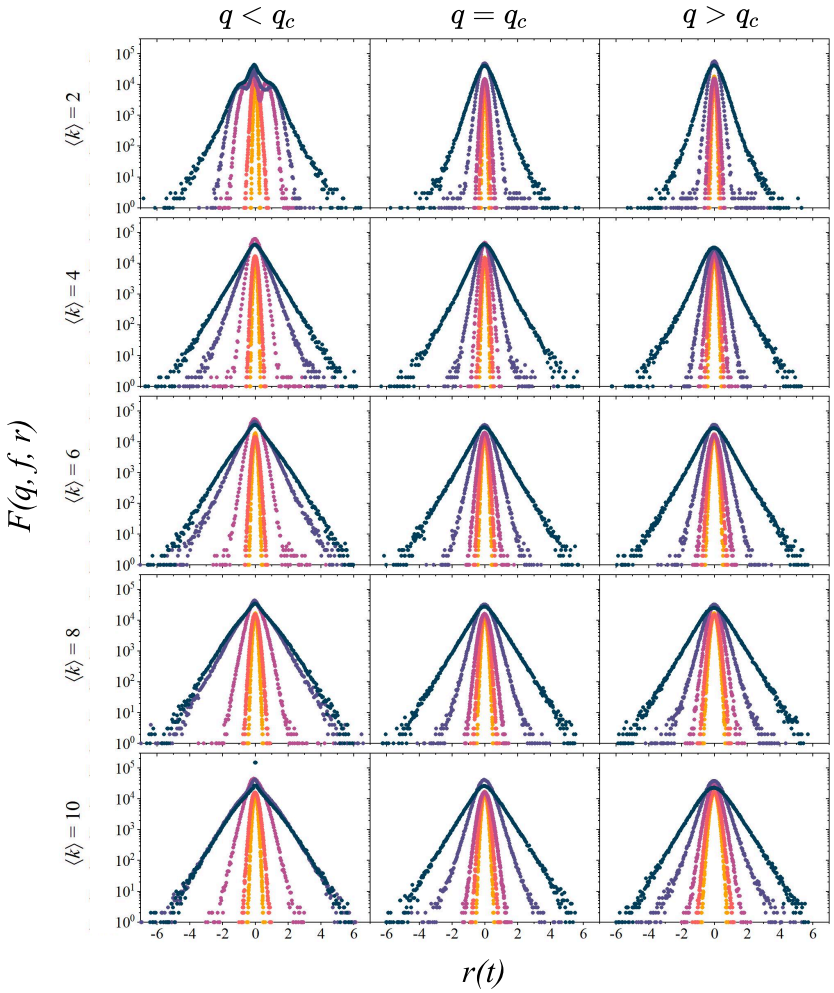

Figure 12: Distributions of logarithmic returns for various noise parameters q and average connectivity $\langle k \rangle$ in the vicinity of $q_c(\langle k \rangle)$ for various concentrations of contrarians: $f = 0.10,\ 0.20,\ 0.30,\ 0.40$, and 0.50 (dark blue, purple, pink, orange, and yellow, respectively).

gradual shift between leptokurtic and mesokurtic regimes. We observe such behavior for most cells in the grid, suggesting that the model is robust over a wide range of topologies and noise parameter values. Nevertheless, we remark on some visible exceptions, such as the distributions for $\langle k \rangle = 2$ below criticality, where lower fractions of contrarians display

unusual behavior. Furthermore, moving vertically (from top to bottom) along a column sheds light on the topological effects of increasing $\langle k \rangle$. In this way, increasing the growth parameter of the network correspondingly increases slightly the spreads and tails of the return distributions, as observed in previous investigations of the two-state global-vote model [27].

We deepen the previous discussion with a quantitative approach by focusing on the system's behavior at the critical point $q = q_c(\langle k \rangle)$, as we did for scale-free and small-world topologies. We fit the volatility distributions of the system for different values of $\langle k \rangle$ according to the symmetric coupled exponential family of distributions Eq. (7) with $\alpha = 2$. Figure 13 displays the heat maps of the fitting parameters corresponding to the nonlinear coupling κ and the scale parameter σ. The rows correspond to distinct values of the average connectivity $\langle k \rangle$, and we explore the influence of different values of the fraction of contrarians f along the rows.

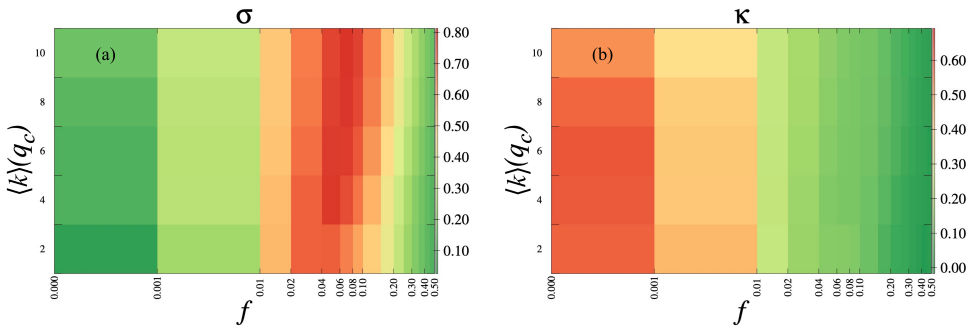

Figure 13: Heat map of (a) the nonlinear statistical coupling κ and (b) the scale parameter σ as a function of the critical noise parameter $q_c(\langle k \rangle)$ at each corresponding average degree $\langle k \rangle$ and the fraction of contrarians f.

Fig. 13(a) depicts the gradual transition from a leptokurtic to a mesokurtic regime with increasing fractions of contrarians, evidence of the loss of heavy tails for all investigated values of $\langle k \rangle$. Similarly, Fig. 13(b) displays the scale parameter's behavior for different system configurations: σ is small for small values of $f \approx 0$, rapidly growing with f; it peaks around the same value of f before decaying for macroscopically large fractions of contrarians. The peak, however, shifts slightly to higher values of f as $\langle k \rangle$ increases, a manifestation of

the effect of increasing the average degree. The scale parameter of the distribution will then tend to decay for larger values of f as the tails weaken and the distributions approach a Gaussian behavior.

Additional quantification of the transition between fat-tailed and normal regimes is obtained via calculating the excess kurtosis of the return distributions, where for $\gamma_2 = 0$, we recall a Gaussian distribution. Thus, in Fig. 14, we plot the excess kurtosis of the return distributions for several values of the fraction of contrarians and different values of network parameters, (a) the growth parameter z for scale-free networks, (b) the rewiring probability p for small-world networks and the average connectivity (c) $\langle k \rangle$ for random networks, at their corresponding real-world market (critical) noise values. We confirm that higher values of f tend to soften the distribution tails for all investigated network topologies, driving the market into a Gaussian regime.

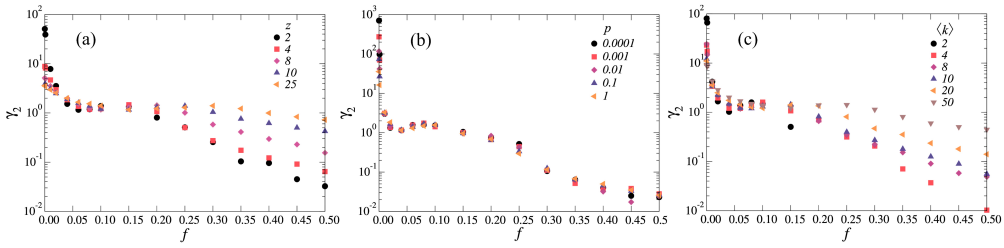

Figure 14: Excess kurtosis of the return distributions for several values of the fraction of contrarians f and different values of the network parameters at their corresponding critical noise values (a) z for scale-free networks, (b) p for small-world networks and (c) $\langle k \rangle$ for random networks. Recall that the excess kurtosis of a Gaussian distribution is $\gamma_2 = 0$.

Furthermore, closer inspection of Fig. 14 reveals the effects of the network's average connectivity on the distribution of logarithmic returns of the model. Recall that the average degree for scale-free networks is $\langle k \rangle = 2z$ whereas $\langle k \rangle = 4$ is constant and independent of the rewiring probability p. Thus, Fig. 14(a) and (c) show that the kurtosis' decay tends to spread out for increasing values of f as we vary the network's average degree of connectivity. We observe that high (low) values of the average individual connectivity promote a slow (rapid) decay of γ_2. Therefore, the network's average degree plays a crucial role in shaping the distribution of returns.

IV. CONCLUSION AND FINAL REMARKS

This work investigates the stochastic dynamics of a three-state economic opinion formation model on complex networks, extending and generalizing previous investigations on the three-state global-vote model for financial markets [26–28]. As in the standard version, two different types of individuals are considered: noise traders who interact locally with their nearest neighbors and tend to agree with the state of the *local majority* with probability $1-q$ and fundamentalists, who are subject to global interactions with the market as a whole and tend to follow the state of the *global minority* with probability $1-q$. The parameter q quantifies the socioeconomic anxiety level.

Financial agents are represented as nodes on complex networks, and the links between neighboring pairs of nodes represent opinion-driven financial interactions. We simulate the dynamics of the model on scale-free, small-world, and random networks and investigate how the distributions of returns are influenced by modifying specific network parameters, namely the growth parameter z for scale-free networks, the rewiring parameter p for small-world networks and the average connectivity $\langle k \rangle$ for random networks. In this work, financial systems comprise three main features: a heterogeneous population of agents with distinct strategies, a complex network of financial interactions, and a level of economic uncertainty near some consensus-dissensus criticality.

By relating changes in the instantaneous financial order of this system to price fluctuations, the model can reproduce the main features of real-world financial markets [17–19]. Our results display such stylized facts of financial time series as fat-tailed distributions of returns, volatility clustering, and long-term memory of the volatility, consistent with the efficient market hypothesis and previous investigations [26–28].

The logarithmic returns of the simulations fit a coupled exponential distribution, which is parameterized by the scale or generalized standard deviation and the shape or nonlinear statistical coupling [50–54]. This family of distributions is typically used within the context of non-extensive statistical mechanics as a tool for the characterization of the complexity of a system. For macroscopically relevant fractions of contrarians, an increase in the contrarians decreases both the scale and the shape of the distributions. This macroscopic effect results from a loss of local order at a microscopic level and the emergence of global order, deviating the dynamics from heavy-tailed real-world to Gaussian distributions of returns.

We frame socioeconomic anxiety levels with the critical point where the opinionization fluctuations diverge in the thermodynamic limit, leading to return distributions with heavy tails and volatility clustering. Furthermore, the topology effects of the underlying network on the returns and volatilities are observed in the distinct ways that the tails decay for networks with different average degrees. The higher the average degree of the network, the slower the decay of the tails of the distributions with increasing fractions of contrarians, as evidenced by the behavior of the performed fits for scale-free and random networks. In contrast, since the average degree for the small-world networks is constant $\langle k \rangle = 4$, the decay of the tails appears to approach a universal behavior independent of the rewiring probability p.

We observe that the larger the fraction of contrarians, the less important the role of the topology is, and the more mean-field the financial system becomes. This observation is reasonable since contrarians do not interact locally with their neighbors. In fact, they interact globally with the state of the market as a whole. Our findings suggest that the behavior of the model is closely tied to broader factors such as the average connectivity of the analyzed network, the level of socioeconomic anxiety, and the proportion of fundamentalist agents, regardless of the detailed topology of the socioeconomic networks.

V. ACKNOWLEDGMENTS

We would like to acknowledge Prof. H. Eugene Stanley for his valuable direction and contributions to the larger scope of this investigation. His advice and guidance, as well as his knowledgeable feedback and inputs, were of paramount importance to all the authors of this manuscript. We acknowledge financial support from SUNY Poly, POLI UPE, DF UFPE and the funding agencies FACEPE (APQ-1129-1.05/24, APQ-0565-1.05/14, APQ-0707-1.05/14), CAPES and CNPq (306068/2021-4), National Natural Science Foundation of China (72071006, 61603011, 62073007).

VI. AUTHOR CONTRIBUTIONS STATEMENT

B. J. Z., M. F. B. G., A. L. M. V., C. W.: Conceptualization, Methodology, Software, Validation, Investigation, Formal Analysis, Writing. K. P. N.: Investigation, Formal analysis,

Writing.

---

[1] B. G. Malkiel, *A Random Walk Down Wall Street: The Time-Tested Strategy for Successful Investing* (W. W. Norton & Company, Inc., New York (United States), 2007).

[2] L. Bachelier, Annales Scientifiques de l'École Normale Supérieure **3**, 21 (1900).

[3] F. Black and M. Scholes, Journal of Political Economy **81**, 637 (1973).

[4] R. N. Mantegna and H. E. Stanley, *An Introduction to Econophysics: Correlations and Complexity in Finance* (Cambridge University Press, Cambridge (United Kingdom), 2000).

[5] A.-L. Barabási and R. Albert, Reviews of Modern Physics **74**, 47 (2002).

[6] D. J. Watts and S. H. Strogatz, nature **393**, 440 (1998).

[7] P. Erdös and A. Rényi, Publications of the Mathematical Institute of the Hungarian Academy of Sciences **5**, 17 (1960).

[8] R. Cont and J.-P. Bouchaud, Macroeconomic Dynamics **4**, 170 (2000).

[9] R. M. Raafat, N. Chater, and C. Frith, Trends in Cognitive Sciences **13**, 420 (2009).

[10] H. Hong, J. D. Kubik, and J. C. Stein, The Journal of Finance **LX**, 2801 (2005).

[11] L. Zhao, G. Yang, W. Wang, Y. Chen, J. P. Huang, H. Ohashi, and H. E. Stanley, Proceedings of the National Academy of Sciences **108**, 15058 (2011), ISSN 0027-8424.

[12] S. Bikhchandani, D. Hirshleifer, and I. Welch, Journal of Political Economy **100**, 992 (1992).

[13] S. Galam, International Journal of Modern Physics C **19**, 409 (2008).

[14] R. J. Shiller, *Irrational Exuberance: Revised and Expanded Third Edition* (Princeton University Press, Princeton (United States), 2015), 3rd ed.

[15] R. H. Day and W. Huang, Journal of Economic Behavior & Organization **14**, 299 (1990).

[16] J. Voit, *The Statistical Mechanics of Financial Markets* (Springer, Berlin (Germany), 2005), 3rd ed., ISBN 3540009787 (softcover : alk. paper).

[17] S. Bornholdt, International Journal of Modern Physics C **12**, 667 (2001).

[18] T. Kaizoji, S. Bornholdt, and Y. Fujiwara, Physica A: Statistical Mechanics and its Applications **316**, 441 (2002).

[19] T. Takaishi, International Journal of Modern Physics C **16**, 1311 (2005).

[20] T. Lux and M. Marchesi, Nature **397**, 498 (1999).

[21] T. Lux and M. Marchesi, International Journal of Theoretical and Applied Finance **3**, 675 (2000).

[22] J. B. De Long, A. Shleifer, L. H. Summers, and R. J. Waldmann, Journal of Political Economy **98**, 703 (1990).

[23] K. Sznajd-Weron and R. Weron, International Journal of Modern Physics C **13**, 115 (2002).

[24] A. Krawiecki, J. A. Holyst, and D. Helbing, Physical Review Letters **89**, 158701 (2002).

[25] M. Bartolozzi, D. B. Leinweber, and A. W. Thomas, Physical Review E **72**, 046113 (2005).

[26] A. L. M. Vilela, C. Wang, K. P. Nelson, and H. E. Stanley, Physica A: Statistical Mechanics and its Applications **515**, 762 (2019).

[27] M. F. B. Granha, A. L. M. Vilela, C. Wang, K. P. Nelson, and H. E. Stanley, Proceedings of the National Academy of Sciences **119** (2022).

[28] B. J. Zubillaga, A. L. M. Vilela, C. Wang, K. P. Nelson, and H. E. Stanley, Physica A: Statistical Mechanics and its Applications **588**, 126527 (2022).

[29] A. Brunstein and T. Tomé, Physical Review E **60**, 3666 (1999).

[30] T. Tomé and A. Petri, Journal of Physics A: Mathematical and General **35**, 5379 (2002).

[31] D. F. F. Melo, L. F. C. Pereira, and F. G. B. Moreira, Journal of Statistical Mechanics: Theory and Experiment **2010**, P11032 (2010).

[32] A. L. M. Vilela, B. J. Zubillaga, C. Wang, M. Wang, R. Du, and H. E. Stanley, Scientific Reports **10**, 1 (2020).

[33] B. J. Zubillaga, A. L. M. Vilela, M. Wang, R. Du, G. Dong, and H. E. Stanley, Scientific Reports **12**, 282 (2022).

[34] P. R. A. Campos, V. M. de Oliveira, and F. G. B. Moreira, Physical Review E **67**, 026104 (2003).

[35] L. F. C. Pereira and F. G. B. Moreira, Physical Review E **71**, 016123 (2005).

[36] F. W. S. Lima, Commun. Comput. Phys **2**, 358 (2007).

[37] F. W. S. Lima, A. O. Sousa, and M. A. Sumuor, Physica A: Statistical Mechanics and its Applications **387**, 3503 (2008).

[38] A. L. M. Vilela and F. G. B. Moreira, Physica A: Statistical Mechanics and its Applications **388**, 4171 (2009).

[39] A. R. Vieira and N. Crokidakis, Physica A: Statistical Mechanics and its Applications **450**, 30 (2016).

[40] A. L. M. Vilela and H. E. Stanley, Scientific reports **8**, 1 (2018).

[41] A.-L. Barabási, R. Albert, and H. Jeong, Physica A: Statistical Mechanics and its Applications **281**, 69 (2000).

[42] M. E. J. Newman, Society for Industrial and Applied Mathematics Review **45**, 167 (2003).

[43] R. Cont, in *Long memory in economics* (Springer, 2007), pp. 289–309.

[44] B. Mandelbrot, The Journal of Business **36**, 394 (1963).

[45] P. Gopikrishnan, V. Plerou, L. A. N. Amaral, M. Meyer, and H. E. Stanley, Physical Review E **60**, 5305 (1999).

[46] R. Cont, Quantitative finance **1**, 223 (2001).

[47] S. Peiris and R. Hunt, Mathematics **11**, 817 (2023).

[48] A. Timmermann and C. W. Granger, International Journal of forecasting **20**, 15 (2004).

[49] B. G. Malkiel, in *Finance* (Springer, 1989), pp. 127–134.

[50] C. Tsallis, C. Anteneodo, L. Borland, and R. Osorio, Physica A: Statistical Mechanics and its Applications **324**, 89 (2003).

[51] S. Queirós, L. G. Moyano, J. de Souza, and C. Tsallis, The European Physical Journal B **55**, 161 (2007).

[52] K. P. Nelson, S. R. Umarov, and M. A. Kon, Physica A: Statistical Mechanics and its Applications **468**, 30 (2017).

[53] K. P. Nelson, M. A. Kon, and S. R. Umarov, Physica A: Statistical Mechanics and its Applications **515**, 248 (2019).

[54] A. E. Biondo, A. Pluchino, and A. Rapisarda, Physical Review E **92**, 042814 (2015).

[55] B. Bollobás and A. Thomason, in *North-Holland Mathematics Studies* (Elsevier, 1985), vol. 118, pp. 47–97.